MSDE

REVIEW

View Article Online
View Journal

Check for updates

Cite this: DOI: 10.1039/d1me00049g

Click-functionalized hydrogel design for mechanobiology investigations

Erica Hui, [a] Jenna L. Sumey [a] and Steven R. Caliari *[ab]

The advancement of click-functionalized hydrogels in recent years has coincided with rapid growth in the fields of mechanobiology, tissue engineering, and regenerative medicine. Click chemistries represent a group of reactions that possess high reactivity and specificity, are cytocompatible, and generally proceed under physiologic conditions. Most notably, the high level of tunability afforded by these reactions enables the design of user-controlled and tissue-mimicking hydrogels in which the influence of important physical and biochemical cues on normal and aberrant cellular behaviors can be independently assessed. Several critical tissue properties, including stiffness, viscoelasticity, and biomolecule presentation, are known to regulate cell mechanobiology in the context of development, wound repair, and disease. However, many questions still remain about how the individual and combined effects of these instructive properties regulate the cellular and molecular mechanisms governing physiologic and pathologic processes. In this review, we discuss several click chemistries that have been adopted to design dynamic and instructive hydrogels for mechanobiology investigations. We also chart a path forward for how click hydrogels can help reveal important insights about complex tissue microenvironments.

Received 7th May 2021,
Accepted 19th July 2021

DOI: 10.1039/d1me00049g

rsc.li/molecular-engineering

Published on 19 July 2021. Downloaded by University of Virginia on 8/10/2021 5:09:05 PM.

Design, System, Application

Over the past few decades researchers have made considerable advancements in the development of hydrogel biomaterial platforms to mimic the complex properties of the body. In particular, click chemistries have emerged as robust tools to rationally design and optimize tissue-mimetic hydrogels to investigate how cells integrate mechanical information from their surroundings to dictate behavior. The simplicity and specificity of click reactions allows for greater user regulation to introduce tissue-relevant mechanical and biochemical cues in a controlled manner. This review covers several click reactions that have shown unique utility in the creation of dynamic and cell-instructive hydrogels, many of which vary in reaction speed, stability or degradability, and response to external triggers including light, temperature, and pH. Continued development of click chemistry-based hydrogel models will further improve our understanding of the complex mechanobiology of pathophysiologic cell behaviors.

1. Introduction

Biomaterials designed to mimic and exploit native tissue signals, such as mechanical and chemical cues, allow improved understanding of a diverse range of physiologic and pathologic conditions from development to wound healing and disease processes.[1,2] In particular, biomaterials have become instrumental in studying how biophysical factors, namely mechanics, influence cell and tissue function, also known as mechanobiology.[3–6] Hydrogels are versatile water-swollen

[a] Department of Chemical Engineering, University of Virginia, 102 Engineer's Way, Charlottesville, Virginia 22904, USA. E-mail: caliari@virginia.edu; Tel: +1 434 243 1821
[b] Department of Biomedical Engineering, University of Virginia, Charlottesville, Virginia 22904, USA

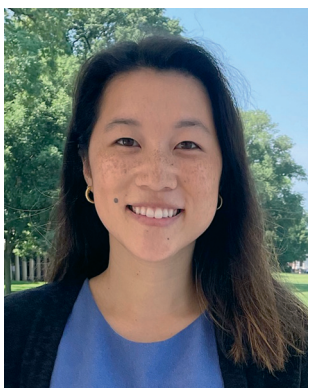

Erica Hui

Erica Hui is a fifth year Ph.D. candidate in Chemical Engineering at the University of Virginia. Her research interests center around developing a class of spatiotemporally dynamic hydrogels to mimic normal and fibrotic tissue processes. In particular, she is interested in the complexity of cell–extracellular matrix interactions and understanding the role of cellular mechanotransduction in disease. She graduated with a B.S. in Chemical Engineering from the University of Kansas in 2016.

Published on 19 July 2021. Downloaded by University of Virginia on 8/10/2021 5:09:05 PM.

polymeric biomaterials that can be designed to recapitulate key attributes of the native microenvironment, enabling further understanding of the interplay between cells and their surrounding extracellular matrix (ECM).[7–10] Many of the key elements that comprise an ideal hydrogel testbed to study mechanobiology can be found within the click chemistry toolbox. The utilization of click chemistries has become a powerful approach to easily and rapidly form hydrogel networks due to their simplicity, high reactivity and reaction specificity, and ability to be carried out under mild reaction conditions without harsh byproducts.[11] From a biomaterials perspective, click reactions are particularly useful in directing material properties through incorporation of mechanical and biochemical cues in a highly specific and bioorthogonal manner (Fig. 1). The ability to independently tune network composition by modulating features such as crosslinker content/concentration and degree of degradation to control a wide range of cell-instructive properties (*e.g.*, stiffness, viscoelasticity, ligand presentation) makes click chemistries specifically advantageous for studying mechanobiology (Table 1). Within the last decade, significant advances have been made in the design of click-based systems to probe mechanistic features of cell–matrix interactions and for various tissue engineering applications.[10,12–19]

Click chemistry is particularly useful in the design and synthesis of hydrogels that mimic salient features of the ECM. The ECM is a highly complex macromolecular network that not only acts as a support structure for cells, but also contains myriad physical, chemical, and mechanical cues that are dynamic in nature, including external and cell-mediated forces, growth factors and other signaling molecules, and changes in tissue architecture and compliance.[20–24] Cells sense mechanical signaling cues provided by the heterogeneous ECM from cell surface receptors (*e.g.*, integrins) that facilitate signal transduction between cells and their surroundings in a process known as mechanotransduction. Integrin-mediated adhesions can initiate conformational changes within the cell body, leading to translocation of relevant proteins and cytoplasmic molecules and activation of downstream signaling pathways.[22,25–27] The bidirectional relationship between ECM mechanics and growth factor presentation, known as dynamic reciprocity, also plays a significant role in regulating and activating disease-relevant signaling pathways.[28,29] For example, matrix remodeling can result in transforming growth factor-β (TGF-β) activation from its latent state and new ECM cytoskeletal and contractile protein expression, which can lead to subsequent promotion of pro-tumorigenic responses such as cellular migration, invasion, and epithelial-to-mesenchymal transition (EMT).[30–33] Similarly, platelet-derived growth factor receptor (PDGFR) isoforms are important in tissue development and homeostasis; overexpression has been linked to fibrosis and cancer, influencing cell proliferation and migration.[34–37]

More recently, mechanical properties such as stiffness,[38–46] topography,[39,47–52] and viscoelasticity[53–61] have been highlighted as critical regulators of cell behavior. For example, during fibrosis, a pathologic scarring process that occurs in most major organs in response to a range of diseases, events such as exposure to toxins, chronic inflammation, and persistent infections trigger the activation of ECM-producing myofibroblasts.[62–64] The contractility of active stress fiber-containing myofibroblasts directly affects the physical ECM *via* continuous profibrotic feed-forward mechanisms driving ECM deposition and dynamic remodeling.[65–68] In turn, aberrant changes in tissue mechanics – declines in tissue viscoelasticity and increases in tissue stiffness *via* lysyl oxidase (LOX)-mediated collagen crosslinking, play a key role in the persistence of mechanotransduction signaling dynamics.[41,46,63,69–71] Importantly, these extracellular cues collectively influence and

Jenna Sumey

Jenna Sumey is a third year Ph.D. student in Chemical Engineering at the University of Virginia. Her research focuses on understanding fibroblast mechanical memory in the context of lung tissue fibrogenesis using mechanically dynamic hyaluronic acid hydrogels. Her research interests include designing hydrogels with tunable mechanical properties as well as exploring the underlying epigenetic alterations that occur following mechanical dosing. She graduated with a B.S. in Chemical Engineering from Virginia Tech in 2018.

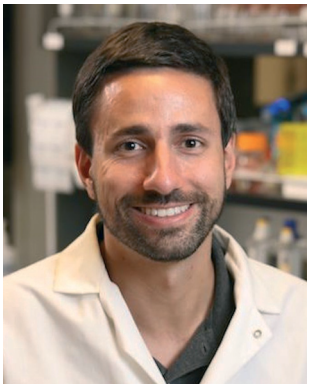

Steven Caliari

Prof. Steven Caliari joined the faculty of the University of Virginia in fall 2016. Prior to joining UVA he was an NIH Postdoctoral Fellow at the University of Pennsylvania. Steven completed his undergraduate and graduate training in Chemical Engineering at the University of Florida and University of Illinois at Urbana-Champaign respectively. His lab designs biomaterials to study the dynamic reciprocity between cells and their microenvironment, applying these platforms to address fundamental human health challenges. Steven recently received the NIH Maximizing Investigators' Research Award (MIRA) and NSF CAREER Award. To learn more about the lab's work, please follow on Twitter www.twitter.com/Caliari_Lab.

This journal is © The Royal Society of Chemistry and IChemE 2021

Published on 19 July 2021. Downloaded by University of Virginia on 8/10/2021 5:09:05 PM.

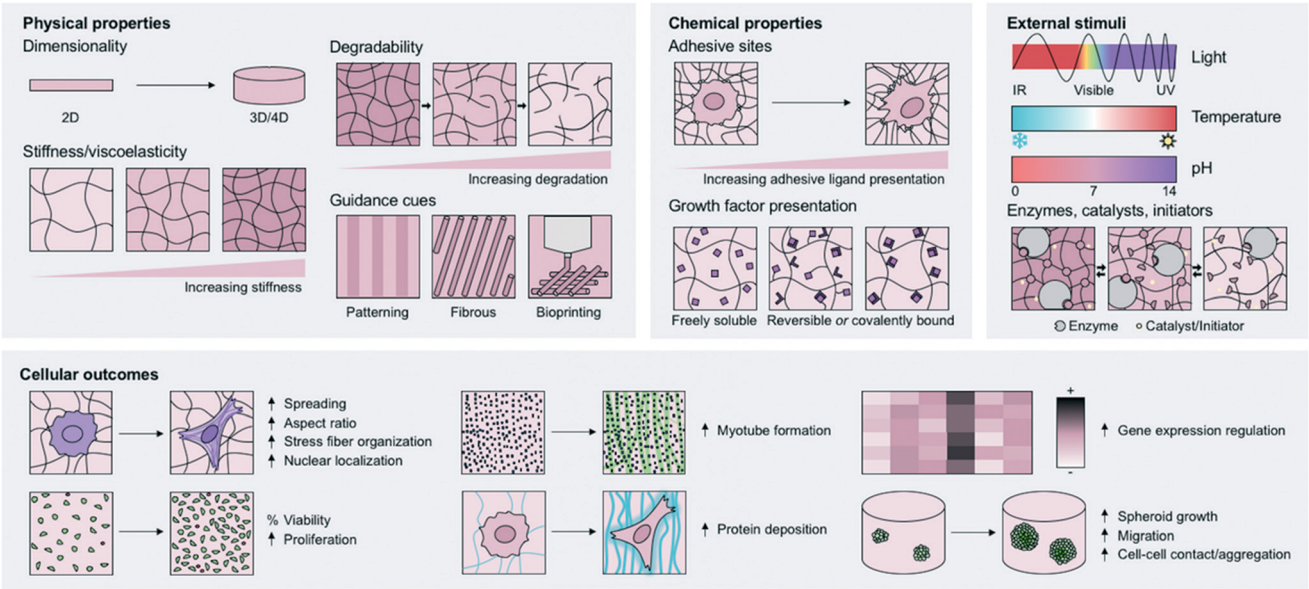

Fig. 1 The click chemistry toolbox enables tuning of tissue-relevant physical (*e.g.*, dimensionality, degradability, stiffness, viscoelasticity, architectural cues) and chemical (*e.g.*, adhesion, growth factor presentation) properties to understand mechanobiological cell responses. Many click reactions are responsive to stimuli such as light, temperature, and pH. This can be exploited to control hydrogel properties including gelation kinetics, secondary crosslinking, and/or degradation. Application of click-functionalized hydrogels can help reveal how individual and combined biophysical factors regulate and influence cell mechanobiology in the context of development, wound healing, and disease processes.

regulate many cell processes such as growth,[25,60,72,73] migration,[74–76] and differentiation[56,77,78] during normal and disease processes. The ability to decouple mechanical and biochemical cues allows researchers to investigate cell–matrix interactions in a controlled manner. As progress continues toward using click chemistry to design biomimetic systems capable of recapitulating dynamic tissue mechanics, these models will enable more nuanced investigations of mechanobiology-influenced complex biological phenomena.

In this review, we highlight the promising applications of click-functionalized hydrogels as cell culture systems for studying mechanobiology. We cover several bioconjugation reactions specifically used for hydrogel fabrication such as thiol-based chemistries, azide–alkyne cycloadditions, Diels–Alder, inverse electron demand Diels–Alder, oxime, hydrazone, and bio-orthogonal platforms combining multiple click reactions. We also discuss the influence of physical (*e.g.*, topography, dimensionality), mechanical (*e.g.*, stiffness, degradability, viscoelasticity), and chemical (*e.g.*, adhesive sites, growth factor presentation) properties on cell mechanobiology, as well as provide commentary on future directions of click-based biomaterial cell culture models.

2. Copper-catalyzed azide–alkyne cycloaddition (CuAAC)

Copper(I)-catalyzed azide–alkyne (CuAAC) reactions were published in 2002 by Meldal and Sharpless, who defined the term "click" chemistry the previous year, making it one of the first categorized click reactions.[89,90] The CuAAC reaction is able to proceed in aqueous solutions and at physiologic temperatures, has fast kinetics, high yield, and is bioorthogonal.[91] The reaction itself involves reacting a terminal alkyne with an organic azide, creating a triazole ring, similar to uncatalyzed Huisgen cycloadditions (Scheme 1). This catalyzed version, however, proceeds much faster and with greater efficiency than the uncatalyzed cycloaddition.

Ossipov *et al.* published the first use of CuAAC to create azide and alkyne functionalized poly(vinyl alcohol) (PVA) hydrogels.[92] These hydrogels could reach stiffnesses (elastic moduli) from ~2–20 kPa depending on the density of the crosslinker and reactive groups available. Other researchers have reported using CuAAC to make hydrogels from other commonly used polymers in the biomaterials field, such as poly(ethylene glycol) (PEG)[93] and hyaluronic acid (HA).[94] This mechanism yields quick gelation times, from 2–30 min, depending on the concentrations of the catalyst and polymer, as well as temperature.[95]

CuAAC reactions, although fast and efficient, are limited in many biological applications due to the presence of copper ions as well as reactive oxygen species formed by the copper ions, which may be toxic to cells and destroy proteins, polysaccharides, and nucleic acids.[96] For many *in situ* cell cultures or *in vivo* analyses, click chemistries that do not require a metal catalyst are more favorable. For more extensive reviews on CuAAC chemistry, including its history and in-depth descriptions of the mechanism, the reader is referred to the following discussions.[97–102] Another disadvantage of the CuAAC mechanism is that the addition

Published on 19 July 2021. Downloaded by University of Virginia on 8/10/2021 5:09:05 PM.

Table 1 Summary of click chemistries covered in this review

Click chemistry	Rate constant k (M^{-1} s^{-1})	Pros	Cons	Common base polymers	Common reactive group 1	Common reactive group 2	Tunable biophysical properties	Reaction method
CuAAC	10–100 (ref. 79)	Fast kinetics, high yield, and bioorthogonal Limited side product formation (azides/alkynes are not present in nature)	Potential catalyst toxicity Mammalian cells can only survive low copper concentrations Catalyst is unstable	Alginate, HA, PEG	Azide	Alkyne	Stiffness	Catalyst Occurs at physiologic conditions
SPAAC	10^{-2}–1 (ref. 80)	No initiator or catalyst required High reactivity to allow rapid cell encapsulation	Complex synthesis of cyclooctynes Cyclooctyne reagents may undergo side reactions with nucleophiles (*e.g.*, sulfhydryl side chain of free cysteines)	Chitosan, dextran, HA, NiPAAm, PEG	Cycloalkyne (DIFO, DBCO, BCN)	Azide	Stiffness, viscoelasticity Degradation Adhesion	Occurs at physiologic conditions
Diels–Alder	10^{-2}–1 (ref. 81 and 82)	No toxic catalyst required Thermal reversibility No reaction byproducts	Slow gelation kinetics	Alginate, chitosan, gelatin, HA, PEG	Furan Furyl Fulvene	Maleimide Dichloromaleic	Stiffness Gelation rate Degradation	Temperature
IEDDA	1–10^6 (ref. 83)	Rapid gelation kinetics at physiologic conditions No initiator or catalyst required 10 000 times faster than CuAAC	Trade-off between reactivity and stability	Alginate, gelatin, HA, PEG	Tetrazine	Norbornene *trans*-Cyclooctene (TCO)	Stiffness, viscoelasticity Gelation rate Adhesion	Occurs at physiologic conditions
Oxime	10^{-3}–10 (ref. 84 and 85)	More stable than hydrazone bonds	Slow gelation kinetics	Alginate, HA, PEG, poly(DMA-*co*-DAAM)	Aldehyde Ketone	Hydroxyl-amine Aminooxy	Stiffness Gelation rate	pH
Hydrazone	10^{-2}–100 (ref. 84–86)	pH reversibility	More likely to undergo hydrolysis compared to oxi mes Slow gelation kinetics	Alginate, ELP, HA, PEG	Aldehyde Ketone	Hydrazine	Viscoelasticity Degradation	Occurs at physiologic conditions pH Temperature
Thiol–ene/–yne (radical-mediated)	N/A	Rapid gelation kinetics Spatiotemporal control	Toxicity of photoinitiators and radicals Cross-reactivity of thiols	Alginate, gelatin, HA, PDMS, PEG	Norbornene	Thiol	Stiffness, viscoelasticity Gelation rate Ligand presentation	Light
Thiol-Michael addition	10^{-6}–100 (ref. 87 and 88)	No photoinitiator needed	Can't as easily control gelation; less spatiotemporal control Cross-reactivity of thiols Often requires basic conditions	Dextran, gelatin, HA, PEG	(Meth)acrylate, vinyl sulfone, maleimide	Thiol	Stiffness, viscoelasticity Gelation rate	pH

This journal is © The Royal Society of Chemistry and IChemE 2021

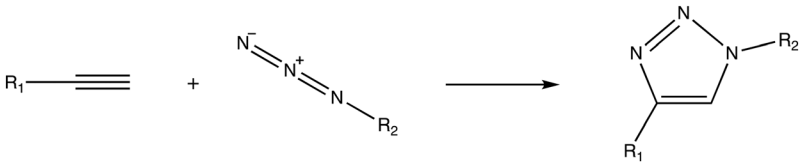

Scheme 1 Mechanism for copper(I)-catalyzed azide–alkyne cycloaddition.

Published on 19 July 2021. Downloaded by University of Virginia on 8/10/2021 5:09:05 PM.

of Cu(I) salt or the reduction of Cu(II) to the Cu(I) catalyst typically provides little to no spatiotemporal control over the reaction, which is often important in tissue engineering and cell culture applications. However, efforts to reduce Cu(II) to the Cu(I) catalyst using photochemical techniques (pCuAAC) resulted in better spatiotemporal control in the crosslinking of alkyne- and azide-functionalized PEG hydrogels. Following initial hydrogel formation through using thiol–yne chemistry, fluorescent patterns could be created in the hydrogel using photomasks where the pCuAAC reaction occurred in the regions exposed to light.[103]

New efforts in designing degradable hydrogels for controlled drug delivery make use of the CuAAC reaction to enable enzymatic[104] or light-mediated hydrogel degradation. For example, Azagarsamy *et al.* reacted visible light degradable azide-functionalized coumarin onto an alkyne-functionalized PEG backbone using the copper catalyzed cycloaddition. The authors reported that higher copper concentration resulted in faster gelation, but with lower shear elastic moduli likely caused by heterogeneous network formation. While this report highlights the ability to engineer user-controlled photodegradable hydrogels, for cytocompatible platforms the authors suggest copper-free click mechanisms.[105]

CuAAC hydrogels for cell culture

While the CuAAC mechanism often involves using cytotoxic amounts of copper catalysts, researchers have still been able to study cellular responses on hydrogels developed with this chemistry as long as cells were incorporated after hydrogel formation.[106,107] Liu *et al.* demonstrated that fibroblasts could attach and proliferate over a period of 7 days when seeded onto tetraacetylene PEG hydrogels functionalized with RGD-containing diazide and formed by the CuAAC mechanism.[95] To better mimic the native ECM, Hu *et al.* developed a hydrogel system consisting of azide-functionalized HA and chondroitin sulfate that underwent crosslinking with alkyne-functionalized gelatin.[108] Following 7 days of culture, they found no significant difference in chondrocyte cell viability on the CuAAC crosslinked hydrogel *versus* standard TCPS, indicating that their system supported cell adhesion and viability. To introduce hydrazone interactions, Lou *et al.* functionalized azide-modified hydrazines onto HA using CuAAC.[61] They subsequently developed interpenetrating networks (IPNs) to create a two-step stress relaxing network that mimicked properties of the native ECM; more details can be found in Section 6 on hydrazone-based hydrogels.

In another study, Seelbach *et al.* used CuAAC to decorate propargylamine-derived hyaluronic acid with either a dendrimer containing an RGDS peptide and one azide, or a thermoresponsive poly(*N*-isopropylacrylamide) with a terminal azide group.[109] This enabled creation of an injectable, thermoresponsive hyaluronic acid hydrogel with controlled presentation of bioactive features. The authors encapsulated bone marrow-derived human mesenchymal stromal cells (hMSCs) by suspending them in the combined polymer solution and forming hydrogel beads following exposure to warm (37 °C) culture media. Cell viability was maintained over a 21 day culture period; however, because this hydrogel did not incorporate degradability – for example, with a matrix metalloproteinase (MMP)-sensitive peptide – the cells did not show significant spreading and maintained spherical morphologies.

Gradient and photopatterned CuAAC hydrogels

Since the reporting of spatiotemporal control of CuAAC using photopatterning, researchers have used this to their advantage to create tailored hydrogels. Chen *et al.* engineered a micropatterned hydrogel consisting of alkyne-functionalized PEG and azide-functionalized bromine plasma polymer using photochemical Cu(II) reduction to Cu(I) to yield the azide–alkyne cycloaddition.[110] The photoinitiator radicals also led to the radical crosslinking of PEG, so using a photomask, the authors could spatially control hydrogel properties with regions of either the PEG hydrogel (patterned) or an azide-functionalized plasma polymer (unpatterned). The authors demonstrated the spatial control of mouse fibroblast attachment on the patterned regions of PEG compared to unpatterned samples.

The controlled presentation of biomolecules using CuAAC has also been explored, predominantly by Becker and colleagues. After developing a method for conjugating azide-functionalized peptides, like RGD, that could undergo CuAAC onto an alkyne gradient containing a self-assembled monolayer (SAM), Gallant *et al.* reported that increasing RGD concentration led to more smooth muscle cell adherence on their gradient system.[111] The conjugation of azide-functionalized RGD was also used to show increased attachment of rabbit corneal epithelial cells onto self-assembled poly(2-methyl-2-carboxytrimethylene carbonate-*co*-D, L-lactide) nanoparticles.[112] An alternative method of conjugating RGD to SAMs was used to investigate hMSC

Published on 19 July 2021. Downloaded by University of Virginia on 8/10/2021 5:09:05 PM.

adhesion and focal adhesion formation, which increased with increasing RGD.[113] This same method was also applied to the conjugation of azide-functionalized osteogenic growth peptide (OGP) to an alkyne gradient to probe preosteoblast adhesion and proliferation. Cell adhesion increased with decreasing OGP concentration over the course of 3 days.[114]

Following the discovery of the first known click chemistry – the CuAAC reaction – advancements in click-based systems rapidly developed. While the CuAAC reaction is amenable to quick crosslinking in aqueous solutions at physiologic conditions, the need for a copper catalyst proved to be cytotoxic for many cell experiments within the biomaterials field. The authors found no reports of CuAAC in the context of mammalian cell encapsulation and only one publication describing the proliferation of encapsulated yeast cells within CuAAC-crosslinked HA.[94] In this study, Crescenzi *et al.* reported 80% cell proliferation 24 hours after encapsulation within these hydrogels, which they formed *in situ* within a few minutes. Although this provides some preliminary evidence to support the use of CuAAC-based systems for tissue engineering applications, the lack of published studies is likely due to the toxicity of the copper ions generated.[94] While more cytocompatible catalysts are in development for use with this rapid crosslinking mechanism, the authors found no report of these different catalysts to create hydrogels for tissue engineering applications.[115] At this time, copper-free click reactions provide more cytocompatible platforms for investigating cell behaviors, including mechanobiology. Although CuAAC is not commonly used in biomaterial design for cell culture, this discovery was crucial to the advancement of more popular click chemistries used today, such as strain-promoted azide–alkyne cycloaddition (SPAAC) or thiol–ene click reactions.

3. Strain-promoted azide–alkyne cycloaddition (SPAAC)

Strain-promoted azide–alkyne cycloaddition (SPAAC) reactions were developed in the early 2000s by Bertozzi and coworkers to address cytotoxicity concerns associated with traditional copper-catalyzed click reactions.[116] SPAAC is bioorthogonal, can occur efficiently under physiologically-relevant conditions without additional reagents (*e.g.*, catalysts, initiators), and results in products with high stability.[117–119] Compared to previous copper-based reactions, SPAAC has more favorable gelation kinetics (second order rate constant, $k \sim 0.1\ M^{-1}\ s^{-1}$) in aqueous conditions, permitting efficient cell encapsulation without significantly impacting cell viability.[117,120,121]

In general, SPAAC proceeds as a (3 + 2) dipolar cycloaddition of a strained cycloalkyne with an organic azide, generating a triazole.[80,117] The reaction is fast and spontaneous due to the release of the strained ring into a fused ring system, as shown in Scheme 2A. Similar to other click chemistries, the balance between reactivity and stability can be influenced by the reactant. Studies have mainly focused on altering the cycloalkyne ring structure to increase reactivity, which can be beneficial for rapid 3D cell encapsulation.

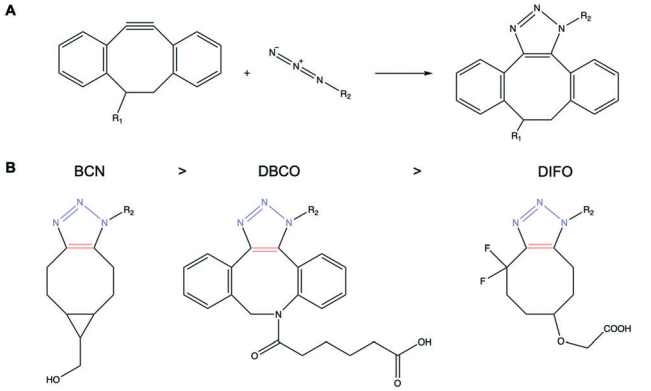

Scheme 2 Strain-promoted azide alkyne cycloaddition (SPAAC). (A) Dibenzylcyclooctyne (DBCO) reacts with a simple aliphatic azide to form the triazole product without the presence of a catalyst or initiator. (B) SPAAC products of common cycloalkynes (listed from most to least reactive), bicyclononyne (BCN), dibenzocyclooctyne (DBCO), and difluorinated cyclooctyne (DIFO), with an azide.

Commonly used cycloalkynes used for hydrogel fabrication include difluorinated cyclooctyne (DIFO),[122,123] dibenzocyclooctyne (DBCO or DIBO),[13,124–127] and bicyclononyne (BCN).[13,128–130] The order of reactant reactivity, BCN > DBCO > DIFO, can be explained by the increasing ring strain imposed onto the carbon atoms (Scheme 2B). Specifically, increased sp^2-hybridized carbons in the cyclooctyne results in increasing ring strain and reactivity.[80,117] Introduction of electron-withdrawing substituents such as fluorine on DIFO can lead to enhanced reactivity. DBCO falls within the class of (di)benzoannulated cyclooctynes, which impart increased reactivity compared to electron-withdrawing groups – the introduction of two adjacent benzene rings increases ring strain and ultimately, reactivity. For BCN, the fusion of cyclooctyne to cyclopropane produces a reactive bicyclo[6.1.0]non-4-yne that outweighs benzoannulated structures.[131] However, a significant limitation to SPAAC is that cyclooctyne synthesis involves several steps (many cyclooctyne derivative syntheses contain around 10 steps) with low overall yield, hindering scale-up. Fortunately, synthesis of BCN and DBCO is relatively simple, requiring only 4–5 steps. Compared to the growing body of literature surrounding the development of various cycloalkynes, modifications to the azide reactant have not been studied as extensively.[80,132,133] The majority of azides that participate in SPAAC reactions for hydrogel synthesis are simple aliphatic azides.

Depending on the reactive functional groups and application, polymerization can take anywhere from 90 seconds to an hour under physiologic conditions. Varying the relative macromer concentrations and degree of functionalization can produce hydrogels with variable stiffness, viscoelasticity, degradation modes, and ligand presentation.[134,135] For example, early SPAAC work by Anseth

This journal is © The Royal Society of Chemistry and IChemE 2021

Published on 19 July 2021. Downloaded by University of Virginia on 8/10/2021 5:09:05 PM.

and co-workers utilized difluorinated cyclooctyne (DIFO3) and azide moieties to quickly form 3D hydrogels within 5 minutes.[122,123] Material degradability can be tuned with pH, where slightly more basic conditions correlate with faster hydrolysis, presenting a promising approach for tissue engineering applications that require quick degradation and material clearance.[136] Increased stability and secondary incorporation of biomolecules can also be achieved by employing orthogonal click chemistries such as photopolymerizable thiol–ene addition, enabling researchers to independently study how variables such as mechanics and ligand presentation affect cell behavior over longer culture periods.[123,135,137]

SPAAC has also been used to tether both adhesive ligands and growth factors to promote migration,[122] stem cell lineage specification,[138,139] and cell release.[140] Arakawa *et al.* demonstrated rapid hydrogel formation using PEG-tetraBCN and a di-azide crosslinker decorated with an adhesive RGD sequence, MMP-degradable sequence, and an *ortho*-nitrobenzyl (*o*NB) group.[130] Hydrogels formed through SPAAC were stable and supported both customizable microvessel generation and long-term viability of encapsulated human umbilical vein endothelial cells (HUVECs). High-resolution spatiotemporal control over vessel formation allowed for a wide range of tunable physical properties such as geometry, thickness, and flow, critical for studying blood vessel function and hemodynamics. Using a similar approach, Shadish *et al.* demonstrated the ability to spatiotemporally immobilize proteins *via* BCN-azide SPAAC chemistry as well as trigger protein photocleavage with potential applications in directing dynamic cellular behaviors.[129] HeLa cells encapsulated within SPAAC hydrogels were subjected to patterned violet light (λ = 400 nm), releasing tethered epidermal growth factor (EGF) from specific regions. Over two weeks, presentation of retained EGF promoted increased cell density and spheroid growth compared to regions without immobilized EGF, highlighting the ability to tether and release bioactive molecules in a spatiotemporal manner to guide cell fate.

Thermoresponsive SPAAC hydrogels

Thermally-responsive hydrogels have also been developed using SPAAC chemistry. Truong *et al.* fabricated chitosan-based hydrogels that were stable at physiologically-relevant conditions.[141] Gelation of azide-functionalized chitosan and propiolic acid ester-functionalized PEG crosslinker occurred within 15 minutes at 37 °C. Increasing polymer concentrations and greater alkyne–azide ratios resulted in faster gelation times (from 55 minutes to 4 minutes) and increased stiffness (up to storage modulus, $G' \sim 44$ kPa). MSCs seeded atop hydrogels for seven days exhibited fibroblastic morphologies typically seen on tissue culture polystyrene, with defined F-actin filaments and vinculin staining, important for adhesion and spreading. In contrast, cell spreading was more restricted in 3D cultures and cells remained rounded.

To promote tissue-specific repair, Guo *et al.* formed thermoresponsive poly(*N*-isopropylacrylamide-*co*-glycidyl methacrylate) (P(NiPAAM-*co*-GMA)) hydrogels capable of biomolecule conjugation *via* SPAAC.[142] The alkyne-containing PEG crosslinker was modified with azide-modified biomolecules designed to promote either chondrogenesis, such as chondroitin sulfate and N-cadherin-mimicking peptide, or osteogenesis, including bone marrow homing peptide 1 and glycine–histidine–lysine. Advantageously, SPAAC-based conjugation of cartilage- and bone-specific biomolecules to the crosslinker occurred through simple mixing at room temperature in water, and presentation of biochemical cues was varied by changing the crosslinker concentration. MSCs encapsulated within cartilage-promoting hydrogels led to cartilage-like matrix synthesis (sulfated glycosaminoglycans) and maintained viability over a month. In contrast, MSCs exposed to bone-specific molecules promoted osteogenesis through expression of osteogenic markers Runt-related transcription factor 2 (RUNX2) and osteopontin.

Viscoelastic SPAAC hydrogels

There is tremendous interest in generating hydrogels that recapitulate the viscoelastic stress relaxing nature of tissues. One method to tune viscoelastic properties is through secondary physical interactions introduced *via* dibenzylcyclooctyne (DBCO) groups. By varying the ratio of covalent DBCO–azide interactions, physical DBCO–DBCO interactions (*i.e.*, hydrophobic and hydrogen bonding interactions), and degradable macromer (*i.e.*, incorporation of a labile ester linkage in PEG–azide), Tan *et al.* was able to match cartilage stiffness, viscoelasticity, and degradability, respectively.[125] Hydrogels formed with an excess of PEG–DBCO exhibited increased stiffness and decreased swelling compared to hydrogels formed with an excess of PEG–azide due to the physical DBCO–DBCO interactions. The increase in non-covalent interactions resulted in faster stress relaxation (stress relaxation time $\tau_{1/2}$ of ~132 min compared to 291–320 min). Stiffer and more viscoelastic hydrogels supported increased chondrocyte proliferation and deposition of type II collagen and glycosaminoglycans, both of which are chondrogenic markers. Degradation also played a key role in maintaining the chondrocyte phenotype; chondrocytes encapsulated in faster-degrading groups showed greater proliferation and more robust deposition of type II collagen.

Combining boronate ester and SPAAC chemistries, Tang *et al.* further demonstrated the importance of stress relaxation timescales on cell–matrix interactions.[127] Viscoelasticity was introduced *via* boronate ester bonds and hydrogels were stabilized through SPAAC chemistry between DBCO and azide groups (Fig. 2A and B), with all hydrogel groups experiencing stress relaxation times of one second or less. In comparison to the previous viscoelastic hydrogel system, this study targeted relaxation timescales to match

Published on 19 July 2021. Downloaded by University of Virginia on 8/10/2021 5:09:05 PM.

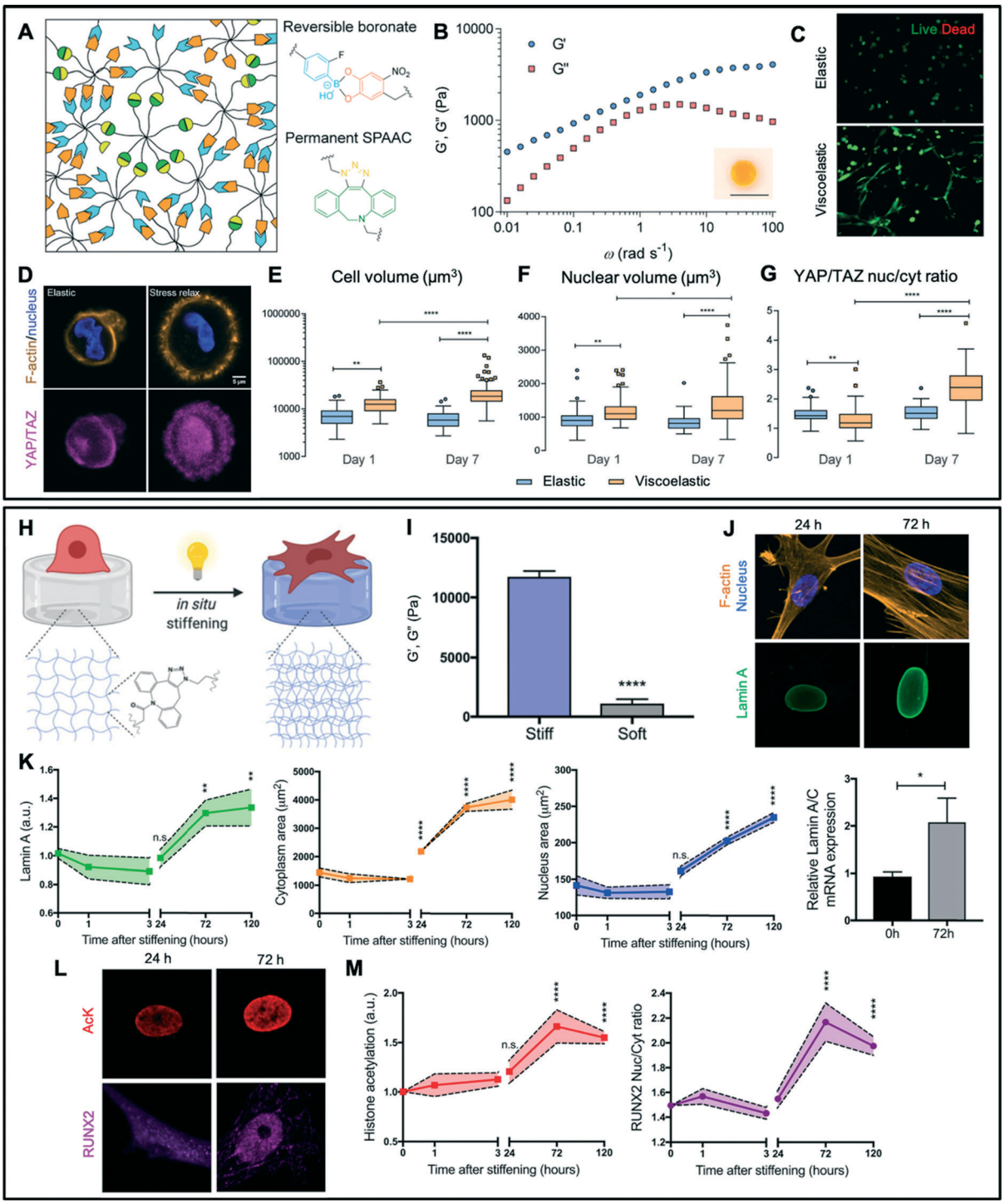

Fig. 2 SPAAC chemistry can be used in combination with secondary crosslinking mechanisms to create dynamic and complex hydrogel networks useful for studying mechanotransduction. (A) A hybrid network containing reversible boronate ester bonds and permanent SPAAC interactions allowed for the fabrication of a stable hydrogel with stress relaxing properties. (B) Frequency sweep of a swollen hydrogel after 7 days (shown in inset photograph, scale bar = 1 cm) demonstrated viscoelasticity and mechanical stability. (C) Cells in viscoelastic (stress relaxing) hydrogels displayed increased cell spread area after 7 days. (D) Immunofluorescent staining for YAP/TAZ (magenta), F-actin (orange), and nuclei (blue) in hMSCs encapsulated for 7 days. Scale bar = 5 μm. (E–G) Quantification of cell volume, nuclear volume, and nuclear localization of YAP/TAZ showed significant increases in all categories for cells in viscoelastic hydrogels. (A–G) adapted with permission from ref. 127. Copyright 2018 Wiley-VCH. (H) Initially formed SPAAC hydrogels can undergo photostiffening in the presence of excess DBCO groups. (I) Average storage moduli, G', of the compliant ($G' \sim 1$ kPa) and stiff ($G' \sim 12$ kPa) hydrogel groups, $n = 3$ hydrogels. (J) Immunofluorescent staining for lamin A (green), F-actin (yellow), and nuclei (blue) in hMSCs 24 and 72 hours after stiffening. (K) Quantification of lamin A intensity and cell areas show gradual increases between 0 and 120 hours after stiffening. (L) Representative hMSCs stained for RUNX2 (purple) and histone acetylation, AcK (red) 24 and 72 hours after stiffening. (M) Quantification of histone acetylation and RUNX2 nuclear localization shows increased levels in hMSCs post-stiffening. (H–M) adapted with permission from ref. 143. Copyright 2020 National Academy of Sciences.

This journal is © The Royal Society of Chemistry and IChemE 2021

Published on 19 July 2021. Downloaded by University of Virginia on 8/10/2021 5:09:05 PM.

those of biological processes (*e.g.*, propagation of mechanical signals from the cytoplasm to the nucleus). In comparison to elastic hydrogels, encapsulated hMSCs in stress relaxing substrates displayed increased spreading, larger cell and nuclear volume, and increased nuclear localization of the transcriptional mechanoregulators YAP/TAZ, extending the ability to easily tune complex mechanics to study cell morphology (Fig. 2C–G).

Dual-crosslinking SPAAC hydrogel systems

Several groups have combined orthogonal click chemistries to achieve spatiotemporally tunable mechanics. After synthesizing initially compliant hydrogels ($G' \sim 700$ Pa) *via* a SPAAC reaction between DBCO and azide groups, Brown *et al.* then further stiffened the network through secondary photopolymerization of excess DBCO groups ($G' \sim 5$ kPa).[126] The on-demand stiffening capabilities of this system enabled a rapid and stable increase in stiffness of hydrogels to between 200–700% of their initial values (given an alkyne : azide ratio of 2–3 : 1), relevant to changes in stiffness related to muscle disease. Indeed, C2C12 myoblasts encapsulated in initially compliant networks ($G' \sim 700$ Pa) showed decreased cell spreading and lower nuclear localization of YAP after immediate photostiffening ($G' \sim 5$ kPa). In contrast, encapsulated myoblasts that underwent photostiffening after seven days were able to spread prior to the delayed stiffening and interestingly, exhibited an overall increase in cell elongation and YAP nuclear localization by day 15. The dual crosslinking modes provide a high level of control over mechanics to recapitulate dynamic disease processes.

One emerging application of tunable hydrogel systems is the ability to study how mechanical cues directly influence cell epigenetic programming and gene expression. Similar to the previous study, Killaars *et al.* formed a PEG-based hydrogel through DBCO–azide interactions that could undergo a secondary photocrosslinking step of excess DBCO groups to enable *in situ* stiffening (Fig. 2H and I).[143] The dynamic nature of this hydrogel platform enables direct analysis of how evolving mechanics can affect epigenetic remodeling as a function of time. hMSCs were seeded atop initially compliant hydrogels ($G' = 1$ kPa) that were stiffened ($G' = 12$ kPa) after one day and analyzed at several timepoints after stiffening (0, 1, 3, 24, 72, and 120 hours). While nuclear localization of YAP occurred within 24 hours, F-actin stress fiber organization was only evident after 72 hours, suggesting that sustained cytoskeletal tension occurs after nuclear localization of mechanosensitive transcriptional co-activators (Fig. 2J and K). The timescale of lamin A intensity, which plays a role in force transmission *via* the LINC complex, correlated with F-actin stress fiber formation. Interestingly, *in situ* stiffening resulted in increased histone acetylation and RUNX2 nuclear localization within the same 72 hour timeframe, suggesting its connection to nuclear tension (Fig. 2L and M). Additionally, increased nuclear tension, caused by stiffening, led to decreased activity of epigenetic modulators histone deacetylases (HDAC)1, 2, and 3 as well as reduced osteogenic fate.

Photochemistry can also be used to introduce biomolecular regulators of cell fate with spatiotemporal control. DeForest *et al.* designed a 3D hydrogel system where initial cell encapsulation occurred *via* SPAAC between azide-functionalized PEG and bis(DIFO3)-functionalized crosslinker with secondary thiol–ene addition enabled biomolecule patterning.[123] The crosslinker contained a photoreactive alkene group and an MMP-cleavable sequence to allow independent control over chemical and mechanical properties, respectively. Specifically, the photoreactive alkene participates in thiol–ene addition to introduce biomolecule patterning and the enzymatically degradable sequence allows cell-mediated remodeling. Fibroblast morphology was assessed in hydrogels with photopatterned regions of thiol-functionalized RGD, and cells encapsulated within the patterned regions displayed greater spreading and elongation compared to those within unpatterned regions, showing the robust capability of the 3D platform to promote and study specific cellular outcomes.

SPAAC for tissue engineering

SPAAC has also been used in the design of tunable tissue engineering models. Han *et al.* developed an HA-based injectable scaffold for chondrocyte encapsulation.[124] HA was modified with DBCO–PEG groups *via* a one-step 1-ethyl-3(3-dimethylaminopropyl)carbodiimide (EDC)/*N*-hydroxysuccinimide (NHS) coupling reaction and mixed with PEG–azide crosslinker to form hydrogels. Varying the crosslinker concentration impacted properties such as stiffness, gelation kinetics, and hydrogel microstructure – to a certain extent, increasing crosslinker concentration correlated with increasing stiffness and decreasing pore size. Chondrocytes encapsulated within the HA hydrogels were found to be uniformly distributed and remain rounded over the 5 day culture period, with observed cell aggregation within stiffer hydrogel groups. Injection of cell-laden hydrogels into mice resulted in regeneration of cartilaginous tissue. Specifically, lower stiffness hydrogels led to host cells migrating into the degraded hydrogels, while intermediate stiffness groups exhibited increased neocartilage formation *in vivo*. Wang *et al.* used azadibenzocyclooctyne–azide SPAAC chemistry to prepare injectable dextran-based hydrogels with varying stiffness ($G' \sim$ 2–6 kPa through increasing polymer concentration and/or polymer modification) and gelation time (as quick as 1.1 min with increasing polymer modification).[144] Using a higher polymer concentration (10%) to support cell encapsulation, chondrocytes exhibited high viability and increasing DNA content over the 3 week culture period. In contrast, DNA content of chondrocyte spheroids showed a more stable output, correlating with slower proliferation. Interestingly, normalized ECM production (glycosaminoglycans and collagen) by chondrocyte spheroids was significantly higher. These results prove promising for cartilage tissue engineering.

Published on 19 July 2021. Downloaded by University of Virginia on 8/10/2021 5:09:05 PM.

The incorporation of a photoreactive nitrobenzyl moiety within the azide-functionalized crosslinker allows for UV-mediated degradation after initial SPAAC hydrogel fabrication. McKinnon *et al.* used a dual reaction scheme to fabricate neural networks for studying axon behavior in neuromuscular junctions after injury.[145] Design and formation of hydrogel channels to promote motor neuron axon extension revealed that the speed and extent of outgrowth was independent of channel width. Co-encapsulation of neuron embryoid bodies and C2C12 myotubes within the hydrogel network facilitated significant branching and axon-myotube interactions, indicated by acetylcholine receptor staining for neuromuscular junctions.

Elastin-like proteins (ELPs) are highly modular and can be designed with elastin-like (*i.e.*, VPG*X*G, where the non-proline *X* residue can be used to incorporate chemical functionalities) and bioactive (*e.g.*, adhesion, degradation) domains to regulate cellular behaviors.[128] Madl *et al.* demonstrated functionalization of ELP lysine residues with either azide or BCN groups to permit SPAAC chemistry. Upon mixing, hydrogel formation occurs within seconds and completes within minutes. Stiffness could be increased by either increasing ELP concentration or the molar ratio of BCN to ELP polymer to yield biologically relevant tissue mechanics (storage modulus, $G' \sim 180$–1200 Pa). Encapsulation of multiple cell types within RGD-containing SPAAC hydrogels resulted in high viability and maintenance of cell phenotypes; hMSCs displayed actin stress fibers and spread morphologies after two days, HUVECs organized into tubular networks and stained positive for endothelial marker CD31 after one week, and murine neural progenitor cells expressed nestin (neural progenitor marker) and were able to differentiate into neurons and astrocytes following the one week growth period.[128,146] Independent tuning of adhesive sites revealed a correlation between increasing adhesive RGD presentation with hMSC spreading and stress fiber formation to a certain stiffness, agreeing with previous studies.[147]

In summary, SPAAC gained momentum as a catalyst-free alternative to CuAAC and has been widely adopted to synthesize hydrogels due to its favorable reaction rate and ability to be combined with other chemistries to produce dual-crosslinked networks. Many of the common cycloalkynes used in SPAAC reactions, including DBCO, support favorable gelation times but more arduous and inefficient syntheses. Fortunately, recent developments in the design of cycloalkynes with increasing strains, such as BCN and DBCO, have led to more rapid gelation times as well as decreased number of synthesis steps and increased overall yield. The utility of the SPAAC reaction extends beyond rapid cell encapsulation and can be demonstrated by its tunability and bioorthogonality. The introduction of secondary crosslinking mechanisms, whether it be between excess cycloalkynes or a reaction mediated by photochemistry, provides endless opportunities to investigate the influence of individual and combined mechanical and biochemical cues on cell behavior and fate. Disease-relevant changes in ECM stiffness, viscoelasticity, degradation, and ligand presentation can all be incorporated within SPAAC hydrogel systems by tuning polymer concentration, ratio of physical interactions, addition of photodegradable groups, and introduction of pendant adhesive cues or growth factors, respectively. In particular, SPAAC has and will continue to be an attractive method to study cell mechanobiology in 3D cultures.

4. Diels–Alder (DA)

The Diels–Alder (DA) reaction is a highly efficient and stereoselective [4 + 2] cycloaddition of a diene and dienophile that can proceed without the use of a catalyst and does not yield any byproducts (Scheme 3A).[148] There are several variations of the traditional electron-demand DA reaction, including intramolecular reactions in which the diene and dienophile are on the same molecule,[149,150] hetero-DA reactions containing at least one heteroatom (commonly nitrogen or oxygen),[151,152] and inverse electron demand DA reactions (section 5). Compared to other functional moieties such as thiols, dienes and dienophiles are less reactive and more stable.[148,153] DA reaction kinetics can be accelerated *via* electron-rich dienes (*e.g.*, alkyls, amines, hydroxyls) and electron-poor dienophiles (*e.g.*, carboxyls, carbonyls, ketones).[148] Gelation rates are improved in aqueous conditions due to increasing hydrophobicity within the reaction center of the diene and hydrophobic interactions from chosen diene–dienophile substituents, making DA cycloadditions particularly useful for creating cytocompatible hydrogels.[81,154,155]

DA reactions are temperature-sensitive and exhibit increased reversibility (*via* a retro-Diels–Alder reaction) at elevated temperatures (>100 °C). By varying diene and dienophile groups, the thermal equilibrium can be shifted to physiologic conditions, which has facilitated the use of DA hydrogels as tunable biomaterial systems for drug delivery and other applications.[156–160] Several studies have investigated this temperature dependency and have shown variability based on parameters such as chosen diene/

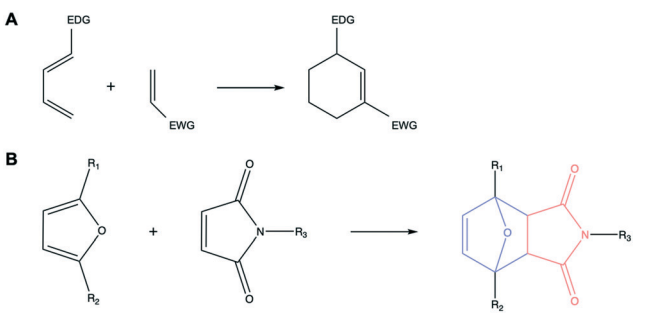

Scheme 3 (A) Conventional electron-demand Diels–Alder (DA) cycloaddition of an electron-rich diene with an electron donating group (EDG) and an electron-poor dienophile bearing an electron withdrawing group (EWG). (B) DA reaction between a furan (EDG) and maleimide (EWG) group.

This journal is © The Royal Society of Chemistry and IChemE 2021

Published on 19 July 2021. Downloaded by University of Virginia on 8/10/2021 5:09:05 PM.

dienophile substituent, concentration of diene/dienophile groups, and molecular weight.[161–163]

Among the growing number of suitable diene–dienophile pairs, furan and maleimide have become the most established for hydrogel fabrication, predominantly for their rapid reaction rate at physiologic temperatures (Scheme 3B). Biomimetic hydrogels synthesized by aqueous DA reaction of furan and maleimide groups were initially reported by Wei *et al.*, demonstrating high stability under mild reaction conditions.[164] Hydrogel formation was shown to be temperature and solvent-dependent, where gelation occurred more rapidly in water (50 min at 37 °C and 10 min at 77 °C) compared to *N*,*N*-dimethylformamide (DMF) over the entire range of studied temperatures. Additionally, Gregoritza *et al.* incorporated various hydrophobic spacers between the polymer backbone and functional groups to enable quicker DA crosslinking.[165] Hydrogels with longer hydrophobic spacers displayed faster gelation, increased crosslinking density and stability, and delayed antibody release profiles. Furan–maleimide DA hydrogels have since been used extensively for tissue engineering and cell culture studies.[14,18,166–171]

Due to its thermally-induced reversibility, DA click chemistry has been used for the development of self-healing, injectable hydrogels. Yu *et al.* studied the shear thinning and self-healing properties of DA-based HA/PEG hydrogels in response to 10–30 cycles of applied stress and demonstrated their ability to easily recover with minimal fatigue. Fan *et al.* successfully fabricated biodegradable HA hydrogels with the ability to release dexamethasone, a corticosteroid that induces cell differentiation, in a sustained manner *via* temperature control.[172] The high tunability afforded by furan–maleimide HA hydrogels, including control of stiffness through varying polymer concentration and degree of furan modification on HA, porosity *via* cryogelation, and pore size distribution by tuning thaw temperature, was demonstrated by Owen *et al.*[167] Additionally, 3D two-photon photopatterning was used to enable spatiotemporal control of protein immobilization, providing a versatile platform for guiding cell fate.[167] By combining thermoresponsive poloxamines modified with DA-friendly maleimide and furyl moieties, rapid hydrogel formation could be induced at 37 °C with controlled stability and triphasic antibody release between 14 and 329 days.[173] Hydrogel stiffness was tuned by varying the ratio of different armed polymer (*e.g.*, 4-arm and 8-arm poloxamine). Hydrogel swelling and degradation both correlated with stiffness – hydrogels with an increased ratio of 8-arm to 4-arm polymer were stiffer and exhibited decreased swelling (quantified by mass) and dissolution in phosphate buffer (pH 7.4) at 37 °C.

By encapsulating model proteins within DA hydrogels, Tan *et al.* successfully controlled drug or protein release by taking advantage of the protein charges.[169] Maleimide- and furan-functionalized HA were synthesized *via* oxidation by sodium periodate and EDC/NHS activation with furan–PEG–NH_2, respectively. Rheological characterization confirmed complete gelation in under an hour, and demonstrated the temperature- and time-dependencies of hydrogel mechanics and swelling behaviors. Negatively-charged insulin and positively-charged lysozyme were encapsulated to enable sustained release. Positively-charged lysozyme demonstrated a slower release profile, perhaps due to electrostatic interactions with negatively-charged HA, compared to the greater burst release profile shown with negatively-charged insulin. Similarly, Koehler *et al.* successfully applied DA chemistry to control the release of dexamethasone toward hMSC osteogenic differentiation.[174] After forming the initial network *via* Michael addition between thiol and maleimide groups, furan-modified dexamethasone was covalently tethered into the hydrogels. By exploiting the dynamic equilibrium between DA products and reactants, sustained release of the tethered dexamethasone was achieved in a precise manner. Robust hMSC osteogenic differentiation was observed over 14 days as shown *via* intense alkaline phosphatase staining and mineral deposition.

The reversible nature of DA reactions lends itself to applications requiring degradability, often a desirable feature in biomaterials. In particular, maleimide-based hydrogels fabricated using step-growth polymerization will readily degrade *via* retro-DA reactions near physiologic temperatures.[175] While gelation is favored at 37 °C, a small number of reactants are still likely present, which can react to form a DA pair or hydrolyze into maleamic derivatives that will not participate in DA reactions. Over time, this can shift the dynamic equilibrium until the DA reaction is reversed.[162,176] By varying the polymer molecular weight and branching factors, the degradation rate can be tuned for specific tissue engineering applications. This feature has been used to develop DA-based hydrogel carriers for temporal protein or drug release.[177–184] Several hydrogel systems have combined DA crosslinking with secondary (physical) interactions to create hydrogels with increased toughness, viscoelasticity, self-healing properties, and responsiveness to external stimulants.[160,185–190] Recent studies have also begun to explore other DA-amenable moieties such as furyl[15,162,171,191] and fulvene[159,192] groups as dienes as well as dichloromaleic[159] groups as dienophiles that exhibit decreased degradability. Additional details on Diels–Alder chemistry can be found in the following reviews.[148,193–195]

DA hydrogels for 2D and 3D cell cultures

Recently, the ability to control relevant features such as substrate stability, mechanics, and ligand presentation have enabled investigations of DA hydrogel properties on cell behavior. Shoichet and co-workers expanded upon initial reports developing DA-based polymers and introduced a host of furan–maleimide DA hydrogels for soft tissue engineering and regenerative medicine applications. A simple, one-step reaction using 4-(4,6-di-methyoxy-1,3,5-triazin-2-yl)-4-methylmorpholinium (DMTMM), an efficient activator of polysaccharide carboxyl groups in aqueous conditions,

Published on 19 July 2021. Downloaded by University of Virginia on 8/10/2021 5:09:05 PM.

allowed furfurylamine coupling to HA carboxylates at a higher yield compared to other methods such as carbodiimide chemistry.[18,196] The addition of bis-maleimide PEG crosslinker enabled DA hydrogel fabrication over a range of soft tissue mechanics (storage modulus, $G' \sim 100$–1000 Pa). Stiffness was manipulated by varying crosslinker concentration (*i.e.*, furan/maleimide ratio) and degradation was monitored with respect to crosslinker amount; it was noted that varying other properties such as macromer molecular weight could also be used to tune stiffness and degradation. Human epithelial cells seeded atop compliant HA hydrogels attached after 24 hours and spread throughout the two-week culture period.

Although hydrogels requiring a more acidic environment (pH 5.5) for gelation are suitable for 2D cell culture, encapsulation of cells within a 3D environment requires stable hydrogel formation under physiologic conditions. To utilize DA click chemistry for 3D cultures, reaction kinetics can be accelerated by modifying the electronic properties of reaction pair substituents. Smith *et al.* functionalized HA with methylfuran groups, resulting in more rapid gelation (average gelation of 12 min compared to 32 min with furan-functionalized HA) without affecting bulk mechanics.[176] The ability to rapidly form hydrogels at physiologically-relevant pH was next demonstrated with multiple cancer cell lines, which exhibited high cell viability over the 7 day culture period as well as characteristic spheroid morphology for the MCF7 breast cancer cell line. Another approach to improve gelation kinetics for cell encapsulation replaced the commonly used furan diene with a more electron-rich group, fulvene.[192] Furan-, methylfuran-, fulvene-, and maleimide-functionalized PEG were synthesized *via* standard amide coupling chemistries. Compared to furan and methylfuran, gelation kinetics for fulvene-maleimide 4-arm PEG hydrogels improved 10-fold (time to reach critical gelation point: 20 min for fulvene, 10 hours for furan, 7 hours for methylfuran) (Fig. 3A–C). By increasing polymer concentration and the number of reactive sites (using 8-arm instead of 4-arm PEG), fulvene-based hydrogels were able to cross the critical gelation point in under 30 seconds. The increased gelation kinetics prevented cell settling during encapsulation. Degradable ELPs containing RGD adhesive sequences were also functionalized with fulvene groups to enable incorporation into the hydrogels (Fig. 3D). Encapsulated hMSCs exhibited high viability and protrusions into the surrounding environment, indicative of cell-mediated remodeling (Fig. 3E–G).

DA click chemistry has also been utilized for co-culture systems. Silva *et al.* synthesized furan-modified gellan gum hydrogels using the DMTMM coupling method described previously.[18,166] Maleimide-RGD adhesive peptides were incorporated *via* the Diels–Alder reaction, and studies showed that neural stem/progenitor cells (NSPCs) migrated and spread with distinctive cytoplasmic extensions in both 2D and 3D cultures. However, without the presence of RGD, increased cell–cell interactions resulted in aggregates of neurospheres. Co-culture of NSPCs and olfactory ensheathing glia (OEG) promoted increased NSPC proliferation in direct and indirect co-culture, indicating that OEG secrete factors that do not require direct cell–cell contact to enhance proliferation.

Thermosensitive DA hydrogels

To address the slower gelation kinetics of the DA reaction that may be unfavorable for injection-based applications, DA hydrogels have been engineered incorporating thermosensitive moieties to enable dual crosslinking. Bi *et al.* explored the use of thermosensitive hydroxypropyl chitin (HPCH) as the backbone polymer for the development of a DA-based injectable hydrogel.[191] The inherent biocompatibility and thermosensitive properties of chitin coupled with furyl–maleimide DA reaction kinetics enabled a dually crosslinked system for both *in vitro* and *in vivo* studies. Even after HPCH modification with furyl moieties *via* etherification, the HPCH demonstrated retention of its ability to gel at physiologic conditions. Initial physical crosslinking of chitin at 37 °C enabled initial cell incorporation and support prior to the two-hour DA gelation between furyl-modified HPCH and bis-maleimide PEG crosslinker. Manipulation of hydrogel mechanical strength correlated with crosslink density, and encapsulated cancer cells displayed rounded morphologies and formed spheroids with increasing aggregate diameter over time. Abandansari *et al.* combined DA crosslinking between furan-functionalized gelatin and bis-maleimide–PEG crosslinker with thermoresponsive interactions *via* chitosan grafted with Pluronic F127 (CP), an FDA-approved thermosensitive copolymer, to create a dual crosslinked hydrogel with more robust mechanics and improved cell retention during injection.[197] Compared to the DA- and CP-only hydrogels ($G' \sim 0.1$–1 kPa and ~4–8 kPa, respectively), the dual crosslinked hydrogel exhibited higher stiffness at 37 °C ($G' > 10$ kPa) due to increased crosslinking as well as lower swelling and higher stability while still being injectable. The injected dual hydrogel led to higher hydrogel (70% on day 3) and cardiomyocyte retention (45% after 24 hours) compared to free cells (15% viable cells after 24 hours) or DA hydrogel (15% material retention on day 3 and 20% cells after 24 hours) groups. Additionally, the hybrid hydrogel induced *in vivo* tissue regeneration and preserved the phenotype of the encapsulated cardiac muscle cells.

DA hydrogels to model tumorigenesis

Efforts to create tumor mimetics have also been explored using DA-based hydrogels. Fisher *et al.* exploited the ability to independently tune multiple HA hydrogel properties, including mechanical (*e.g.*, stiffness, degradability) and chemical (*e.g.*, adhesion) cues (Fig. 3H and I).[14] Similar to previous studies, crosslink density and HA concentration were decoupled by varying the degree of furan modification on HA while maintaining the same crosslinker concentration for all formulations (Fig. 3J). Hydrogels with a lower crosslink density (Young's modulus, $E \sim 3.5$ kPa) resulted in greater

This journal is © The Royal Society of Chemistry and IChemE 2021

Published on 19 July 2021. Downloaded by University of Virginia on 8/10/2021 5:09:05 PM.

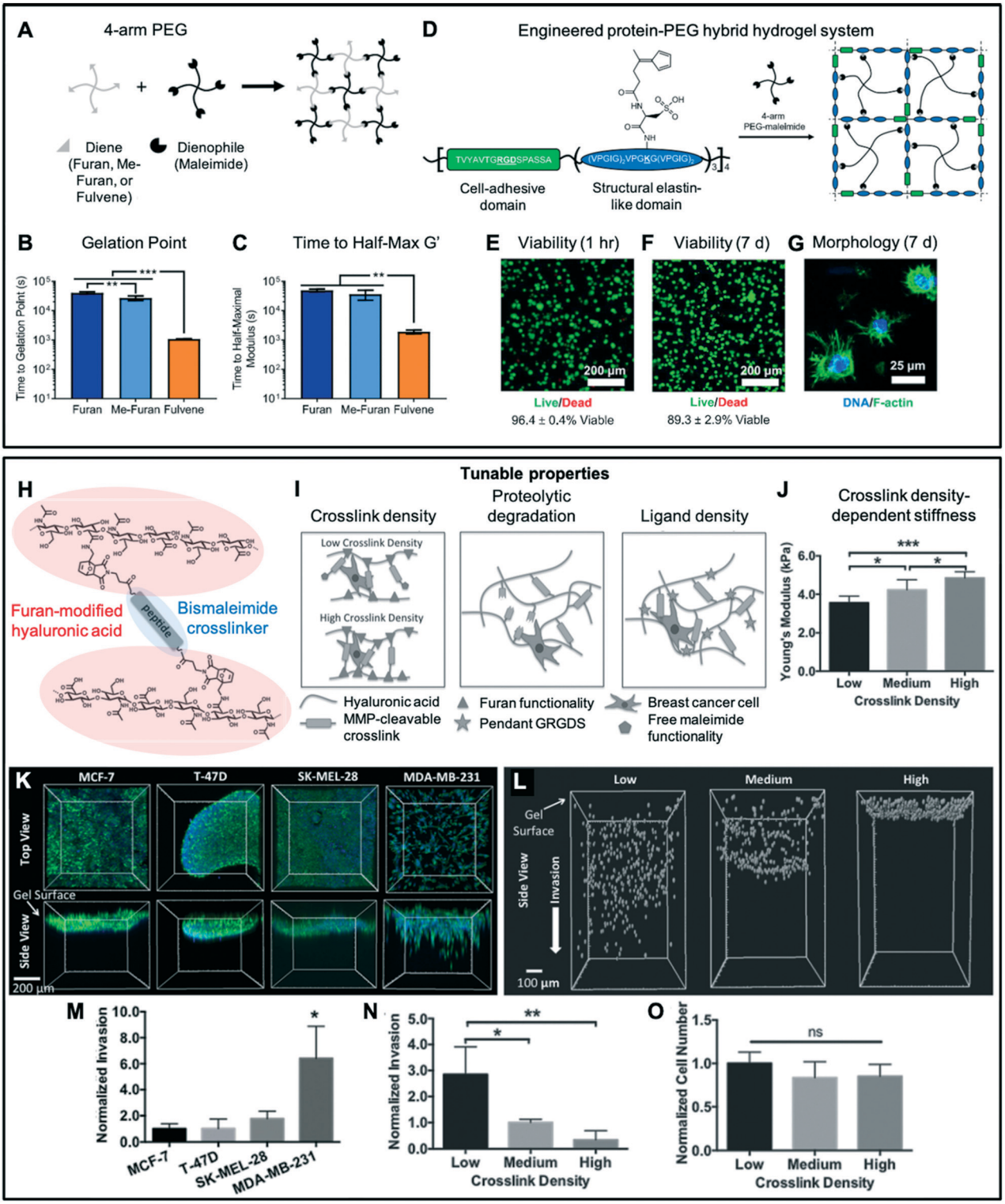

Fig. 3 Diels Alder (DA) hydrogel tunability can be used to explore the influence of matrix mechanics on cell behaviors. (A) DA hydrogels can be synthesized by mixing a diene (furan, methylfuran, or fulvene) with a dienophile (maleimide). (B and C) the point of gelation and the time it takes to reach half of the maximum storage modulus, *G'*, can be tuned by varying the diene group. Compared to furan and methylfuran, the more electron-rich fulvene demonstrated faster gelation times. (D) Engineered ELPs functionalized with fulvenes can be used to fabricate hydrogels with cell adhesive and structural domains. (E–G) Encapsulated hMSCs maintained high viability after 7 days and spread. (A–G) adapted with permission from ref. 192. Copyright 2019, American Chemical Society. (H) DA hydrogels can be fabricated using furan-modified HA and bismaleimide crosslinkers. (I) Several modifications can be made using DA chemistry to tune stiffness (crosslink density), degradation, and bioactive molecule presentation (ligand density). (J) Young's moduli of hydrogels increased as crosslink density increased. (K) Invasion of MCF-7, T-47D, SK-MEL-28, and MDA-MB-231 cancer cell lines in medium crosslinked hydrogels revealed different morphologies and infiltration mechanisms based on cell type. (L–O) MDA-MB-231 invasion was stifled as hydrogel stiffness increased. (H–O) Adapted with permission from ref. 14. Copyright 2015 WILEY-VCH.

Published on 19 July 2021. Downloaded by University of Virginia on 8/10/2021 5:09:05 PM.

MDA-MB-231 breast cancer cell invasion into the hydrogels compared with cells within stiffer hydrogels ($E \sim 5$ kPa) (Fig. 3K–O). Incorporation of MMP-degradable crosslinks also correlated with increased cell invasion independent of stiffness. Interestingly, increased adhesive ligand density led to greater cell proliferation but did not affect the degree of cellular invasion into the hydrogel.

This model was further exploited as a high-throughput metastatic cancer drug screening platform.[168] In addition to the DA chemistry, methylcellulose was covalently incorporated into the matrix to introduce hydrophobic interactions and consequently, tunable stress relaxation properties. The platform was then used to independently assess cell viability and invasion over a range of pharmacological treatments and hydrogel compositions in a lung cancer model, lymphangioleiomyomaosis (LAM). Compared to elastic hydrogel controls, LAM smooth muscle cells displayed increased invasion in 3D viscoelastic substrates due to stress relaxation properties. Drug screening was then tested within a 384-well format to enable higher-throughput analysis, and candidates that showed a decrease in both cell viability and invasion included those that impacted cell cycle (*e.g.*, cyclin-dependent kinase inhibitors) and autophagy (*e.g.*, IRE1 inhibitors). Overall, the hydrogel platform allowed for several physicochemical properties to be varied (*e.g.*, stiffness, viscoelasticity, biochemical composition) with increased throughput to study cell responses to treatments.

In summary, DA chemistry is a highly selective cycloaddition involving facile synthesis, no side reactions or byproducts, and accelerated reaction kinetics in water. While many DA reactions demonstrate slower gelation kinetics compared to other click reactions, this can be overcome by substituting more hydrolytically stable diene–dienophile pairs.[164,198] The slower DA reaction has also been used in conjunction with secondary assembly mechanisms such as fast-gelling thermosensitive polymers. The DA reaction is also thermosensitive, with higher temperatures resulting in faster gelation times. Under certain conditions such as increased temperature or choice of diene–dienophile pair, the reaction is also reversible, enabling controlled degradation. In the context of mechanobiology, DA chemistry is particularly useful for allowing tailored ligand presentation (*e.g.*, adhesive peptides), mechanics (*e.g.*, stiffness, degradation), and DA-mediated biomolecule release within hydrogel systems for studying cell–matrix interactions.

5. Inverse electron demand Diels–Alder (IEDDA)

Inverse electron demand Diels–Alder (IEDDA) reactions are fast, chemoselective, and readily proceed at mild conditions without requiring additives such as initiators or catalysts.[199,200] Compared to the normal Diels–Alder (DA) cycloaddition, where an electron-rich diene reacts with an electron-poor dienophile, the IEDDA reaction mechanism involves an electron-poor diene and an electron-rich dienophile (Scheme 4A). These reactions demonstrate irreversible kinetics on experimental timescales, producing only nitrogen during product formation.[201,202] IEDDA reactions were first discovered through the use of 1,2,4,5-tetrazine, a nitrogen-containing electron-poor diene with electron withdrawing groups (EWG), and demonstrated quicker reaction rates influenced by changes in electronic properties.[203] While other cyclic azines such as pyridazine and triazine have shown suitability as diene candidates, the majority of IEDDA reactions utilize tetrazine for its increased reactivity and orthogonality with respect to other click chemistries such as CuAAC and thiol-Michael addition, which is particularly valuable within the biomaterials community.[10,118,204–209] However, studies have shown a trade-off between fast reactivity and stability; compared to tetrazines, some less reactive dienes such as 1,2,4-triazines exhibit higher stability under physiologic conditions.[118,199,210,211] Despite this limitation, tetrazine-based reactions have proven stable within characteristic cellular timescales and are a popular route for tissue engineering and hydrogel systems (Scheme 4B and C).[211–219]

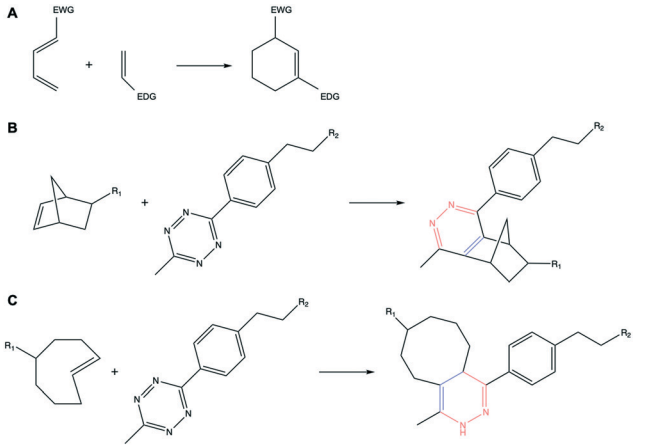

Scheme 4 (A) Inverse electron demand Diels–Alder (IEDDA) cycloaddition between an electron-poor diene and an electron-rich dienophile. (B) IEDDA reaction between a norbornene and tetrazine group. (C) IEDDA reaction between a *trans*-cyclooctene (TCO) and tetrazine.

Compared to other common click-based cycloadditions such as CuAAC and SPAAC, IEDDA has a significantly faster reaction rate (IEDDA[83,220,221] second-order rate constant $k \sim 1–10^6$ M^{-1} s^{-1} *versus* $k \sim 10–100$ M^{-1} s^{-1} and $k \sim 10^{-2}–1$ M^{-1} s^{-1} for CuAAC[79] and SPAAC,[80] respectively). Adding electron-withdrawing (*i.e.*, electron-poor) groups such as carboxylates to dienes increases overall reactivity by lowering the energy of the lowest unoccupied molecular orbital (LUMO).[195,222] Likewise, adding electron-donating (*i.e.*, electron-rich) groups such as olefins and enamines to dienophiles raises the dienophile's highest occupied molecular orbital (HOMO), which greatly impacts kinetic behavior.

IEDDA reaction kinetics can also be controlled by varying substituent features such as dienophile ring strain and solvent type. Decreasing the internal angle of cyclic dienophiles increases ring strain and results in lower

This journal is © The Royal Society of Chemistry and IChemE 2021

Published on 19 July 2021. Downloaded by University of Virginia on 8/10/2021 5:09:05 PM.

distortion energy to reach the transition-state geometry, which correlates with increased reactivity.[211,223] Norbornene groups have become a common dienophile for their low cost and cell encapsulation-friendly gelation kinetics.[212,224] Similarly, the *trans* configuration encourages increased ring strain compared to the *cis* configuration – computational analysis revealed that the 'crown' conformation of *trans*-cyclooctene (TCO) was seven orders of magnitude more reactive toward tetrazines than *cis*-cyclooctene due to a lower activation energy.[222,223] Furthermore, TCO has demonstrated faster reaction rates compared to norbornenes ($k \sim 10^3$–10^6 M^{-1} s^{-1} for TCO *versus* $k \sim 2$ M^{-1} s^{-1} for norbornenes in aqueous solution at room temperature).[83,224,225] The influence of dienophile stereochemistry on reaction rates is similar to that of the normal DA reaction; *endo*-isomers are typically more thermodynamically favorable and exhibit faster kinetics than *exo*-positioned groups.[199,226–228] However, in some cases, this selectivity can be reversed due to differences in functional group distortions (*e.g.*, norbornenes[224,229]) and electrostatic repulsions (*e.g.*, cyclopentadiene[230]). Accelerated reaction rates in water have also been observed due to increased hydrophobic interactions and stabilization of the activated complex *via* hydrogen bonding, which becomes advantageous for cell culture systems.[81,211,231,232] In particular, the influence of protic solvents on reaction rate has mainly centered around the use of tetrazines.[201]

In an effort to increase tetrazine stability, Shoichet and co-workers designed an IEDDA-based hydrogel system involving norbornene and methylphenyltetrazine (mpT), where the inclusion of electron-donating groups increased hydrolytic stability while compromising high reactivity.[214,215] Using HA as the polymer backbone, Delplace *et al.* confirmed that gelation time was not significantly affected; depending on polymer and crosslinker concentrations, hydrogel gelation occurred within one hour and could be formed in as little as 5 minutes at high polymer concentrations.[214] Interestingly, at a constant mpT : norbornene ratio, hydrogel swelling was independent of HA–mpT molar mass as well as HA–norbornene concentration. Encapsulated cells maintained high viability over several days, particularly in hydrogels with lower polymer concentrations, and also confirmed the correlation between gelation time and cell sedimentation. Using the same IEDDA click chemistry, Delplace *et al.* also developed a methylcellulose-based hydrogel system for the co-delivery of neural stem cells and chondroitinase ABC (ChABC) enzyme for glial scar degradation.[215] Gelation occurred within 15 minutes with Young's moduli ranging between 0.5–1.5 kPa, similar to brain tissue. Using affinity-controlled release, controlled release of ChABC could be extended to 4 days. Interestingly, neurospheres containing neural progenitor cells within degradable IEDDA hydrogels appeared to maintain viability and resulted in increased neurosphere size with the formation of new, smaller neurospheres. Dual-crosslinked systems have also been used to form robust hydrogels. For example, Truong *et al.* created cytocompatible, tough PEG-based IPNs with compressive stresses of ~15 MPa through a one-step fabrication involving IEDDA between tetrazine and norbornene groups and a nucleophilic thiol–yne click reaction.[209] This system provides a structurally supportive hydrogel network with robust mechanical strength that can maintain high cell viability and accommodate ligand functionalization.

Tetrazine–norbornene hydrogels

Many IEDDA hydrogel systems have utilized the high reactivity and bioorthogonality of tetrazine–norbornene interactions. Lueckgen *et al.* fabricated alginate hydrogels using carbodiimide chemistry to modify alginate with norbornene and tetrazine groups.[233] Similar to a previous system developed by Mooney, Joshi, and co-workers, alginate was chosen as the backbone polymer for its degradability *via* controlled oxidation using sodium periodate.[234] Gelation kinetics and stiffness were tuned by altering the oxidation state of alginate, degree of norbornene modification, and the ratio of norbornene to tetrazine. Hydrogel mechanics were varied from 2–20 kPa, with lower degrees of alginate substitution and oxidation resulting in more compliant hydrogels with slower gelation kinetics. Regulating these parameters enabled control over degradation – increased crosslinking density *via* backbone modification and norbornene : tetrazine ratio slowed degradation. Compared to degradable substrates, mouse pre-osteoblasts seeded atop hydrogels proliferated more on non-degradable hydrogels. The stability of IEDDA reactions at physiologic conditions lends favorably to 3D culture applications as well. Lueckgen *et al.* expanded their previous alginate 2D cell culture model into a 3D system, and encapsulated mouse pre-osteoblasts retained a more rounded morphology over all hydrogel groups without significant proliferation.[233] Finally, *in vivo* hydrogel implantation revealed that the degradable, oxidized substrates promoted cell infiltration after 8 weeks compared to non-degradable controls.

Alge *et al.* successfully fabricated tunable 3D PEG hydrogels for cell encapsulation and protein patterning using tetrazine–norbornene chemistry.[212] 4-arm PEG was functionalized with tetrazine groups *via* acid amine conjugation between PEG-amines and carboxylic acid-bearing tetrazines. Di-norbornene MMP-degradable crosslinker and mono-norbornene adhesion peptides were incorporated for hydrogel fabrication and introduction of adhesive sites, respectively. Varying polymer concentration and norbornene-functionalized pendant peptides enabled control of parameters such as stiffness and adhesive ligand density. Under physiologic conditions initial gelation occurred in a few minutes and plateaued within 15 minutes. Encapsulated hMSCs showed high viability but a low degree of spreading, suggesting the need for optimizing hydrogel parameters (*e.g.*, stiffness, degradability, adhesion presentation). Koshy *et al.* used the natural adhesivity and degradability of gelatin to fabricate "click gelatin hydrogels" (ClickGel) to support increased cell spreading.[216] The addition of norbornene and

Published on 19 July 2021. Downloaded by University of Virginia on 8/10/2021 5:09:05 PM.

tetrazine functional groups resulted in decreased gelation temperature and viscosity, making the hydrogel precursors easier to pipet and mix at room temperature. Similar to previous studies, gelation occurred spontaneously and rapidly within minutes, and gelation rate correlated with increased polymer concentration. Encapsulation of enhanced green fluorescent protein (EGFP)-expressing NIH3T3 fibroblasts in 5 and 10 wt% hydrogels revealed the influence of polymer concentration on cell behavior. Cells within the softer 5% ClickGel groups displayed elongated morphologies after a 3 day culture period and remained spherical after treatment with MMP-inhibitor Marimastat, suggesting that cell spreading was largely mediated by enzymatic degradation. Similarly, encapsulated hMSCs within the 5% ClickGels elongated extensively and displayed organized actin stress fibers due to matrix remodeling, and *in vivo* injection of the hydrogel led to almost complete degradation over 120 days.

Dual-crosslinked hydrogels

Similar to DA-based reactions, several groups have exploited the orthogonal nature of IEDDA chemistry toward the rational design of dual-crosslinked systems. By combining IEDDA chemistry with photoinduced thiol–ene addition, Lueckgen *et al.* demonstrated spatial control over hydrogel biophysical and biochemical properties to study and guide wound healing responses.[235] The IEDDA crosslinks enabled compliant hydrogel formation prior to thiol–ene patterning regions of higher stiffness *via* non-degradable crosslinkers (Fig. 4A and B), degradation *via* incorporation of degradable crosslinkers, or biomolecules through immobilization of cell adhesive peptides. Interestingly, for initially IEDDA-crosslinked hydrogels, later UV exposure resulted in stiffer patterned regions by almost an order of magnitude ($E \sim 1$–2 kPa with early secondary crosslinking *vs.* 9–10 kPa for later crosslinking), enabling spatiotemporal control over stiffness. On regions of patterned stiffness (9–10 kPa), fibroblasts aligned in the direction of the striped pattern, covered more surface area, and displayed both increased cell area and significantly decreased circularity (Fig. 4C). Similarly, patterned regions of cell adhesive RGD and degradable crosslinker led to preferential attachment and lower stiffness respectively compared to non-patterned control regions. As expected, on stiffness-patterned substrates, adipogenic and osteogenic differentiation increased on soft and stiff regions, respectively (Fig. 4D). These trends were quantified by cell attachment as well as oil droplet area (adipogenic) and mineralized area (osteogenic).

In addition to varying stiffness, Vining *et al.* varied ionic (between alginate and calcium) and covalent (between norbornene and tetrazine) crosslinking ratios to tune hydrogel viscoelasticity.[237] The viscoelastic properties of the hydrogels, measured by loss angle, were achieved without altering the microscale architecture of the hydrogel network by maintaining constant alginate concentration. To study the impact of physical properties on cell function, MSCs were encapsulated within hydrogels of varying stiffness (storage moduli, $G' \sim 0.5$ kPa and 2.5 kPa) and viscoelasticity (loss moduli, $G'' \sim 50$ Pa and 250 Pa, respectively). Interestingly, after 72 hours, MSCs exhibited increased cell cross-sectional area in the stiffer more elastic hydrogels containing the covalent IEDDA network. Immunomodulatory markers such as cyclooxygenase-2 and TNFα-stimulated gene-6 were upregulated to varying degrees based on hydrogel stiffness and viscoelasticity, with gene expression increasing as both stiffness and viscoelasticity increased.

While IEDDA reactions can occur spontaneously in aqueous conditions without an initiator or catalyst, the addition of a catalyst can both increase stability and trigger gelation. Carthew *et al.* demonstrated the use of horseradish peroxidase (HRP) to increase material stability *via* oxidation and activate faster crosslinking.[238] To bypass the limitation of tetrazine oxidation over time, synthesis of dihydrogen tetrazine-functionalized PEG (dHTz-PEG) *via* carbodiimide coupling provided precursor stability, where mild oxidation to tetrazine could easily occur using a low concentration of HRP. Mixing norbornene-functionalized gelatin, which was synthesized through the same coupling method, dHTz-PEG, and HRP quickly formed a hydrogel within 5 minutes. Encapsulated hMSCs over a 32 day culture period displayed extended filopodia, particularly in the more compliant hydrogel group ($G' \sim 1.2$ kPa) where star-shaped cellular morphologies were seen. As hydrogel stiffness increased ($G' \sim 3.8$ kPa), cells remained more rounded with decreased spreading. Overall, the facile synthesis method and ability for the hydrogels to remain stable over a month-long culture are highly attractive for long-term mechanobiology studies.

TCO–tetrazine hydrogels

While norbornenes offer greater stability, TCO–tetrazine reactions demonstrate faster reaction rates, providing an alternative dienophile for rapid hydrogel fabrication. Strategies involving TCO have taken advantage of the increased reactivity to uniquely study cell–matrix interactions in 3D hydrogels. Zhang *et al.* synthesized liquid microspheres composed of an outer HA shell fabricated *via* IEDDA click chemistry capable of 3D biomolecule patterning and cell culture.[239] Microspheres were created by adding HA–tetrazine droplets to a solution of bis-TCO, triggering nearly instant TCO–tetrazine crosslinking at the droplet surface, where subsequent crosslinking occurred through bis-TCO crosslinker diffusion into the hydrogel. The diffusion-driven crosslinking mechanism enabled biomolecule patterning by switching the solution to generate multilayer structures within the microsphere without an initiator or catalyst. Applying the hydrogel system to mimic an *in vitro* tumor microenvironment, homogeneously encapsulated prostate cancer cells continuously proliferated within the compliant microspheres ($G' \sim 135$ Pa) and formed rounded cell clusters with cells displaying cortical actin filaments.

This journal is © The Royal Society of Chemistry and IChemE 2021

Published on 19 July 2021. Downloaded by University of Virginia on 8/10/2021 5:09:05 PM.

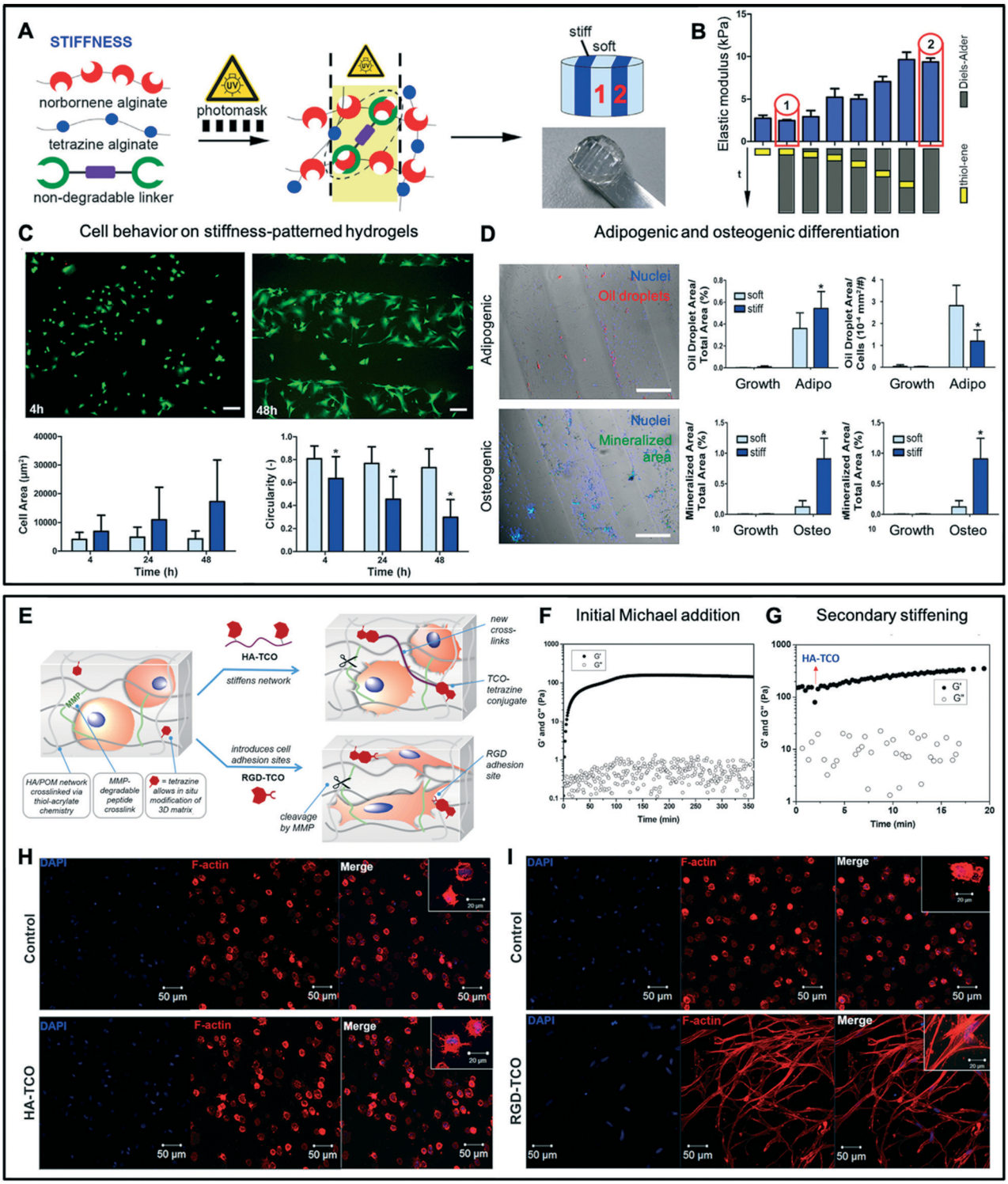

Fig. 4 Inverse electron demand Diels–Alder (IEDDA) can be used on its own or with secondary crosslinking mechanisms to rapidly and precisely control hydrogel mechanical properties for studying cell mechanobiology. (A) Additional modifications, such as stiffness (shown), biomolecule presentation, and degradation sites, can be photopatterned within IEDDA-based alginate hydrogels. (B) Elastic moduli of dual-crosslinked hydrogels were measured by compression testing, showing increased stiffness in regions exposed to UV-mediated thiol–ene addition. (C) Fibroblast attachment, spread area, and circularity on stiffness-patterned 2D cultures show distinct behaviors based on mechanics. Scale bar = 200 μm. (D) Adipogenic and osteogenic differentiation increased on unpatterned (compliant) and patterned (stiff) regions, respectively. Lineage specification was measured by oil droplet and mineralized area. Scale bar = 500 μm. (A–D) adapted with permission from ref. 235. Copyright 2020 Elsevier Ltd. (E) IEDDA can facilitate *in situ* stiffening and adhesive ligand presentation without external triggers. (F and G) After initial hydrogel formation, diffusion-controlled secondary crosslinking results in IEDDA-mediated stiffening. (H) Matrix stiffening (bottom) led to rounded hMSCs with distinct cortical actin. Scale bars = 50 μm. (I) The addition of RGD–TCO adhesive cues resulted in hMSC elongation with F-actin (red) stress fiber bundles. Scale bars = 50 μm. (E–I) adapted with permission from ref. 236. Copyright 2018, American Chemical Society.

Published on 19 July 2021. Downloaded by University of Virginia on 8/10/2021 5:09:05 PM.

TCO–tetrazine interactions also enable temporal hydrogel stiffening and introduction of tethered biomolecules.[236] Following initial Michael-type addition between thiolated HA, a hydrophilic co-polymer with acrylate and methyltetrazine groups at mildly basic conditions, and MMP-degradable crosslinker, secondary stiffening of the primary network was achieved *via* incorporation of HA–TCO (through solution diffusion into the hydrogel) to introduce TCO–tetrazine interactions (Fig. 4E–G). Incorporation of cell adhesive sites through the addition of pendant RGD–TCO groups was achieved in a similar manner. The 9 day cell culture revealed the influence of secondary stiffening, where hMSCs displayed more pronounced actin-rich processes from the generally rounded encapsulated cells (Fig. 4H). However, introduction of cell adhesive sites resulted in significant hMSC spreading and elongation, creating a mesh-like cellular network with distinct stress fiber bundles (Fig. 4I). In the absence of degradable crosslinkers, spreading was inhibited even with the addition of RGD sequences, again highlighting the importance of degradation in supporting 3D cell spreading.

In summary, the IEDDA click reaction has been gaining recognition as a bioorthogonal crosslinking mechanism that exhibits rapid gelation at physiologic conditions. Similar to Diels–Alder, varying the diene and dienophile pairs can influence gelation rate. For example, the use of dienophiles with greater strain (*e.g.*, TCO) increases reaction rates by several orders of magnitude compared to their *cis*-counterparts. For this reason, IEDDA reactions are highly advantageous for cell encapsulation studies. Hydrogel properties, including stiffness, viscoelasticity, and biomolecule presentation, can be efficiently tuned with precise control. More recently, the fast encapsulation properties of IEDDA reactions have been used in hydrogels containing dual crosslinking modes to engineer complex mechanics for studying cellular responses while maintaining a high level of user control. One limitation with IEDDA chemistry is the trade-off between reactivity and stability, with less reactive dienophiles demonstrating higher stability in aqueous conditions. However, the majority of reactions involving tetrazine, a highly reactive but slightly less stable diene, maintain stability within relevant cellular timescales. Continued optimization of reaction pairs to increase stability for longer cell culture studies will only add to the beneficial properties of IEDDA hydrogels to study mechanobiology.

6. Imine-derivatives (oximes and hydrazones)

Imines are formed through the dehydration reaction of a primary amine with an aldehyde or ketone. In general, the mechanism involves a proton-catalyzed attack of the α-nucleophile on the carbonyl carbon atom, followed by proton transfer and dehydration of the hydroxyl group to yield an imine or imine-derivative (*e.g.*, oxime, hydrazone).[240–242] Imines are considered covalent bonds that are reversible within experimental timescales, termed dynamic covalent chemistry

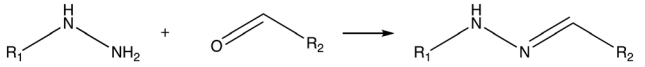

Scheme 5 Oxime bond formation between an aminooxy and an aldehyde.

(DCC).[242] In general, the carbonyl reaction can be accelerated under acidic conditions (especially between pH values of 3–7), enabling control over gelation time and mechanical properties *via* pH.

Hydrazones and oximes share structural similarities with imines with nitrogen and oxygen neighboring the carbon–nitrogen double bond, respectively. Under aqueous conditions, more electronegative heteroatoms (O, oxime > NH, hydrazone > CH_2, imine) create a negative inductive effect and provide addition stability at physiologic pH to oximes and hydrazones compared to imines.[243] As a result, hydrazone and oxime bonds have become particularly appealing bioorthogonal approaches for tunable biomaterial synthesis and cell behavior studies.[244–249]

Oxime bond formation (Scheme 5) is a highly efficient and chemoselective reaction that occurs between either an aldehyde or ketone and an alkoxyamine (typically a hydroxylamine).[250] Compared to hydrazones, oximes have a higher stability owing to steric and electronic differences. While oxime bioconjugation reactions were studied as early as 1882, previously complex hydroxylamine synthesis techniques limited its utility.[250,251] The development of more facile hydroxylamine syntheses such as the Mitsunobu reaction and BOC deprotection coupled with the increased stability and stimulus-responsiveness of oximes has allowed researchers to exploit the dynamic covalent reaction for both minimally invasive *in vivo* experiments and longer-term cell culture studies.[249,250] In particular, pH has been widely used as a method to alter bond reversibility while maintaining tissue-relevant stiffnesses.[252–257]

Similar to oximes, hydrazones are dynamic covalent bonds that form between a hydrazine and a carbonyl, usually an aldehyde or ketone (Scheme 6). While they are more stable than imines, they are more likely to undergo hydrolysis compared to oximes; the rate constant for oxime hydrolysis is nearly 1000-fold lower than for hydrazones.[242,243,258,259] The degree of acid lability is dependent on the carbonyl group selected; hydrazone bonds formed with ketones exhibit slower reaction rates and are less labile compared to aldehydes. However, aromatic aldehydes have shown more stability than aliphatic aldehydes.[245,259–261] These subtle differences in chemistry have been shown to greatly impact stress relaxation timescales for hydrogel systems.[61,262,263] Notably, many systems have taken advantage of hydrazone

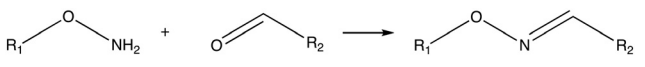

Scheme 6 Hydrazone bond formation between a hydrazine and an aldehyde.

This journal is © The Royal Society of Chemistry and IChemE 2021

Published on 19 July 2021. Downloaded by University of Virginia on 8/10/2021 5:09:05 PM.

tunability and reversibility *via* alterations in pH, temperature, and/or polymer groups to develop hydrogels with dynamic covalent properties and/or shear-thinning and self-healing capabilities.[264–279] Recent approaches utilizing bioorthogonal mechanisms, such as secondary photocrosslinking or photocleavage, have also enabled the design of systems with spatiotemporal control over mechanical and biochemical cues.[280,281] For more in-depth discussion of oxime and hydrazone bioconjugation techniques, readers are referred to the following reviews.[86,245,250,257]

Viscoelastic oxime hydrogels

Maynard and co-workers first reported the use of oxime click chemistry as a method of hydrogel fabrication.[256] Eight-armed aminooxy PEG (AO-PEG) was crosslinked with glutaraldehyde and functionalized with a ketone-modified RGD adhesive peptide to support cell culture. By varying AO-PEG concentration or crosslinker density, hydrogel stiffness could be tuned from storage moduli G' of about 250 Pa to over 4 kPa. Subsequently, viscoelastic properties were also altered by increasing stiffness (loss modulus, $G'' \sim 10$ Pa to around 50 Pa, respectively). Hydrogel gelation was also pH-dependent, with more acidic solutions resulting in quicker gelation. At a more physiologic pH of 7.2, oxime formation occurred in 30 minutes (compared to 5 minutes at a pH of 6) without compromising stiffness to allow 3D encapsulation of MSCs. MSCs were metabolically active and proliferated over the 7 day culture period, demonstrating material cytocompatibility. In the absence of any enzymatically-degradable crosslinkers, encapsulated cells remained rounded during the 7 day culture, indicative of oxime bond stability and non-degradability. Grover *et al.* also demonstrated the ability to tune gelation and stiffness using oxime conjugation. By altering either the concentration of AO-PEG and aldehyde-PEG (ald-PEG) or ald/AO ratios, gelation rate (2–400 seconds) or hydrogel stiffness ($G' \sim 450$ Pa to 1.4 kPa) could be manipulated, respectively.[282] Interestingly, while the PEG-functionalized hydrogel inhibited 3T3 fibroblast adhesion regardless of the degree of polymer modification, verified by rounded cell morphologies in 2D cultures, functionalization enabled hydrogel adherence to *ex vivo* cardiac tissues to improve material retention for future *in vivo* studies.

The pH-responsive nature of oxime bonds has also been used to incorporate time-dependent properties into hydrogels. Toward this approach, Sánchez-Morán *et al.* synthesized aldehyde-containing oxidized alginate (NaAlg-Ald) by oxidizing alginate diols using sodium metaperiodate ($NaIO_4$), where the diol/$NaIO_4$ ratio could be tuned to control oxidation and subsequently, degree of modification.[283] Alkoxyamine alginate (NaAlg-AA) was synthesized *via* a Mitsunobu reaction followed by a hydrazinolysis to yield an alkoxyamine group. Stiffness and viscoelasticity were controlled by varying polymer concentrations, Ald/AA ratio, and the degree of NaAld-Ald oxidation – as Ald/AA decreased, both storage and loss moduli increased ($G' \sim 0.1$–12 kPa and $G'' \sim 1$–30 Pa). Gelation studies demonstrated the dependence of oxime bond formation on pH and temperature; more rapid gelation occurred in mildly acidic conditions (pH 4–6) and at higher temperatures. However, the addition of a nucleophilic aniline catalyst, which has been previously shown to improve gelation kinetics and mechanical properties, enabled gelation across the entire spectrum.[283–285] Mean relaxation times, $\langle\tau\rangle$, were fitted to experimental stress relaxation profiles. As the Ald/AA ratio increased, faster stress relaxation occurred – for a hydrogel with an Ald/AA ratio of 9, $\langle\tau\rangle \sim 4$ h compared to ~27 h for a hydrogel with an Ald/AA ratio of 0.3. Increasing oxidation levels also led to faster stress relaxation ($\langle\tau\rangle \sim 13$ h *versus* ~56 h for 100% and 25% oxidation, respectively). Encapsulation of murine B lymphoma cell line 2PK-3 in oxime hydrogels with faster stress relaxation resulted in increased cell size, proliferation, and migration.

Oximes can also be used to trigger cell adhesion and influence cell mechanobiology. Criado-Gonzalez *et al.* explored this approach by combining stable oxime-based PEG networks with enzyme-assisted peptide self-assemblies.[286] Poly(dimethylacrylamide-*co*-diacetoneacrylamide) (poly(DMA-*co*-DAAM), PDD) was synthesized *via* reversible addition-fragmentation chain-transfer (RAFT) polymerization and varying polymer concentrations were crosslinked with bis-aminooxy PEG (AOP) at a pH of 7.4 to create hydrogel networks with mechanics ranging from $G' \sim 0.3$ kPa ($G'' \sim 4$ Pa) to $G' \sim 1.8$ kPa ($G'' \sim 8$ Pa) (Fig. 5A–C). Embedding alkaline phosphatase within the bulk PDD–AOP hydrogel prior to diffusion of Fmoc-FFpY peptides led to enzyme-assisted peptide dephosphorylation and intercalated Fmoc-FFY self-assemblies without affecting hydrogel stiffness. The presence of self-assembled Fmoc-FFY also allowed incorporation of Fmoc-F-RGD to provide additional adhesion sites. After confirmation of peptide supramolecular self-assembly *via* circular dichroism spectroscopy, the influence of self-assembled peptides on cell adhesion was studied using NIH3T3 fibroblasts. A combinatorial study demonstrated that fibroblast area, spreading, and formation of vinculin spots at the tips of actin microfilaments only occurred in the presence of the self-assembled Fmoc-FFY, and these cell metrics were enhanced with the addition of RGD (Fig. 5D–F). Thus, this hydrogel platform allowed decoupled investigation of the influence of mechanical and adhesive cues on fibroblast behavior.

Oxime hydrogels to mimic the tumor microenvironment

Oxime chemistry can be combinatorially leveraged with secondary crosslinking methods to enable independent control of mechanical and biochemical properties. By modifying HA with aldehyde and methyl furan groups, Baker and co-workers designed a system allowing initial oxime ligation between HA–aldehyde and bis(oxyamine)-PEG, followed by Diels–Alder click chemistry to facilitate presentation of biochemical cues.[287] Through rational design

Published on 19 July 2021. Downloaded by University of Virginia on 8/10/2021 5:09:05 PM.

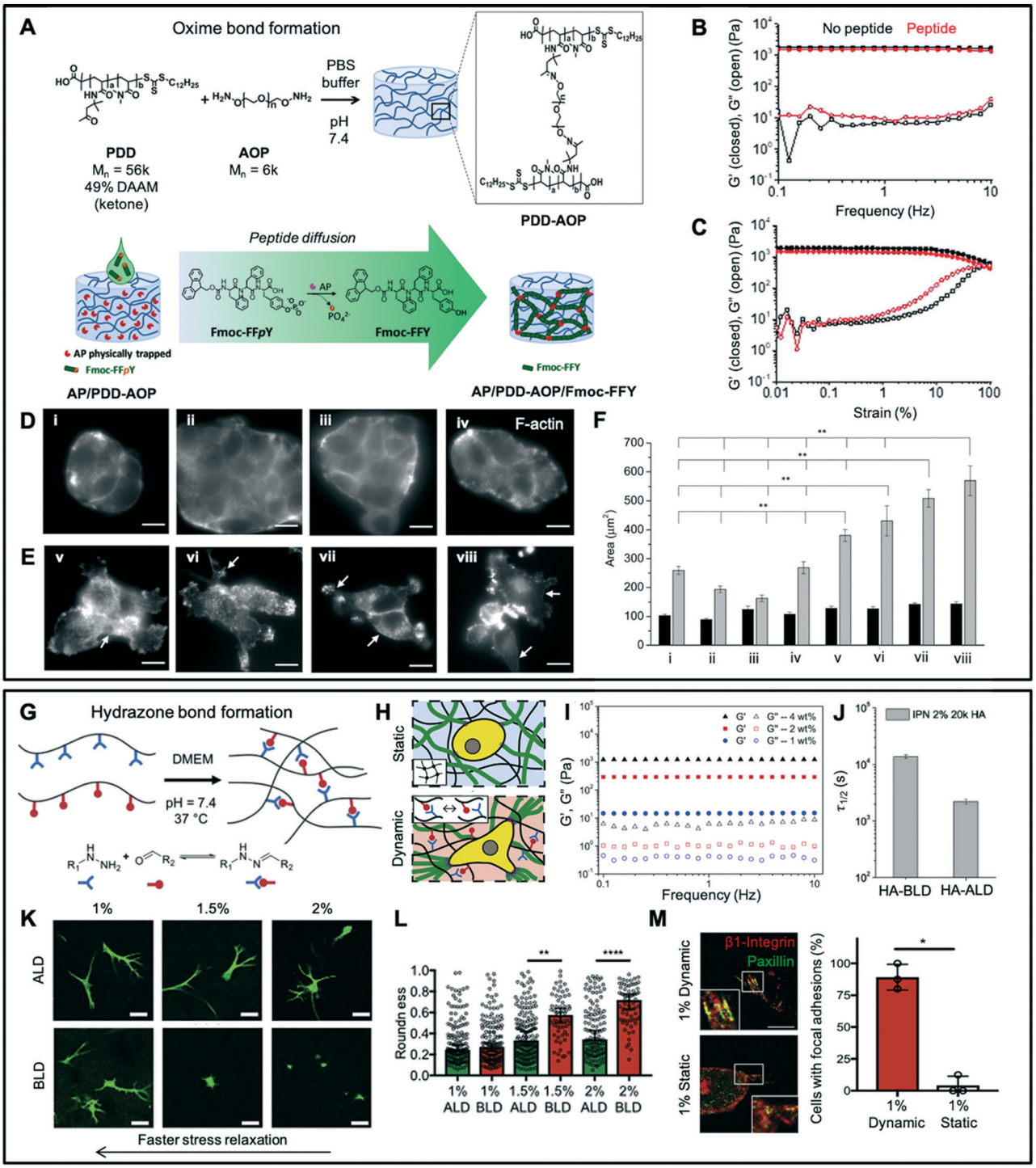

Fig. 5 Viscoelastic oxime and hydrazone hydrogels can be employed to study the influence of dynamic mechanics on cell behaviors. (A) An oxime-based PEG network containing embedded enzyme alkaline phosphatase enables peptide supramolecular self-assemblies when infused with a peptide solution. (B and C) Storage (G') and loss (G'') moduli showing negligible differences in stiffness before and after peptide incorporation. (D–F) F-Actin staining revealed distinct increases in cell protrusions and spreading on hydrogels with peptide self-assemblies (v–viii), compared to more rounded morphologies without distinct F-actin fibers when peptide self-assembly was absent (i–iv). Scale bars = 10 μm. (A–F) Adapted from ref. 286 with permission from The Royal Society of Chemistry 2020. (G) Hydrazone interactions occur at physiologically-relevant conditions and are reversible. (H) Dynamic hydrazone bonds introduce stress relaxation behaviors that are commonly displayed in natural tissues. (I) Frequency sweep of hydrogels with varying polymer concentrations demonstrates ability to modulate stiffness and viscoelasticity. (J) HA hydrogels modified with either aliphatic aldehydes (HA–ALD) or benzyl aldehydes (HA–BLD) were formed to tune stress relaxation profiles with HA–ALD hydrogels displaying faster relaxation. (K and L) Cell spreading is influenced by stress relaxation timescale, with increasing MSC spreading in fast relaxing HA–ALD compared to slower relaxing HA–BLD hydrogels. Increasing HA concentration also resulted in decreased cell spreading. Scale bars = 50 μm. (M) Focal adhesion formation increased significantly in viscoelastic substrates capable of stress relaxing. Scale bar = 10 μm. (G–M) Adapted with permission from ref. 61. Copyright 2017 Elsevier Ltd.

This journal is © The Royal Society of Chemistry and IChemE 2021

Published on 19 July 2021. Downloaded by University of Virginia on 8/10/2021 5:09:05 PM.

of hydrogel parameters, they were able to optimize long-term breast cancer epithelial cell growth in spheroids. Cells cultured on optimally compliant matrices ($E \sim 0.6$ kPa) formed acinar-like spheroids compared to a flattened morphology on tissue culture polystyrene. Similarly, breast cancer cells on stiffer hydrogels ($E \sim 2.3$ kPa) also deviated from the optimal spheroid morphology in favor of flat monolayers. Increasing concentrations of the laminin-derived IKVAV peptide on the 0.6 kPa substrates also led to cell flattening, highlighting the combined effects of mechanical and adhesive cues in regulating disease-relevant cell behaviors.

Oxime and hydrazone hydrogels for *in vivo* applications

The dynamic covalent interactions of oxime bonds can also be manipulated for *in vivo* studies that favor minimally invasive approaches. Hardy *et al.* demonstrated the clinical relevance of a hydrogel composed of oxime-crosslinked HA, PEG, and collagen for central or peripheral nervous system applications.[288] Aldehyde-functionalized HA (HA–ALD) was crosslinked with linear aminooxy-terminated PEG to rapidly form oximes at a pH of 7.4, and mechanical properties such as stiffness and degradability were adjusted by tuning the ratios of PEG and HA derivatives. Cell adhesion was mediated by incorporating various amounts of α-1-type collagen. hMSCs seeded atop hydrogels displayed spread morphologies, with increased viability on stiffer substrates.

Within the regenerative medicine field, *in situ* formation and sutureless implantation are ideal characteristics for drug and cell delivery. The Skottman group developed an implantable tissue adhesive hydrogel for corneal regeneration based on a HA hydrogel system enabling corneal cell attachment and high viability of encapsulated human adipose stem cells (hASCs).[289,290] Koivusalo *et al.* applied this model toward the design of a tissue adhesive scaffold containing distinctly compartmentalized cells to promote regeneration after implantation.[290] Dopamine was functionalized onto hydrazone-crosslinked HA hydrogels (HA–DOPA) to enable adhesion of the scaffold to the defect site. Advantageously, the introduction of dopamine allowed for thiolated collagen IV (col IV-SH) cell adhesive peptide to be conjugated to the hydrogel surface *via* Michael addition. Compared to DOPA-free HA hydrogels (HA–HA), limbal epithelial stem cells (LESCs) on col IV-SH-conjugated HA–DOPA hydrogels displayed greater adhesion and long-term viability. Interestingly, LESC attachment was observed on unmodified col IV-coated HA–DOPA groups, owing to the adhesive properties of DOPA. On HA–DOPA, LESCs retained their progenitor-like phenotype *via* expression of the limbal stem cell marker $\Delta Np63\alpha$ (indicated by $p63\alpha$ and $p40$ nuclear co-localization) in combination with low expression of epithelial maturation marker cytokeratin 12. Covalent attachment of col IV was also necessary for continued cell growth and maintenance of LESCs. Encapsulated hASCs displayed increased elongation within HA–DOPA hydrogels compared to a more rounded phenotype in HA–HA hydrogels, potentially due to DOPA residues promoting the retention of ECM proteins deposited by cells.

Viscoelastic hydrazone hydrogels

Hydrazone-based hydrogels have been used most extensively for their unique dynamically covalent crosslinks, imparting viscoelasticity and rapid shear-thinning and self-healing capabilities at physiologic conditions. Recent efforts by the Anseth group have utilized dynamic covalent hydrazone bonds to provide a stable crosslinked network for cell culture and with tunable stress relaxation profiles. McKinnon *et al.* formed hydrogels composed of aliphatic hydrazine- and aldehyde-functionalized 4-arm PEG at a pH of 7.4 to allow for cell encapsulation.[262] Stress relaxation timescales were tuned by varying the ratio of aliphatic (AA) and aryl (BA) aldehyde crosslinker; AA hydrazone bonds were shown to relax 100% of the imposed stress within a minute, whereas BA hydrazone bonds only relaxed about 75% of the total stress over the course of 14 hours. Encapsulated C2C12 myoblasts remained morphologically rounded in BA hydrazone networks but displayed filopodia and lamellipodia with extended processes in faster stress relaxing substrates with increased AA/BA ratio. Additionally, viscoelastic hydrogels with AA hydrazone linkages supported myoblast fusion into multinucleated myotube-like structures, demonstrating the ability for the dynamic network to permit cell behaviors necessary for myotube maturation. A subsequent study demonstrated the compatibility of the hydrogel system with sensitive cell types and the ability to characterize how biophysical signals influenced the level of cellular force involved in adhesion and motor neurite extension.[291] Increasing the stoichiometric ratio of PEG-hydrazine to PEG-aldehyde (2 : 1) resulted in lower cell toxicity and neurite extension from embryoid bodies in a 3D scaffold compared to 1 : 1 hydrazine-aldehyde hydrogels. This finding is supported by the fact that excess reactive aldehydes can potentially contribute to neurodegenerative diseases.[292]

Similarly, by varying the percentage of alkyl aldehyde (aHz) and benzylaldehyde (bHz) in a hydrazone-crosslinked hydrogel, Richardson *et al.* achieved stress relaxation times ranging from one hour to one month ($\langle\tau\rangle \sim 4 \times 10^3$ s to $\sim 3 \times 10^6$ s, respectively).[293] Hydrogels were fabricated by reacting nucleophilic PEG-hydrazine with either alkyl- or benzylaldehyde-modified PEG; rheological characterization demonstrated that increased bHz crosslinking corresponded with slower relaxation times. While both primarily elastic (100% bHz, slow relaxing) and highly stress relaxing (>88% aHz, fast relaxing) hydrogels suppressed chondrocyte proliferation and cellularity, hydrazone hydrogels with a combination of aHz and bHz crosslinks supported cellular proliferation. In particular, a significant increase in proliferation, glycosaminoglycan deposition, and collagen deposition was observed in the 22% bHz hydrogels (stress relaxation ~3 days). These results suggest that an average stress relaxation timescale of ~3 days is relevant for dense

Published on 19 July 2021. Downloaded by University of Virginia on 8/10/2021 5:09:05 PM.

chondrocyte growth and formation of high quality neocartilaginous tissue. This hydrogel system was then used to understand how mechanical deformation, similar to a load-bearing joint, would influence chondrocyte morphology.[294] Chondrocytes were encapsulated in elastic (0% aHz), viscoelastic (100% aHz), and mixed (78% aHz, 22% bHz) hydrogels and exposed to 20% uniaxial compressive strain for 10 hours. Chondrocytes in the elastic hydrogels retained an ellipsoidal morphology over the strain period and only recovered once the strain was removed. Conversely, chondrocytes in viscoelastic hydrogels were able to recover to their unstrained rounded morphology during deformation due to creep compliance behavior of the hydrogel network. The optimized mixed viscoelastic hydrogel resulted in a slower recovery of the rounded morphology, indicating that the network is composed of elastic and viscoelastic interactions. The viscoelastic hydrogel groups (100% and 78% aHz) also showed greater distribution of nascent ECM protein deposition and subsequently, decreased cellular deformation when subjected to compressive strain.

Hydrazone hydrogels incorporating protein cues

The stress relaxation properties of hydrazone bonds can also be exploited to recapitulate fibrillar ECM. Lou and co-workers designed a HA-based IPN consisting of hydrazone bonds and type I collagen with tunable viscoelastic regimes (Fig. 5G–I).[61] Instead of using oxidation to modify the HA backbone with aldehydes (a common and quick method that can potentially compromise the molecular weight distribution of the polymer backbone), aldehyde functionalization was added to HA by first modifying HA carboxyl groups with alkynes (*via* carbodiimide coupling), followed by a copper-catalyzed reaction to attach azide-functionalized hydrazines, aliphatic aldehydes (HA–ALD), and benzyl aldehydes (HA–BLD). Consistent with previous findings, the hydrogels containing hydrazine–aliphatic aldehyde hydrazone bonds displayed faster relaxation kinetics compared to hydrazone bonds with benzyl aldehydes (Fig. 5J). MSCs encapsulated within faster relaxing dynamic substrates supported increased cell spreading (Fig. 5K), reduced roundness (Fig. 5L), protrusions up to 100 μm in length, collagen fiber alignment, and focal adhesion formation indicative of robust integrin binding (IPN with HA–BLD > IPN with HA–ALD) (Fig. 5M).[61,262]

Recent interest in independent tuning of mechanical and biochemical cues has led to the design of hydrogels containing engineered ELPs.[268,295] Zhu and co-workers designed a hydrazine-functionalized ELP (ELP-HYD) with modular repeats of structural and cell adhesive sequences.[295] When combined with aldehyde-modified HA (HA–ALD) at room temperature, gelation rapidly occurred and stabilized within one minute. Hydrogel stiffness was varied by controlling the crosslinking ratio between hydrazines and aldehydes as well as through polymer concentrations. In general, higher polymer concentrations resulted in increasing stiffness, and this was more sensitive to changes in ELP concentration. To minimize thermally-induced stiffening effects and produce a group of hydrogels with similar storage moduli (G'), a lower concentration of ELP was fixed (1.8 wt%) while HA concentration was varied (1.5, 3, or 5 wt%). Interestingly, increasing HA caused a dose-dependent increase in gene expression of cartilage markers by encapsulated chondrocytes, including aggrecan (*Acan*), SRY (sex determining region Y)-box 9 (*Sox9*), and type II collagen (*Col2a1*). In addition, markers related to the undesirable fibrocartilage phenotype, type I and type X collagens, were downregulated. Matrix metalloproteinase-13 (MMP-13), a marker of cartilage remodeling, increased as HA concentration decreased – this suggests that lower levels of HA enable greater degradation and matrix remodeling. Similarly, decreasing HA concentration led to increased chondrocyte proliferation. Deposition of cartilage-specific matrix (sulfated GAGs) correlated with cartilage marker expression trends, and these observations were consistent with previous reports showing increased matrix deposition resulting in decreased cell proliferation. Overall, this study highlighted the importance of decoupling mechanical and biochemical cues to probe cell–matrix interactions.

Disease-mimetic hydrazone systems

Several groups have also exploited the cytocompatible nature of hydrazone reactions toward the design of relevant disease models. Dahlmann *et al.* designed an alginate- and HA-based hydrogel system mimicking contractile myocardial tissue with hydrazone crosslinking capabilities to enable a wide range of mechanophysical properties.[296] Gelation kinetics, stiffness, and viscoelasticity were adjustable *via* the chosen polymer backbone, degree of polymer functionalization, and temperature. Interestingly, incorporation of type I collagen into HA-containing substrates led to increased active contraction force compared to collagen alone; passive forces were also dependent on the substrate material properties (alg–alg > HA–alg > HA–HA > collagen). Finally, cardiomyocytes on all hydrazone-based constructs exhibited elongated, aligned morphologies with cross-striations and expression of the gap junction protein connexin 43, comparable to native myocardium.

One important aspect in the design of pathologically-relevant disease models is the influence of culture dimensionality on cell behaviors, particularly because of their differences in cell–cell and cell–matrix interactions. Toward this objective, Suo *et al.* developed degradable hydrazone hydrogels to compare cell morphology and growth factor expression as a function of culture dimensionality.[297] Increasing the ratio of aldehyde-modified HA (oxidized HA, AHA) to hydrazide-modified HA (glycidyl methacrylated 3,3′-dithiobis(propionic hydrazide), GHHA) resulted in increased hydrogel stiffness. To control degradation, hyaluronidase and glutathione concentrations were varied, demonstrating that the hydrogels were susceptible to enzymatic hydrolysis and reduction. Human breast cancer MCF-7 cell morphologies differed between 2D and 3D cultures, displaying more

This journal is © The Royal Society of Chemistry and IChemE 2021

Published on 19 July 2021. Downloaded by University of Virginia on 8/10/2021 5:09:05 PM.

polygonal spreading in 2D compared to more rounded and spherical morphologies throughout the 3D culture, similar to those seen in tumors. Interestingly, cells in 3D hydrogels also proliferated at a greater rate due to increased area to grow. Expression of breast cancer-relevant cytokines – vascular endothelial growth factor (VEGF), interleukin 8 (IL-8), and basic fibroblast growth factor (bFGF) – as well as cell migration and invasion were all significantly increased in 3D cultures. This suggests that the 3D microenvironment, which is more hypoxic compared to 2D cultures, potentially provides increased tumorigenic capacity by supporting more disease-relevant cell–cell and cell–matrix interactions.

In summary, dynamic covalent chemistries such as oximes and hydrazones have become particularly attractive for the development of dynamic and mechanically compliant hydrogel systems. The reactions proceed at physiologic conditions and tissue-relevant properties such as viscoelasticity can be easily tuned. For this reason, both oxime and hydrazone chemistries have been utilized in applications requiring shear-thinning and self-healing properties as well as for studies focusing on the impact of material stress relaxation timescales on cell mechanobiology. While oxime bonds are more stable than hydrazone bonds, hydrazone-based hydrogels have been explored more in the biomaterials space because of their increased stress relaxation capabilities. Additionally, imine bond formation is pH- and temperature-sensitive. Not surprisingly, one drawback to these mechanisms is the slow gelation kinetics. However, recent approaches combining imine reactions with secondary crosslinking mechanisms have generated rapidly gelling hydrogels that are structurally stable and viscoelastic.

7. Thiols

Thiol-based click hydrogel formation typically occurs under one of two mechanisms: the radical thiol–ene/–yne reaction and the thiol-Michael addition.[16] Both mechanisms meet the criteria for click chemistry with fast reaction kinetics, high yields of one regioselective product, requiring only a small amount of catalyst, taking place in mild solvents, and reacting in air or water. Since the thiol itself, which contains a sulfhydryl group attached to a carbon, is what distinguishes these reactions from other click chemistries it is worth discussing key characteristics of this chemical species. There are a few commonly used thiols including alkyl thiols, aromatic thiols, thiolpropionates, and thiol glycolates.[298] A number of biomaterials researchers have also taken advantage of the sulfhydryl group in cysteine to incorporate peptide-based pendant groups and crosslinkers in hydrogels.[299–305] The high nucleophilicity allows for greater selectivity during crosslinking. Further, as outlined by Fairbanks *et al.*, thiol-based click photopolymerization offers an advantage over some other click chemistries in that it allows precise spatiotemporal control over the reaction, which they demonstrated by toggling light exposure on and off to illustrate modulus increase and stagnation, respectively.[306] A comprehensive discussion of thiols with respect to pK_a, nucleophilicity, and electrophilicity characteristics is covered in Hoyle *et al.*[307]

Radical thiol–ene/–yne chemistry

Thiol–ene addition reactions function by a radical-mediated crosslinking mechanism where a thiol attaches to an alkene. Thiol–yne photopolymerization reactions are similar to thiol–ene, with the substitution of an alkyne for an alkene. While the thiol–ene mechanism follows a 1:1 stoichiometric ratio of the two groups, the thiol–yne utilizes a 2:1 thiol–alkyne ratio.[308] This reaction mechanism results in greater crosslink density and conversion rates compared to the thiol–ene reaction.[309] Thiol–ene/–yne reactions are most commonly done using light and a photoinitiator to produce radicals,[306,310] as opposed to other methods like temperature.[311] This mechanism is efficient, with crosslinking occurring on time scales of seconds to several minutes, is useful for several different alkene functional groups, and results in high yields.[306] Photoinitiators like lithium phenyl(2,4,6-trimethylbenzoyl)phosphinate (LAP) and Irgacure 2959 (I2959) are used to generate the initial radicals that propagate through thiols upon light exposure. Briefly, once thiyl radicals are formed, they follow an addition reaction across the double bond in the –ene, which in turn results in a radical centered on a carbon that attaches to a thiol, producing another thiyl radical (Scheme 7). This reaction follows a step-growth mechanism which includes initiation, propagation, and termination steps. The termination step depends on the amount of thiol initially added, the number of available –enes, the amount of photoinitiator, and/or the removal of the light source generating the radicals.

This reaction mechanism has been widely used in the field of macromolecules, with exemplary work in the early 2000s by Bowman who studied the reaction kinetics[312–314] as well as its potential use in biomaterials applications.[315] While this mechanism enables facile regulation of the crosslinking density and spatiotemporal control of the hydrogel formation, the use of toxic photoinitiators which produce reactive radicals and light within the UV range may be harmful in certain cell culture applications. However, highly sensitive pancreatic β-cells remained viable following encapsulation in UV (365 nm) photopolymerized PEG-norbornene hydrogels, and resulted in higher cell viability compared to chain growth PEG-diacrylate polymerization mechanisms.[316] This result is just one of many examples highlighting the tunability of the functional group presentation and polymerization factors that can accommodate a variety of cell types.

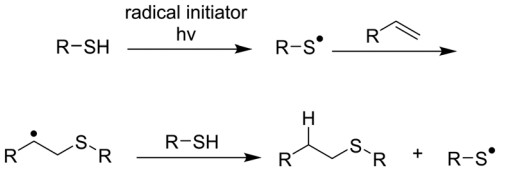

Scheme 7 Mechanism for radical initiated thiol–ene addition.

Published on 19 July 2021. Downloaded by University of Virginia on 8/10/2021 5:09:05 PM.

Thiol-Michael chemistry

Since the first publication of the thiol-Michael reaction in 1964, this mechanism has been widely applied in the area of polymer chemistry, and more specifically biomaterial design.[317] By the early 2000s, the thiol-Michael reaction was being used to synthesize PEG hydrogels which paved the way for developing thiol-Michael fabricated hydrogels for cell culture.[318,319] The thiol-Michael addition reaction is a specific class of thiol–ene chemistry that occurs by crosslinking a thiol with a double bond such as those found in commonly used functional groups for hydrogel design like maleimides, vinyl sulfones,[318,320–322] and (meth)acrylates.[320] This reaction typically proceeds more rapidly under basic conditions. The more electron-deficient the double carbon bond is, the more readily it will undergo the thiol-Michael reaction.[315]

The base-catalyzed Michael addition leads to a thiolate anion which directly adds to the β-carbon of a double bond, producing a carbanion (Scheme 8). The carbanion obtains a proton from another thiol or the conjugate acid and continues to completion. The yield as well as the kinetics rely on the base strength and amount, the pK_a and steric accessibility the thiol. In biomaterials applications, commonly used bases are triethylamine or triethanolamine[323] mixed in PBS.

The Michael addition reaction does not require an especially strong base to produce a high yield of crosslinks and does not generate reactive radicals like the thiol photopolymerization reactions, enabling the formation of hydrogels with Young's moduli ranging from 1 kPa (ref. 324) to 300 kPa.[320] Along with the light-mediated thiol–yne reaction, there exists a non-radical mechanism that occurs at a physiologic pH.[325] This has advantages over the photopolymerization mechanism, namely by not producing radicals or requiring light sources which may be detrimental to cells and sensitive therapeutic payloads. For more rapid thiol-Michael reactions, such as thiol–maleimide, nonuniform crosslinking can result in more heterogeneous network formation.[326–328] The Peyton laboratory designed a set of experiments exploring how the buffer concentration and pH, as well as polymer concentration, changed the rate of the polymerization and subsequently investigated cancer cell cytocompatibility within these systems.[326] Using a slightly acidic pH of ~6.0 and a lower strength catalytic buffer afforded more optimal hydrogel properties with increased network homogeneity, as measured by visual inspection and small particle diffusion experiments using fluorescent beads. Darling *et al.* further examined how heterogeneous network formation of thiol–maleimide PEG hydrogels led to a broader distribution of human dermal fibroblast spreading compared to those encapsulated within hydrogels with more homogeneous network crosslinks.[327]

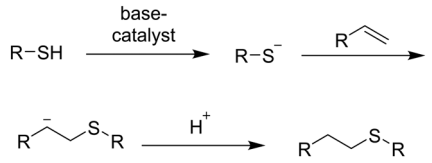

Scheme 8 Mechanism for the base-catalyzed thiol-Michael addition.

Ligand-decorated thiol-based hydrogels

Kasko's group studied the effects of material stiffness and adhesive peptide presentation on lung fibroblast activation by transforming growth factor β (TGF-β).[329] The thiol–ene mechanism enabled facile crosslinking of PEG-diacrylate to thiol-functionalized peptides of different concentrations. By tuning the molecular weight of the monomer and the concentration of the peptide, hydrogels were fabricated with storage moduli ranging from 10 kPa to 1 MPa. Additionally, the type and concentration of the adhesive peptide could be tuned to control ligand presentation. The authors chose an arginine–glycine–aspartic acid–serine (RGDS) sequence since it is found in numerous ECM components like type I collagen, fibronectin, fibrinogen, and vitronectin. They also examined aspartic acid–glycine–glutamic acid–alanine (DGEA) and IKVAV sequences, which are found in type I collagen and laminin, respectively. Fibroblasts adhered to both RGDS and DGEA-functionalized hydrogels, though the latter required extreme concentrations. While it was demonstrated that stiffness alone did not activate fibroblasts, the RGDS-incorporated hydrogels altered actin cytoskeletal organization and focal adhesion formation. Further, expression of the myofibroblast marker α-smooth muscle actin (α-SMA) increased over time for cells on the stiffer materials, indicating that stiffness progressively drives fibroblast activation.

In addition to investigating cell–matrix interactions, recent work has used thiol-Michael chemistry to understand the combined effects of cell–cell and cell–matrix cues on MSC mechanobiology.[330] Methacrylated HA hydrogels were functionalized *via* thiol-Michael addition with thiolated HAVDI and RGD peptides to investigate cell–cell N-cadherin interactions and cell–matrix integrin-mediated adhesion respectively. The presence of HAVDI decreased cell contractility as well as YAP/TAZ nuclear translocation in MSCs at intermediate stiffnesses ($E \sim 10$ kPa) through reduction of Rac1 activity, indicating that cell–cell N-cadherin interactions can alter how cells sense and interpret the mechanics of their environment.

Degradable thiol-crosslinked hydrogels

Recent work using thiol–ene chemistries to design cell-degradable hydrogels has advanced our understanding of how cells sense their surrounding dynamic environments.[302,331] Caliari *et al.* studied how hydrogel stiffness and degradability influenced hMSC behavior in both 2D and 3D cultures using norbornene-modified HA (NorHA) crosslinked with dithiol peptides *via* thiol–ene photopolymerization (Fig. 6A and B).[331] While hMSCs demonstrated more spreading and YAP/TAZ nuclear

This journal is © The Royal Society of Chemistry and IChemE 2021

Published on 19 July 2021. Downloaded by University of Virginia on 8/10/2021 5:09:05 PM.

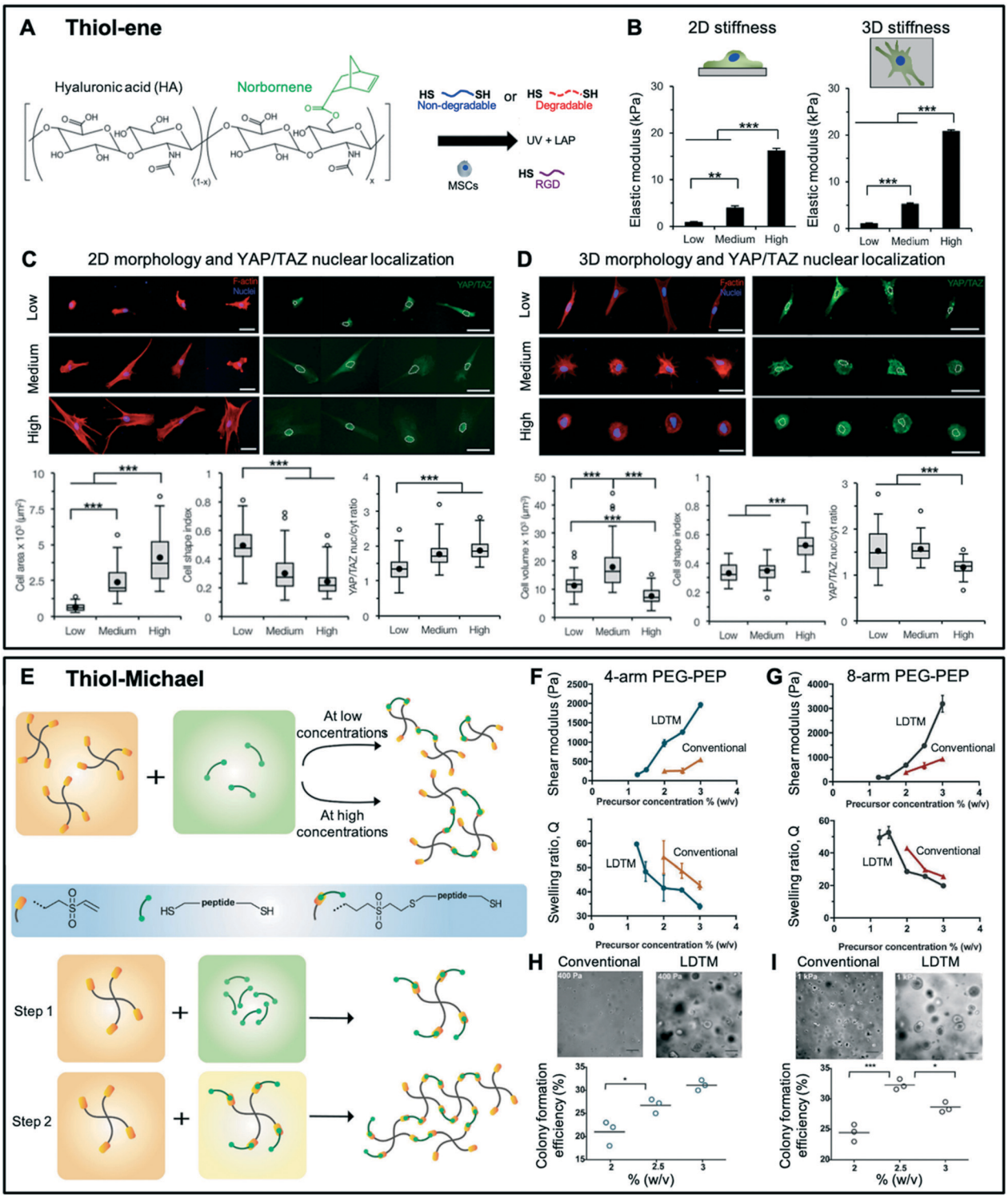

Fig. 6 Thiol click mechanisms are useful to explore cell behaviors in a variety of contexts. (A) Norbornene-functionalized hyaluronic acid (NorHA) hydrogels were fabricated using UV light-mediated thiol–ene addition with either non-degradable or MMP-degradable peptide crosslinkers. (B) 4 wt% hydrogels with variable crosslinking densities were formed for 2D and 3D hMSC cultures to present a range of mechanical cues. (C) Representative images and quantification show that for 2D cultures, increased stiffness led to increased MSC spreading, reduced circularity, and greater YAP/TAZ nuclear translocation. (D) In 3D culture, cell volume, circularity, and YAP/TAZ nuclear localization trends were reversed from 2D cultures as stiffness increased. Scale bars = 50 μm. (A–D) Adapted with permission from ref. 331. Copyright 2016 Elsevier Ltd. (E) Thiol-Michael gelation was used to create 4-arm PEG macromers containing bi-functional peptides, either at low or high polymer concentrations in which the hydrogels were formed through stepwise co-polymerization with 4-arm PEG-vinyl sulfone and tetra-thiol peptide-functionalized PEG macromers. (F) 4-Arm and (G) 8-arm low defect thiol Michael (LDTM) hydrogels showed higher shear moduli and lower swelling ratios compared to conventional peptide-containing PEG hydrogels. (H) In both 4-arm and (I) 8-arm LDTM hydrogels of 2.5% w/v, 1×10^{-3} M RGD, mouse intestinal stem cells formed colonies within 4 days of culture. Scale bars = 100 μm. (E–I) Adapted with permission from ref. 332. Copyright 2020 WILEY-VCH.

Published on 19 July 2021. Downloaded by University of Virginia on 8/10/2021 5:09:05 PM.

translocation as hydrogel stiffness increased from 1 kPa to 20 kPa on 2D cultures (Fig. 6C), encapsulated cells showed opposite trends with more spreading and YAP/TAZ nuclear localization in lower stiffness ($E < 5$ kPa) proteolytically-degradable 3D hydrogels (Fig. 6D). Importantly, hMSCs encapsulated in mechanically equivalent but non-degradable 3D hydrogels spread less and had reduced YAP/TAZ in the nucleus. These results indicate that mechanosensing, specifically through YAP/TAZ, depends on hydrogel stiffness as well as culture dimensionality and degradability.

It is critical to consider matrix degradation in 3D hydrogel cultures since cells are encapsulated and sterically hindered within crosslinked networks, as opposed to 2D cultures where cells can more easily spread and migrate. With this in mind, Lutolf *et al.* developed a multi-arm PEG hydrogel containing vinyl sulfone moieties that underwent thiol-Michael addition with cysteine-containing RGD integrin-binding domains and MMP-degradable peptides for cell adhesion and enzymatic degradation, respectively (Fig. 6E–G).[321] They investigated human fibroblast invasion from within fibrin clots encapsulated in the hydrogel network, where peptides with increased MMP sensitivity enhanced cell invasion rates compared to less sensitive and insensitive peptides. The results also indicated an optimal RGD concentration, with a peak in the extent of fibroblast outgrowth occurring in the median range of concentrations investigated (42.5 and 85 μM, with a range from 2.5 to 340 μM). Crosslink structure within the 3D PEG hydrogels was found to influence cell migration, with significantly lower invasion rates with increasing crosslink density. Interestingly, the authors used the information gained from this *in vitro* study to implant MMP-degradable hydrogels loaded with BMP-2 within rat cranial defects and found cells permeated throughout the entire hydrogel within 4 weeks of implantation. Notably, the enhanced healing response and bone regeneration depended on the increased sensitivity of the MMP-degradable peptide, corroborating the *in vitro* results. Recently, Lutolf and coworkers improved upon this design by successfully decreasing the network defects often found in thiol-Michael hydrogels. With this system, they reported robust mouse intestinal organoid development that was similar to those formed by the gold standard Matrigel (Fig. 6H and I).[332]

Griffith's group utilized the thiol–vinyl sulfone Michael addition to couple PEG–vinyl sulfone with a variety of matrix-binding peptides, such as collagen I-derived, RGD, laminin 5-derived, basement membrane binding, and MMP-sensitive peptides.[300] Epithelial cells and stromal fibroblasts co-cultured within these hydrogels remained biologically active for two weeks of culture as indicated by production of various cytokines and growth factors. The cell behavior depended on hydrogel properties, including incorporation of an adhesive ligand recognized by both cell types, cell-specific peptides that stabilize the secreted ECM, as well as a proteolytically degradable peptide linker that allowed the cells to remodel the hydrogel networks. In an extension of this work, crosslinkers susceptible to a sortase A (SrtA)-mediated transpeptidase reaction were produced to enable user-directed and cell-independent hydrogel degradation to retrieve the co-cultured cells for further downstream analyses.[333] While the control group involving typical protease degradation damaged roughly half of the cytokines and growth factors secreted by the cells that the authors tested, the SrtA treatment only affected the IL-15 protein. These results provide a method for recovering cells from within hydrogels with minimal damage to investigate transcriptional and proteomic changes over time as the cells interact with each other and their surrounding matrix.

Fairbanks *et al.* also reported on the ability to biochemically control a PEG-norbornene hydrogel crosslinked by incorporating MMP-degradable dithiol peptides.[306] In comparison to the previously discussed thiol-Michael hydrogels from Lutolf and Hubbell,[321] PEG-norbornene thiol–ene polymerized hydrogels displayed higher moduli even at similar molecular weights, likely caused by an increased conversion of the functional groups in the radical photopolymerization. RGDS functionalization was necessary for encapsulated MSC spreading; without RGDS the cells remained rounded for all of the degradable peptides studied. The degree of cell spreading at constant RGDS density depended on the structure of the MMP-cleavable peptide, where MMP-tryptophan and MMP-alanine resulted in the highest and lowest cell spreading, respectively. In a similar system, the Anseth group investigated the effects of neuronal axon outgrowth when exposed to different cysteine-functionalized biochemical cues, RGDS and YIGSR.[334] Within 12 hours of encapsulation in peptide-modified hydrogels, motor axons exhibited outgrowth and shapes typical of native motor neurons compared to unmodified PEG hydrogels or PEG hydrogels without the MMP-degradable crosslinker.

Lin's group also used thiol–ene photopolymerization to study the encapsulation of pancreatic ductal epithelial cells (PDEC) in an MMP-degradable PEG-norbornene hydrogel.[335] Within just 4 days, the PDECs arranged into clusters, but their growth was limited by MMP sensitivity, adhesion ligand presentation, and hydrogel mechanical properties. Notably, the authors found that the laminin-derived YIGSR adhesive peptide promoted increased epithelial cell marker expression, like β-catenin and E-cadherin, but less cell growth compared to RGDS presentation. The RGDS ligand also enhanced cyst-like morphologies in the PDECs, owing to how different ECM-mimetic ligands produce different cell behaviors. In another study, the same group incorporated cysteine-containing SrtA-sensitive peptides for user-controlled matrix degradation and found that hydrogel softening increased encapsulated hMSC spread area.[318,336] Notably, a SrtA-sensitive sequence was incorporated into a bis-cysteine peptide which allowed the authors to cyclically stiffen and soften the PEG-norbornene hydrogel.[337] Pancreatic cancer cells displayed either a decrease or increase in spheroid size upon hydrogel stiffening or softening, respectively. Encapsulating Huh7 or HepG2 liver cells into PEG-norbornene hydrogels resulted in increased urea secretion, CYP3A4 – an important enzyme responsible

This journal is © The Royal Society of Chemistry and IChemE 2021

Published on 19 July 2021. Downloaded by University of Virginia on 8/10/2021 5:09:05 PM.

for toxin removal – and mRNA of hepatocyte genes CYP3A4, BESP, and NTCP, which helped elucidate mechanisms of hepatitis B virology *in vitro.*[338] Huh7 cells encapsulated within thiol–norbornene hydrogels comprised of gelatin with varying stiffness or gelatin concentration showed no significantly altered CYP3A4 activity or urea secretion.[339] However, the immobilization of heparin – a sulfated glycosaminoglycan commonly found in the liver – onto the hydrogel network led to Huh7s displaying greater urea secretion and CYP3A4 activity compared to the hydrogels without heparin, which was likely caused by modified cell signaling due to isolated growth factors in the media or released from cells.[340] In a similar study, Lin *et al.* studied the effects of matrix crosslinking and degradability on YAP regulation in encapsulated Huh7 cells[341] using a modified PEG system containing acrylate groups that could undergo cytocompatible visible light photocrosslinking with thiol moieties.[342,343] YAP expression was suppressed in 3D *versus* 2D cultures and also in hydrogels that did not contain RGD.

Mechanically dynamic and viscoelastic thiol-crosslinked hydrogels

To better model the dynamic mechanical properties of native ECM during development, wound repair, and disease, sequential crosslinking reactions allow control of hydrogel stiffness in the presence of cells to probe the resulting cell–matrix interactions. Hydrogels formed using methacrylated HA (MeHA) crosslinked through base-catalyzed thiol-Michael addition displayed initial stiffnesses (E) of ~3 to 100 kPa, dependent on the thiol crosslinker concentration.[344] hMSCs exhibited either rounded or elongated morphologies when cultured atop soft or stiff hydrogels, respectively. Following *in situ* chain-growth UV photopolymerization of the remaining methacrylates, which stiffened initially compliant hydrogels from 3 to 30 kPa, hMSC morphology changed to more closely match that of cells initially seeded on the stiffer 30 kPa matrix. Long-term culture on these hydrogels illustrated the effects of stiffening on differentiation, where earlier or later stiffening promoted preferential adipogenic or osteogenic differentiation, respectively.

As a model for liver fibrosis progression, which results in gradual tissue stiffening, hepatic stellate cells seeded on a similar hydrogel system displayed markers of myofibroblast activation including more spreading, YAP/TAZ nuclear translocation, and α-SMA stress fiber organization when stiffening under more cytocompatible blue light occurred at later timepoints.[46] Interestingly, the authors suggested that the decreased cell spreading and myofibroblast marker expression seen in earlier stiffening may be due to a lag in cell mechanosensing following enzymatic primary cell isolation, an important consideration for mechanobiology studies using freshly isolated cells. To mimic fibrosis resolution, incorporation of a thiol crosslinker containing hydrolytically labile ester groups (combined with a non-degradable thiolated crosslinker) resulted in gradual softening, but not complete hydrolysis, of the MeHA hydrogel.[345] Stellate cells seeded on the softening hydrogel demonstrated a reduction in myofibroblast activation with decreased cell spreading as well as YAP/TAZ and α-SMA expression, but assumed an intermediate phenotype and did not completely return to baseline behaviors exhibited on static soft hydrogels. Notably, re-stiffening through blue light photopolymerization resulted in markedly rapid myofibroblast re-activation. The authors suggested that this mimics *in vivo* hepatic stellate cell behavior following fibrosis resolution and subsequent re-insult.

Groups have also looked at exploiting thiol-based click chemistries in multiple steps to investigate the role of stiffness,[324] ligand presentation,[346] and ECM deposition[347,348] on the mechanoregulation of cell behavior. Petrou *et al.* leveraged the thiol-Michael and subsequent thiol–ene photopolymerizations to investigate the effects of hydrogel mechanical cues on PDGFRα+ fibroblast behavior.[377] They found that fibroblasts cultured on the stiff as well as temporally stiffened PEG α-methacrylate hydrogels showed greater cell activation, as measured by α-SMA and Col1a1 expression, than those on the soft PEG. A previously developed labeling method[350] using SPAAC was implemented to visualize nascent protein deposition by cells encapsulated in a variety of hydrogels, including Michael addition-formed MeHA and thiol–ene photopolymerized NorHA substrates.[347,348] MSCs displayed spreading, preferential osteogenic differentiation, and YAP/TAZ nuclear localization within either MMP-sensitive covalently crosslinked or dynamic viscoelastic HA hydrogels. However, when nascent protein secretion or remodeling was inhibited, the cells exhibited opposite trends, including preferential adipogenic differentiation, indicating that cellular interactions with nascent proteins in 3D hydrogels are critical to mechanosensing.

Anseth's group is well-known for their work involving PEG-based click reactions to study cell behavior. Valvular interstitial cells (VICs) encapsulated within thiol–ene photopolymerized PEG-norbornene hydrogels displayed more elongation and α-SMA expression, which decreased following *in situ* secondary thiol–ene photocrosslinking.[351] This study also highlighted the opposing trends seen between 2D and 3D cultures, underscoring that culture dimensionality is a key factor to consider when investigating cell behavior. More recently, the researchers explored VIC contractility within this hydrogel system.[352] Through a combinatorial modeling and experimental approach, they discovered that VIC contraction resulted in an increase in the effective shear modulus of the 3D system, and that this contractility depended on the hydrogel mechanics as well as the concentration of adhesion ligands.

Aside from PEG, researchers have investigated these click reactions in a variety of other polymeric materials. Naturally-derived gelatin hydrogels provide adhesive ligands and enzymatic degradation as opposed to unmodified synthetic systems like PEG. Lin's group utilized thiol–ene

Published on 19 July 2021. Downloaded by University of Virginia on 8/10/2021 5:09:05 PM.

photocrosslinking of gelatin-based systems[353] to create mechanically static soft or tyrosine-induced stiffening hydrogels[354] either with or without HA to investigate encapsulated pancreatic ductal adenocarcinoma (PDAC) cell morphology. They found that either a stiffening hydrogel without HA or a soft HA-containing hydrogel reduced PDAC growth, but HA-containing stiffening hydrogels resulted in significantly increased spreading. The authors suggest this is due to upregulation of Rac1, Rac2, RhoA, and Raf1 mRNAs, which are all involved in Ras/MAPK signaling. Notably, they also found upregulated genes involved in fibrosis, specifically TGF-β2, EGFR, and TGFβR1 for cells encapsulated in HA-containing stiffening hydrogels.[355]

Recently, a 4D hydrogel developed by Zheng *et al.* allowed control of biochemical and mechanical cues in 3D culture through an initial thiol-Michael addition with methacrylated dextran and dicysteine-containing MMP-sensitive peptides.[304] At the same time, cysteine-bearing cyclo[RGD(DMNPB)fC] also attached to the methacrylates where subsequent UV light cleaved the DMNPB group to activate the RGD peptide, allowing for control of cell adhesion in a spatiotemporal manner. Under visible light and in the presence of a photoinitiator, the remaining methacrylate groups underwent chain growth polymerization to further stiffen the hydrogel. Fibroblasts encapsulated as embedded spheroids remained confined and did not migrate within the initial hydrogel; however, when RGD was activated the fibroblasts migrated out of the spheroid and into the surrounding dextran hydrogel. When the RGD-activated hydrogel underwent secondary blue light stiffening, fibroblasts stopped migrating due to the increased crosslinks within the hydrogel network. These results highlight the incredible tunability afforded with click-based chemistries in hydrogel design as well as the competing effects of biochemical and biophysical hydrogel properties on regulating cell behaviors such as migration.

Others have even leveraged photopatterning techniques to enable spatiotemporal control of biochemical and biophysical hydrogel properties. Thiol–ene photopolymerization offers an advantage in being relatively mild and quick which helps maintain the stability and function of added signaling moieties. The Burdick group is most noted for their efforts in photopatterning HA-based materials.[323,356,357] Khetan *et al.* developed acrylate-modified HA to investigate cell morphology when encapsulated in hydrogels crosslinked by either thiol-Michael addition, chain growth photopolymerization, or sequential addition and photopolymerization in the presence of RGD, MMP-degradable dithiol crosslinker, or both peptides.[323] In the sequential method, photomasks were used to spatially control the secondary crosslinking reaction, where cells exposed to the additional non-degradable crosslinks displayed rounded morphologies while the hydrogel areas only containing MMP-degradable crosslinks exhibited spindle-like shapes. This system was then applied to investigate aortic arch growth and MSC differentiation.[358] Encapsulated arches as well as MSCs in MMP-degradable hydrogels demonstrated robust outgrowth, while those in the non-degradable photopolymerized hydrogels did not; the same results occurred for arches and MSCs within hydrogels patterned with regions of the secondary photopolymerization, underscoring the importance of degradability for creating 3D hydrogels permissive to normal mechanical signaling. Gramlich *et al.* made use of the thiol–ene photoclick reaction to first create a norbornene-modified HA hydrogel that could undergo secondary thiol-mediated photocrosslinking to pattern regions of increased crosslinking and/or pendant thiolated peptides like RGD.[357]

Numerous recent studies have highlighted the importance of designing hydrogels mimicking the viscoelasticity of native tissue to study mechanobiology.[57,61,359,360] For example, dynamic PDMS substrates, which are inherently viscoelastic, could be stiffened using thiol–ene chemistry to promote increased cardiac fibroblast activation compared to softer PDMS matrices.[361] Noting that many native tissues are viscoelastic and display time-dependent stress relaxation, Hui *et al.* developed NorHA hydrogels photopolymerized with dithiol crosslinkers while also containing β-cyclodextrin-functionalized HA and thiolated adamantane-modified peptides to create a hybrid hydrogel network combining stable covalent crosslinks and guest–host supramolecular interactions to impart viscoelasticity.[57] Human hepatic stellate cells (LX-2s) seeded atop the viscoelastic hydrogels exhibited reduced spreading, actin stress fiber organization, and MRTF-A nuclear localization compared to elastic hydrogels. Additionally, thiol–ene photochemistry was leveraged to spatially pattern stiffer more elastic hydrogel regions interspersed within more compliant and viscoelastic non-patterned regions to mimic the heterogeneous emergence of fibrotic nodules in liver fibrosis. Stellate cells responded to the patterned mechanical properties in a spatially selective manner with cells more spread in the stiffer elastic photopatterned regions.

Structured thiol-based hydrogels

Thiol–ene photopolymerizations also afforded the ability to create hydrogels with hierarchical structures by tethering self-assembling collagen-mimicking peptide fibrils to tetra-thiol PEG.[362] hMSCs displayed more elongation as the concentration of the collagen peptide mimic increased, with the authors describing notable "hole" regions where the cells seem to form donut clusters, in stark contrast to typical cell behavior in PEG hydrogels crosslinked with non-assembling peptides. In a similar study, Reynolds *et al.* formed an initial cell-laden fibrillar collagen structure that was later reinforced with photocrosslinked PEG-norbornenes and -dithiols to create an IPN mimicking *in vivo* collagen microarchitecture.[363] By confining metastatic breast cancer cells to increasingly stiff IPNs, the cells expressed less malignant behavior such as proliferation, therefore impeding tumorigenesis.

Along with incorporating fibrillar architecture into hydrogel networks, researchers also have taken advantage of microgels to engineer microscale porosity into 3D culture systems. Xin *et al.*

This journal is © The Royal Society of Chemistry and IChemE 2021

Published on 19 July 2021. Downloaded by University of Virginia on 8/10/2021 5:09:05 PM.

packed PEG-norbornene microgels together and photocrosslinked them with the addition of PEG-dithiol.[301] hMSCs proliferated around the microgels and into the surrounding micropores within 24 h following encapsulation, but this behavior depended on the concentration of the crosslinker and the photoinitiator; cell proliferation increased for microgels made with lower PEG concentrations, even though the microgel porosity decreased. Cells displayed greater YAP nuclear localization in microgels of increasing stiffness, indicating that mechanical properties of the microgel scaffold influence cell mechanosensing in a similar manner to 2D cell culture. Using this same system, cell response was evaluated to either fast tryptophan-functionalized or slow proline-containing degradable crosslinks incorporated within the microgels.[364] hMSCs proliferated more in both degradable groups, especially in the fast degrading group, compared to non-degradable microgels after 2 days of culture, suggesting that the degradability allowed for enhanced cell proliferation. Further, cells secreted OPG, a marker of osteogenic differentiation, in the fast degrading group with either the α5β1 peptide c(RRETAWA) – which induces osteogenesis – or RGDS modification. Segura's group also explored the design of microporous annealed particle scaffolds to study human dermal fibroblast mechanobiology.[365] HA–norbornene microgels were formed through photocrosslinking with dithiothreitol before annealing with a PEG-tetrazine crosslinker that was synthesized through base-catalyzed thiol-Michael addition. Fibroblasts displayed increased spreading and proliferation when cultured within scaffolds made with a lower degree of annealing since they could more easily remodel the scaffold network.

In summary, significant advantages of thiol-based click reactions over other click chemistries include the versatile range of groups that can undergo click reactions with thiols and the ability to typically perform these reactions under mild conditions. This has led to a wide breadth of hydrogel designs with reaction kinetics that are often faster than other click chemistries. However, because thiols are so highly reactive in both radical or catalyzed conditions, these mechanisms may not be as selective as other chemistries since they can undergo both reactions simultaneously, which may complicate therapeutic delivery if the payload contains reactive thiols or –ene groups, for example.[366,367] For more information regarding thiols, the complete chemistry of the thiol–ene/–yne and Michael-type reactions, and other applications of thiol-based reactions, the reader is referred to more extensive reviews on these mechanisms.[16,298,307,308,366,368]

8. Conclusions and future directions

Native tissues are highly dynamic and intricate systems containing hierarchical levels of physical and biochemical cues spanning multiple length and time scales. As researchers endeavor to uncover important details about the cell–cell and cell–matrix interactions governing cell behavior in both normal and diseased tissue states, the development of advanced multi-responsive biomaterial models of tissue becomes increasingly important. Click chemistry is a powerful tool to guide the design of tunable biomaterials for studying cell mechanobiology. Several classes of click reactions have been identified and are continuously being refined to meet various design criteria of cell culture systems. Importantly, click-based hydrogels allow simple, independent manipulation of critical cell-instructive cues such as stiffness, viscoelasticity, degradability, adhesion, and growth factor presentation.

The diversity in click chemistries and reaction pairs, from initial efforts applying CuAAC chemistry to achieve fast and efficient kinetics with limited side product formation, is ideal for the development of a suite of hydrogel systems covering multivariate applications (Table 2). Hydrogel mechanics and gelation kinetics can easily be tuned by varying polymer concentration (stiffness), click pair reactivity (reaction rate), ratio of reagents (stiffness, viscoelasticity), crosslinking density and type (stiffness, viscoelasticity), and biomolecule ligand presentation. Rational selection of click reaction pairs – using electron-rich dienes or electron-poor dienophiles for Diels–Alder hydrogels, increasing SPAAC cycloalkyne strains, or substituting in more electron-withdrawing groups in an IEDDA system – has enabled more efficient gelation rates. Increasing reaction kinetics can allow more rapid cell encapsulation for 3D cultures. Slower gelation *via* Diels–Alder, hydrazone, and oxime chemistries, has shown utility for creating cell-laden injectable and self-healing platforms. Varying hydrazone and oxime reactive group ratios allows for modulation of time-dependent, viscoelastic properties like stress relaxation. External stimuli such as temperature, pH, initiators, or catalysts can also aid in primary and secondary chemistries to enable spatiotemporal control over physical and biochemical cues. Radical- and light-mediated thiol–ene and thiol–yne additions yield systems with high levels of spatiotemporal control, useful for studying the impact of multiple cues on cell behaviors.

The simplicity of click reactions allows for a more in-depth perspective into how particular mechanisms, such as stress relaxation timescales, can influence cell morphology, nuclear localization of transcriptional mechanoregulators, migration, and differentiation in both 2D and 3D cell culture systems. Several click chemistries can be spatiotemporally combined within a single system, creating an array of dynamic materials in which cell-instructive cues can be added to coincide with disease progression. For instance, a simple yet effective approach that has been applied to several systems is to introduce a secondary photomediated thiol–ene reaction for spatiotemporal presentation of stiffness, viscoelastic, or adhesive cues as well as tethered biomolecules. Dynamic chemistries utilizing dual crosslinking schemes have been used to influence subsequent mechanical properties in the presence of cells (*e.g.*, using orthogonal wavelengths of light to trigger hydrogel stiffening or softening). These multi-factorial systems have enhanced our understanding of the complex mechanisms governing biological processes. Although

Published on 19 July 2021. Downloaded by University of Virginia on 8/10/2021 5:09:05 PM.

Table 2 Summary of current and future applications for each click chemistry reaction

Click chemistry	Common applications/uses	Future directions
CuAAC	2D cell cultures[106,107] Biomolecule conjugation[369–372] Patterned hydrogels *via* photochemical Cu(II) reduction[103]	Non-toxic catalyst for 3D cultures[115,373]
SPAAC	3D cell cultures[122,123] pH-Mediated degradation[136] Biomolecule conjugation[129,142] Stress relaxing hydrogels[125,127]	Dual-crosslinked hydrogels[126,143] Tissue regeneration applications[124,144]
Diels–Alder	Shear thinning and self-healing (injectable) materials[172] Controlled degradation *via* temperature or pH[172,173,191] Drug/protein delivery[169,174] Tumor models[14,168]	Biomolecule presentation and release[167] Thermosensitive hydrogels for controlled degradation[162,175,176] Tissue regeneration applications[170,171]
IEDDA	3D cell cultures[212,233] Biomolecule bioconjugation[236,239] Dual-crosslinked hydrogels[235]	Multilayer hydrogel microsphere formation[239] Cancer cell spheroid encapsulation[215]
Oxime	pH- and temperature-mediated viscoelastic hydrogels[256,283]	Dual-crosslinked hydrogels[287] Photo-mediated oxime ligation[247]
Hydrazone	Viscoelastic hydrogels[262,293,294] Sutureless tissue implantation[289,290] Biomolecule conjugation[295]	Interpenetrating network (IPN) hydrogels[61] 3D bioprinting of cell-laden scaffolds[271]
Thiol-based	3D cell cultures[306,321,338,352] Biomolecule conjugation[300,329,330] Dual-crosslinked hydrogels (in combination with other click chemistries)[103,123,174,209,235,236] Structured hydrogels (*e.g.*, fibrillar architecture)[362,363]	Spatially patterned hydrogels[57,304,323,357] 3D bioprinting of cell-laden scaffolds[271,374,375] Dynamic platforms with temporal control over mechanical and chemical instructive cues[46,344,345,349,351,354]

current studies have already begun to demonstrate the power of click chemistry to design and tune biomaterials for cell culture, further research is needed to improve our understanding of how physical cues individually contribute to tissue regeneration and disease processes, as well as how we can exploit the specific and quick nature of click reactions to repair, replace, and treat diseased tissue.

Continued development toward integrating multiple mechanical and chemical cues in a user-controlled manner will be essential to mimic the complex behaviors of tissues, particularly during disease processes. Fortunately, there are several emerging areas that click-assembled cell culture models could specifically help address. Advancements toward spatiotemporally patterned biomaterials that capture the heterogeneity of healthy and diseased tissues will help establish models that can be used to study pathological cell behaviors. For example, photoclick chemistries such as radical-mediated thiol–ene addition have already shown promise toward achieving this objective because there is a high degree of control of when and where the reaction will take place. Dynamic materials, such as those involving dual-crosslinking approaches, allow cell-instructive cues (*e.g.*, stiffness, viscoelasticity, ligand presentation) to be added to coincide with disease progression, furthering our understanding of how temporally presented signals regulate cell phenotype. Another promising avenue is multi-stimuli responsive hydrogels that can respond to various triggers such as light, pH, temperature, and redox state to independently manipulate physical, chemical, and mechanical properties. Utilizing click chemistry, development of these techniques will continue to expand the field toward the rational design of dynamic yet well-controlled hydrogel platforms. Looking ahead, click reactions should provide accessibility toward investigating complex combinatorial microenvironments. High-throughput arrays that can easily introduce physical cues and bioactive molecules in a single step can help address challenges in trying to increase clinical relevance of biomaterial systems without sacrificing user control or convenience.[376]

Conflicts of interest

There are no conflicts of interest to declare.

Acknowledgements

The authors thank Ivan Basurto, Beverly Miller, and Mackenzie Grubb for helpful discussions. This work was supported by the NIH (R35GM138187, T32GM008715) and NSF (CAREER DMR/BMAT 2046592). The content is solely the responsibility of the authors and does not necessarily represent the official views of the National Institutes of Health.

References

1 C. Bonnans, J. Chou and Z. Werb, *Nat. Rev. Mol. Cell Biol.*, 2014, **15**, 786–801.
2 K. S. Midwood, L. V. Williams and J. E. Schwarzbauer, *Int. J. Biochem. Cell Biol.*, 2004, **36**, 1031–1037.
3 K. A. Jansen, D. M. Donato, H. E. Balcioglu, T. Schmidt, E. H. J. Danen and G. H. Koenderink, *Biochim. Biophys. Acta, Mol. Cell Res.*, 2015, **1853**, 3043–3052.

 This journal is © The Royal Society of Chemistry and IChemE 2021

Published on 19 July 2021. Downloaded by University of Virginia on 8/10/2021 5:09:05 PM.

4 G. V. Shivashankar, M. Sheetz and P. Matsudaira, *Integr. Biol.*, 2015, **7**, 1091–1092.
5 D. Mohammed, M. Versaevel, C. Bruyère, L. Alaimo, M. Luciano, E. Vercruysse, A. Procès and S. Gabriele, *Front. Bioeng. Biotechnol.*, 2019, **7**, 162.
6 J. Eyckmans, T. Boudou, X. Yu and C. S. Chen, *Dev. Cell*, 2011, **21**, 35–47.
7 S. R. Caliari and J. A. Burdick, *Nat. Methods*, 2016, **13**, 405–414.
8 H. H. G. Song, K. M. Park and S. Gerecht, *Adv. Drug Delivery Rev.*, 2014, **79**, 19–29.
9 J. H. Lee and H. W. Kim, *J. Tissue Eng.*, 2018, **9**, 0–3.
10 Y. Jiang, J. Chen, C. Deng, E. J. Suuronen and Z. Zhong, *Biomaterials*, 2014, **35**, 4969–4985.
11 H. C. Kolb, M. G. Finn and K. B. Sharpless, *Angew. Chem., Int. Ed.*, 2001, **40**, 2004–2021.
12 C. M. Madl and S. C. Heilshorn, *Adv. Funct. Mater.*, 2018, **28**, 1–21.
13 H. Zhan, H. De Jong and D. W. P. M. Löwik, *ACS Appl. Bio Mater.*, 2019, **2**, 2862–2871.
14 S. A. Fisher, P. N. Anandakumaran, S. C. Owen and M. S. Shoichet, *Adv. Funct. Mater.*, 2015, **25**, 7163–7172.
15 F. Yu, X. Cao, Y. Li and X. Chen, *ACS Macro Lett.*, 2015, **4**, 289–292.
16 D. P. Nair, M. Podgórski, S. Chatani, T. Gong, W. Xi, C. R. Fenoli and C. N. Bowman, *Chem. Mater.*, 2014, **26**, 724–744.
17 S. Yigit, R. Sanyal and A. Sanyal, *Chem. – Asian J.*, 2011, **6**, 2648–2659.
18 C. M. Nimmo, S. C. Owen and M. S. Shoichet, *Biomacromolecules*, 2011, **12**, 824–830.
19 J. Gopinathan and I. Noh, *Tissue Eng. Regener. Med.*, 2018, **15**, 531–546.
20 K. A. Jansen, P. Atherton and C. Ballestrem, *Semin. Cell Dev. Biol.*, 2017, **71**, 75–83.
21 F. Martino, A. R. Perestrelo, V. Vinarský, S. Pagliari and G. Forte, *Front. Physiol.*, 2018, **9**, 1–21.
22 J. D. Humphrey, E. R. Dufresne and M. A. Schwartz, *Nat. Rev. Mol. Cell Biol.*, 2014, **15**, 802–812.
23 N. Wang, J. D. Tytell and D. E. Ingber, *Nat. Rev. Mol. Cell Biol.*, 2009, **10**, 75–82.
24 M. Urbanczyk, S. L. Layland and K. Schenke-Layland, *Matrix Biol.*, 2020, **85–86**, 1–14.
25 K. H. Nakayama, L. Hou and N. F. Huang, *Adv. Healthcare Mater.*, 2014, **3**, 628–641.
26 R. Changede and M. Sheetz, *BioEssays*, 2017, **39**, 1–12.
27 N. Wang, *Nat. Mater.*, 2017, **16**, 1173–1174.
28 R. G. Wells and D. E. Discher, *Sci. Signaling*, 2008, **1**, 1–4.
29 A. B. Roberts, B. K. McCune and M. B. Sporn, *Kidney Int.*, 1992, **41**, 557–559.
30 J. L. Leight, M. A. Wozniak, S. Chen, M. L. Lynch, C. S. Chen and Y. Wang, *Mol. Biol. Cell*, 2012, **23**, 1–11.
31 M. Lodyga and B. Hinz, *Semin. Cell Dev. Biol.*, 2020, **101**, 123–139.
32 T. R. Cox and J. T. Erler, *Dis. Models Mech.*, 2011, **4**, 165–178.
33 R. L. Furler, D. F. Nixon, C. A. Brantner, A. Popratiloff and C. H. Uittenbogaart, *Cancers*, 2018, **10**, 1–18.
34 N. Noskovičová, M. Petřek, O. Eickelberg and K. Heinzelmann, *Am. J. Respir. Cell Mol. Biol.*, 2015, **52**, 263–284.
35 R. Li, K. Bernau, N. Sandbo, J. Gu, S. Preissl and X. Sun, *eLife*, 2018, **7**, 1–20.
36 L. Gouveia, C. Betsholtz and J. Andrae, *Development*, 2018, **145**(7), 1–9.
37 M. Endale, S. Ahlfeld, E. Bao, X. Chen, J. Green, Z. Bess, M. T. Weirauch, Y. Xu and A. K. Perl, *Dev. Biol.*, 2017, **425**, 161–175.
38 J. D. Mih, A. Marinkovic, F. Liu, A. S. Sharif and D. J. Tschumperlin, *J. Cell Sci.*, 2012, **125**, 5974–5983.
39 Kshitiz, J. Afzal, H. Chang, R. Goyal and A. Levchenko, *Curr. Stem Cell Rep.*, 2016, **2**, 62–72.
40 S. Asano, S. Ito, K. Takahashi, K. Furuya, M. Kondo, M. Sokabe and Y. Hasegawa, *Physiol. Rep.*, 2017, **5**, 1–11.
41 A. Santos and D. Lagares, *Curr. Rheumatol. Rep.*, 2018, **20**, 1.
42 P. A. Janmey, D. A. Fletcher and C. A. Reinhart-King, *Physiol. Rev.*, 2020, **100**, 695–724.
43 A. M. Handorf, Y. Zhou, M. A. Halanski and W. J. Li, *Organogenesis*, 2015, **11**, 1–15.
44 D. E. Discher, P. Janmey and Y. L. Wang, *Science*, 2005, **310**, 1139–1143.
45 C. F. Guimarães, L. Gasperini, A. P. Marques and R. L. Reis, *Nat. Rev. Mater.*, 2020, **5**, 351–370.
46 S. R. Caliari, M. Perepelyuk, B. D. Cosgrove, S. J. Tsai, G. Y. Lee, R. L. Mauck, R. G. Wells and J. A. Burdick, *Sci. Rep.*, 2016, **6**, 1–10.
47 A. Parandakh, A. Anbarlou, M. Tafazzoli-Shadpour, A. Ardeshirylajimi and M. M. Khani, *Colloids Surf., B*, 2019, **173**, 194–201.
48 Y. R. Chang, V. K. Raghunathan, S. P. Garland, J. T. Morgan, P. Russell and C. J. Murphy, *J. Mech. Behav. Biomed. Mater.*, 2014, **37**, 209–218.
49 S. A. Abdellatef, A. Ohi, T. Nabatame and A. Taniguchi, *Int. J. Mol. Sci.*, 2014, **15**, 4299–4317.
50 B. M. Baker and C. S. Chen, *J. Cell Sci.*, 2012, **125**, 3015–3024.
51 M. D. Davidson, K. H. Song, M. H. Lee, J. Llewellyn, Y. Du, B. M. Baker, R. G. Wells and J. A. Burdick, *ACS Biomater. Sci. Eng.*, 2019, **5**, 3899–3908.
52 K. H. Song, S. J. Heo, A. P. Peredo, M. D. Davidson, R. L. Mauck and J. A. Burdick, *Adv. Healthcare Mater.*, 2020, **9**, 1–10.
53 L. Cacopardo, N. Guazzelli, R. Nossa, G. Mattei and A. Ahluwalia, *J. Mech. Behav. Biomed. Mater.*, 2019, **89**, 162–167.
54 Y. M. Efremov, T. Okajima and A. Raman, *Soft Matter*, 2019, **16**, 64–81.
55 M. Hemshekhar, R. M. Thushara, S. Chandranayaka, L. S. Sherman, K. Kemparaju and K. S. Girish, *Int. J. Biol. Macromol.*, 2016, **86**, 917–928.
56 E. E. Charrier, K. Pogoda, R. G. Wells and P. A. Janmey, *Nat. Commun.*, 2018, **9**, 1–13.
57 E. Hui, K. I. Gimeno, G. Guan and S. R. Caliari, *Biomacromolecules*, 2019, **20**, 4126–4134.
58 Z. Gong, S. E. Szczesny, S. R. Caliari, E. E. Charrier, O. Chaudhuri, X. Cao, Y. Lin, R. L. Mauck, P. A. Janmey, J. A.

Published on 19 July 2021. Downloaded by University of Virginia on 8/10/2021 5:09:05 PM.

Burdick and V. B. Shenoy, *Proc. Natl. Acad. Sci. U. S. A.*, 2018, **115**, E2686–E2695.
59 O. Chaudhuri, L. Gu, D. Klumpers, M. Darnell, S. A. Bencherif, J. C. Weaver, N. Huebsch, H. P. Lee, E. Lippens, G. N. Duda and D. J. Mooney, *Nat. Mater.*, 2016, **15**, 326–334.
60 O. Chaudhuri, L. Gu, M. Darnell, D. Klumpers, S. A. Bencherif, J. C. Weaver, N. Huebsch and D. J. Mooney, *Nat. Commun.*, 2015, **6**, 1–7.
61 J. Lou, R. Stowers, S. Nam, Y. Xia and O. Chaudhuri, *Biomaterials*, 2018, **154**, 213–222.
62 J. L. Balestrini, S. Chaudhry, V. Sarrazy, A. Koehler and B. Hinz, *Integr. Biol.*, 2012, **4**, 410–421.
63 F. Klingberg, B. Hinz and E. S. White, *J. Pathol.*, 2013, **229**, 298–309.
64 T. A. Wynn and T. R. Ramalingam, *Nat. Med.*, 2012, **18**, 1028–1040.
65 P. Pakshir and B. Hinz, *Matrix Biol.*, 2018, **68–69**, 81–93.
66 S. D. Varney, C. B. Betts, R. Zheng, L. Wu, B. Hinz, J. Zhou and L. Van De Water, *J. Cell Sci.*, 2016, **129**, 774–787.
67 G. Halder, S. Dupont and S. Piccolo, *Nat. Rev. Mol. Cell Biol.*, 2012, **13**, 591–600.
68 M. Jang, J. An, S. W. Oh, J. Y. Lim, J. Kim, J. K. Choi, J. H. Cheong and P. Kim, *Nat. Biomed. Eng.*, 2021, **5**, 114–123.
69 F. Liu, J. D. Mih, B. S. Shea, A. T. Kho, A. S. Sharif, A. M. Tager and D. J. Tschumperlin, *J. Cell Biol.*, 2010, **190**, 693–706.
70 R. G. Wells, *Biochim. Biophys. Acta, Mol. Basis Dis.*, 2013, **1832**, 884–890.
71 X. H. Zhao, C. Laschinger, P. Arora, K. Szászi, A. Kapus and C. A. McCulloch, *J. Cell Sci.*, 2007, **120**, 1801–1809.
72 A. J. Engler, S. Sen, H. L. Sweeney and D. E. Discher, *Cell*, 2006, **126**, 677–689.
73 A. Bauer, L. Gu, B. Kwee, W. A. Li, M. Dellacherie, A. D. Celiz and D. J. Mooney, *Acta Biomater.*, 2017, **62**, 82–90.
74 M. L. Gardel, I. C. Schneider, Y. Aratyn-Schaus and C. M. Waterman, *Annu. Rev. Cell Dev. Biol.*, 2010, **26**, 315–333.
75 W. J. Hadden, J. L. Young, A. W. Holle, M. L. McFetridge, D. Y. Kim, P. Wijesinghe, H. Taylor-Weiner, J. H. Wen, A. R. Lee, K. Bieback, B. N. Vo, D. D. Sampson, B. F. Kennedy, J. P. Spatz, A. J. Engler and Y. S. Cho, *Proc. Natl. Acad. Sci. U. S. A.*, 2017, **114**, 5647–5652.
76 K. Burridge and C. Guilluy, *Exp. Cell Res.*, 2016, **343**, 14–20.
77 A. S. Rowlands, P. A. George and J. J. Cooper-White, *Am. J. Physiol.*, 2008, **295**, C1037–C1044.
78 J. H. Wen, L. G. Vincent, A. Fuhrmann, Y. S. Choi, K. C. Hribar, H. Taylor-Weiner, S. Chen and A. J. Engler, *Nat. Mater.*, 2014, **13**, 979–987.
79 S. I. Presolski, V. Hong, S. H. Cho and M. G. Finn, *J. Am. Chem. Soc.*, 2010, **132**, 14570–14576.
80 J. Dommerholt, F. P. J. T. Rutjes and F. L. van Delft, *Top. Curr. Chem.*, 2016, **374**, 1–20.
81 A. Meijer, S. Otto and J. B. F. N. Engberts, *J. Org. Chem.*, 1998, **63**, 8989–8994.
82 M. Vauthier, L. Jierry, M. L. Martinez Mendez, Y. M. Durst, J. Kelber, V. Roucoules and F. Bally-Le Gall, *J. Phys. Chem. C*, 2019, **123**, 4125–4132.
83 A. Darko, S. Wallace, O. Dmitrenko, M. M. Machovina, R. A. Mehl, J. W. Chin and J. M. Fox, *Chem. Sci.*, 2014, **5**, 3770–3776.
84 D. Larsen, A. M. Kietrys, S. A. Clark, H. S. Park, A. Ekebergh and E. T. Kool, *Chem. Sci.*, 2018, **9**, 5252–5259.
85 A. Dirksen, S. Dirksen, T. M. Hackeng and P. E. Dawson, *J. Am. Chem. Soc.*, 2006, **128**, 15602–15603.
86 E. T. Kool, D. H. Park and P. Crisalli, *J. Am. Chem. Soc.*, 2013, **135**, 17663–17666.
87 F. Saito, H. Noda and J. W. Bode, *ACS Chem. Biol.*, 2015, **10**, 1026–1033.
88 P. Schelté, C. Boeckler, B. Frisch and F. Schuber, *Bioconjugate Chem.*, 2000, **11**, 118–123.
89 C. W. Tornøe, C. Christensen and M. Meldal, *J. Org. Chem.*, 2002, **67**, 3057–3064.
90 V. V. Rostovtsev, L. G. Green, V. V. Fokin and K. B. Sharpless, *Angew. Chem., Int. Ed.*, 2002, **41**, 2596–2599.
91 J. F. Lutz and Z. Zarafshani, *Adv. Drug Delivery Rev.*, 2008, **60**, 958–970.
92 D. A. Ossipov and J. Hilborn, *Macromolecules*, 2006, **39**, 1709–1718.
93 M. Malkoch, R. Vestberg, N. Gupta, L. Mespouille, P. Dubois, A. F. Mason, J. L. Hedrick, Q. Liao, C. W. Frank, K. Kingsbury and C. J. Hawker, *Chem. Commun.*, 2006, 2774–2776.
94 V. Crescenzi, L. Cornelio, C. Di Meo, S. Nardecchia and R. Lamanna, *Biomacromolecules*, 2007, **8**, 1844–1850.
95 S. Q. Liu, P. L. Rachel Ee, C. Y. Ke, J. L. Hedrick and Y. Y. Yang, *Biomaterials*, 2009, **30**, 1453–1461.
96 E. Lallana, R. Riguera and E. Fernandez-Megia, *Angew. Chem., Int. Ed.*, 2011, **50**, 8794–8804.
97 J. F. Lutz, *Angew. Chem., Int. Ed.*, 2007, **46**, 1018–1025.
98 V. D. Bock, H. Hiemstra and J. H. Van Maarseveen, *Eur. J. Org. Chem.*, 2006, 51–68.
99 W. H. Binder and R. Sachsenhofer, *Macromol. Rapid Commun.*, 2008, **29**, 952–981.
100 R. A. Evans, *Aust. J. Chem.*, 2007, **60**, 384–395.
101 J. E. Moses and A. D. Moorhouse, *Chem. Soc. Rev.*, 2007, **36**, 1249–1262.
102 H. Nandivada, X. Jiang and J. Lahann, *Adv. Mater.*, 2007, **19**, 2197–2208.
103 B. J. Adzima, Y. Tao, C. J. Kloxin, C. A. DeForest, K. S. Anseth and C. N. Bowman, *Nat. Chem.*, 2011, **3**, 256–259.
104 M. Van Dijk, C. F. Van Nostrum, W. E. Hennink, D. T. S. Rijkers and R. M. J. Liskamp, *Biomacromolecules*, 2010, **11**, 1608–1614.
105 M. A. Azagarsamy, D. D. McKinnon, D. L. Alge and K. S. Anseth, *ACS Macro Lett.*, 2014, **3**, 515–519.
106 G. Huerta-Angeles, M. Němcová, E. Příkopová, D. Šmejkalová, M. Pravda, L. Kučera and V. Velebný, *Carbohydr. Polym.*, 2012, **90**, 1704–1711.
107 A. M. Testera, A. Girotti, I. G. de Torre, L. Quintanilla, M. Santos, M. Alonso and J. C. Rodríguez-Cabello, *J. Mater. Sci.: Mater. Med.*, 2015, **26**, 1–13.
108 X. Hu, D. Li, F. Zhou and C. Gao, *Acta Biomater.*, 2011, **7**, 1618–1626.

 This journal is © The Royal Society of Chemistry and IChemE 2021

Published on 19 July 2021. Downloaded by University of Virginia on 8/10/2021 5:09:05 PM.

109 R. J. Seelbach, P. Fransen, M. Peroglio, D. Pulido, P. Lopez-Chicon, F. Duttenhoefer, S. Sauerbier, T. Freiman, P. Niemeyer, C. Semino, F. Albericio, M. Alini, M. Royo, A. Mata and D. Eglin, *Acta Biomater.*, 2014, **10**, 4340–4350.
110 R. T. Chen, S. Marchesan, R. A. Evans, K. E. Styan, G. K. Such, A. Postma, K. M. McLean, B. W. Muir and F. Caruso, *Biomacromolecules*, 2012, **13**, 889–895.
111 N. D. Gallant, K. A. Lavery, E. J. Amis and M. L. Becker, *Adv. Mater.*, 2007, **19**, 965–969.
112 J. Lu, M. Shi and M. S. Shoichet, *Bioconjugate Chem.*, 2009, **20**, 87–94.
113 G. A. Hudalla and W. L. Murphy, *Langmuir*, 2009, **25**, 5737–5746.
114 N. M. Moore, N. J. Lin, N. D. Gallant and M. L. Becker, *Biomaterials*, 2010, **31**, 1604–1611.
115 D. Soriano Del Amo, W. Wang, H. Jiang, C. Besanceney, A. C. Yan, M. Levy, Y. Liu, F. L. Marlow and P. Wu, *J. Am. Chem. Soc.*, 2010, **132**, 16893–16899.
116 N. J. Agard, J. A. Prescher and C. R. Bertozzi, *J. Am. Chem. Soc.*, 2004, **126**, 15046–15047.
117 M. F. Debets, S. S. Van Berkel, J. Dommerholt, A. J. Dirks, F. P. J. T. Rutjes and F. L. Van Delft, *Acc. Chem. Res.*, 2011, **44**, 805–815.
118 E. Kim and H. Koo, *Chem. Sci.*, 2019, **10**, 7835–7851.
119 C. J. Pickens, S. N. Johnson, M. M. Pressnall, M. A. Leon and C. J. Berkland, *Bioconjugate Chem.*, 2018, **29**, 686–701.
120 S. M. Hodgson, E. Bakaic, S. A. Stewart, T. Hoare and A. Adronov, *Biomacromolecules*, 2016, **17**, 1093–1100.
121 J. Xu, T. M. Filion, F. Prifti and J. Song, *Chem. – Asian J.*, 2011, **6**, 2730–2737.
122 C. A. DeForest and K. S. Anseth, *Nat. Chem.*, 2011, **3**, 925–931.
123 C. A. Deforest, B. D. Polizzotti and K. S. Anseth, *Nat. Mater.*, 2009, **8**, 659–664.
124 S. S. Han, H. Y. Yoon, J. Y. Yhee, M. O. Cho, H. E. Shim, J. E. Jeong, D. E. Lee, K. Kim, H. Guim, J. H. Lee, K. M. Huh and S. W. Kang, *Polym. Chem.*, 2018, **9**, 20–27.
125 Y. Tan, H. Huang, D. C. Ayers and J. Song, *ACS Cent. Sci.*, 2018, **4**, 971–981.
126 T. E. Brown, J. S. Silver, B. T. Worrell, I. A. Marozas, F. M. Yavitt, K. A. Günay, C. N. Bowman and K. S. Anseth, *J. Am. Chem. Soc.*, 2018, **140**, 11585–11588.
127 S. Tang, H. Ma, H. C. Tu, H. R. Wang, P. C. Lin and K. S. Anseth, *Adv. Sci.*, 2018, **5**, 1800638.
128 C. M. Madl and S. C. Heilshorn, *Bioconjugate Chem.*, 2017, **28**, 724–730.
129 J. A. Shadish, A. C. Strange and C. A. Deforest, *J. Am. Chem. Soc.*, 2019, **141**, 15619–15625.
130 C. K. Arakawa, B. A. Badeau, Y. Zheng and C. A. DeForest, *Adv. Mater.*, 2017, **29**, 1–9.
131 J. Dommerholt, S. Schmidt, R. Temming, L. J. A. Hendriks, F. P. J. T. Rutjes, J. C. M. Van Hest, D. J. Lefeber, P. Friedl and F. L. Van Delft, *Angew. Chem., Int. Ed.*, 2010, **49**, 9422–9425.
132 J. Dommerholt, O. Van Rooijen, A. Borrmann, C. F. Guerra, F. M. Bickelhaupt and F. L. Van Delft, *Nat. Commun.*, 2014, **5**, 1–7.
133 E. S. Zimmerman, T. H. Heibeck, A. Gill, X. Li, C. J. Murray, M. R. Madlansacay, C. Tran, N. T. Uter, G. Yin, P. J. Rivers, A. Y. Yam, W. D. Wang, A. R. Steiner, S. U. Bajad, K. penta, W. Yang, T. J. Hallam, C. D. Thanos and A. K. Sato, *Bioconjugate Chem.*, 2014, **25**, 351–361.
134 C. D. Hermann, D. S. Wilson, K. A. Lawrence, X. Ning, R. Olivares-Navarrete, J. K. Williams, R. E. Guldberg, N. Murthy, Z. Schwartz and B. D. Boyan, *Biomaterials*, 2014, **35**, 9698–9708.
135 C. A. Deforest, E. A. Sims and K. S. Anseth, *Chem. Mater.*, 2010, **22**, 4783–4790.
136 H. Jiang, S. Qin, H. Dong, Q. Lei, X. Su, R. Zhuo and Z. Zhong, *Soft Matter*, 2015, **11**, 6029–6036.
137 J. C. Grim, T. E. Brown, B. A. Aguado, D. A. Chapnick, A. L. Viert, X. Liu and K. S. Anseth, *ACS Cent. Sci.*, 2018, **4**, 909–916.
138 H. Li, J. Zheng, H. Wang, M. L. Becker and N. D. Leipzig, *J. Biomater. Appl.*, 2018, **32**, 1222–1230.
139 C. A. Deforest and D. A. Tirrell, *Nat. Mater.*, 2015, **14**, 523–531.
140 V. X. Truong, K. M. Tsang, G. P. Simon, R. L. Boyd, R. A. Evans, H. Thissen and J. S. Forsythe, *Biomacromolecules*, 2015, **16**, 2246–2253.
141 V. X. Truong, M. P. Ablett, H. T. J. Gilbert, J. Bowen, S. M. Richardson, J. A. Hoyland and A. P. Dove, *Biomater. Sci.*, 2014, **2**, 167–175.
142 J. L. Guo, A. Li, Y. S. Kim, V. Y. Xie, B. T. Smith, E. Watson, G. Bao and A. G. Mikos, *J. Biomed. Mater. Res., Part A*, 2020, **108**, 684–693.
143 A. R. Killaars, C. J. Walker and K. S. Anseth, *Proc. Natl. Acad. Sci. U. S. A.*, 2020, **117**, 21258–21266.
144 X. Wang, Z. Li, T. Shi, P. Zhao, K. An, C. Lin and H. Liu, *Mater. Sci. Eng., C*, 2017, **73**, 21–30.
145 D. D. McKinnon, T. E. Brown, K. A. Kyburz, E. Kiyotake and K. S. Anseth, *Biomacromolecules*, 2014, **15**, 2808–2816.
146 C. M. Madl, L. M. Katz and S. C. Heilshorn, *Adv. Funct. Mater.*, 2016, **26**, 3612–3620.
147 N. Huebsch, P. R. Arany, A. S. Mao, D. Shvartsman, O. A. Ali, S. A. Bencherif, J. Rivera-Feliciano and D. J. Mooney, *Nat. Mater.*, 2010, **9**, 518–526.
148 M. Gregoritza and F. P. Brandl, *Eur. J. Pharm. Biopharm.*, 2015, **97**, 438–453.
149 M. M. Heravi and V. F. Vavsari, *RSC Adv.*, 2015, **5**, 50890–50912.
150 A. Duan, P. Yu, F. Liu, H. Qiu, F. L. Gu, M. P. Doyle and K. N. Houk, *J. Am. Chem. Soc.*, 2017, **139**, 2766–2770.
151 M. M. Heravi, T. Ahmadi, M. Ghavidel, B. Heidari and H. Hamidi, *RSC Adv.*, 2015, **5**, 101999–102075.
152 C. Grosso, M. Liber, A. F. Brigas, T. M. V. D. Pinho E Melo and A. Lemos, *J. Chem. Educ.*, 2019, **96**, 148–152.
153 I. Altinbasak, R. Sanyal and A. Sanyal, *RSC Adv.*, 2016, **6**, 74757–74764.
154 W. Blokzijl, M. J. Blandamer and J. B. F. N. Engberts, *J. Am. Chem. Soc.*, 1991, **113**, 4241–4246.
155 D. C. Rideout and R. Breslow, *J. Am. Chem. Soc.*, 1980, **102**, 7816–7817.

Published on 19 July 2021. Downloaded by University of Virginia on 8/10/2021 5:09:05 PM.

156 Y. Chujo, K. Sada and T. Saegusa, *Macromolecules*, 1990, **23**, 2636–2641.
157 S. Jung, S. Y. Kim, J. C. Kim, S. M. Noh and J. K. Oh, *RSC Adv.*, 2017, **7**, 26496–26506.
158 P. Reutenauer, E. Buhler, P. J. Boul, S. J. Candau and J. M. Lehn, *Chem. – Eur. J.*, 2009, **15**, 1893–1900.
159 Z. Wei, J. H. Yang, X. J. Du, F. Xu, M. Zrinyi, Y. Osada, F. Li and Y. M. Chen, *Macromol. Rapid Commun.*, 2013, **34**, 1464–1470.
160 R. K. Kramer, M. N. Belgacem, A. J. F. Carvalho and A. Gandini, *Int. J. Biol. Macromol.*, 2019, **141**, 493–498.
161 G. F. Wang, H. J. Chu, H. L. Wei, X. Q. Liu, Z. X. Zhao and J. Zhu, *Chem. Pap.*, 2014, **68**, 1390–1399.
162 S. Kirchhof, F. P. Brandl, N. Hammer and A. M. Goepferich, *J. Mater. Chem. B*, 2013, **1**, 4855–4864.
163 V. Froidevaux, M. Borne, E. Laborbe, R. Auvergne, A. Gandini and B. Boutevin, *RSC Adv.*, 2015, **5**, 37742–37754.
164 H. L. Wei, Z. Yang, L. M. Zheng and Y. M. Shen, *Polymer*, 2009, **50**, 2836–2840.
165 M. Gregoritza, V. Messmann, A. M. Goepferich and F. P. Brandl, *J. Mater. Chem. B*, 2016, **4**, 3398–3408.
166 N. A. Silva, M. J. Cooke, R. Y. Tam, N. Sousa, A. J. Salgado, R. L. Reis and M. S. Shoichet, *Biomaterials*, 2012, **33**, 6345–6354.
167 S. C. Owen, S. A. Fisher, R. Y. Tam, C. M. Nimmo and M. S. Shoichet, *Langmuir*, 2013, **29**, 7393–7400.
168 R. Y. Tam, J. Yockell-Lelièvre, L. J. Smith, L. M. Julian, A. E. G. Baker, C. Choey, M. S. Hasim, J. Dimitroulakos, W. L. Stanford and M. S. Shoichet, *Adv. Mater.*, 2019, **31**, 1–9.
169 H. Tan, J. P. Rubin and K. G. Marra, *Macromol. Rapid Commun.*, 2011, **32**, 905–911.
170 D. Xing, L. Ma and C. Gao, *J. Bioact. Compat. Polym.*, 2017, **32**, 382–396.
171 F. Yu, X. Cao, L. Zeng, Q. Zhang and X. Chen, *Carbohydr. Polym.*, 2013, **97**, 188–195.
172 M. Fan, Y. Ma, Z. Zhang, J. Mao, H. Tan and X. Hu, *Mater. Sci. Eng., C*, 2015, **56**, 311–317.
173 M. Gregoritza, V. Messmann, K. Abstiens, F. P. Brandl and A. M. Goepferich, *Biomacromolecules*, 2017, **18**, 2410–2418.
174 K. C. Koehler, D. L. Alge, K. S. Anseth and C. N. Bowman, *Biomaterials*, 2013, **34**, 4150–4158.
175 S. Kirchhof, A. Strasser, H. J. Wittmann, V. Messmann, N. Hammer, A. M. Goepferich and F. P. Brandl, *J. Mater. Chem. B*, 2015, **3**, 449–457.
176 L. J. Smith, S. M. Taimoory, R. Y. Tam, A. E. G. Baker, N. Binth Mohammad, J. F. Trant and M. S. Shoichet, *Biomacromolecules*, 2018, **19**, 926–935.
177 C. García-Astrain and L. Avérous, *Int. J. Biol. Macromol.*, 2019, **137**, 612–619.
178 M. Montiel-Herrera, A. Gandini, F. M. Goycoolea, N. E. Jacobsen, J. Lizardi-Mendoza, M. Recillas-Mota and W. M. Argüelles-Monal, *Carbohydr. Polym.*, 2015, **128**, 6–12.
179 S. Kirchhof, M. Gregoritza, V. Messmann, N. Hammer, A. M. Goepferich and F. P. Brandl, *Eur. J. Pharm. Biopharm.*, 2015, **96**, 217–225.
180 S. A. Stewart, M. Backholm, N. A. D. Burke and H. D. H. Stöver, *Langmuir*, 2016, **32**, 1863–1870.
181 M. Zhang, J. Wang and Z. Jin, *Int. J. Biol. Macromol.*, 2018, **114**, 381–391.
182 O. Guaresti, C. García-Astrain, R. H. Aguirresarobe, A. Eceiza and N. Gabilondo, *Carbohydr. Polym.*, 2018, **183**, 278–286.
183 N. Cengiz, T. N. Gevrek, R. Sanyal, R. Sanyal, A. Sanyal and A. Sanyal, *Bioconjugate Chem.*, 2020, **31**, 1382–1391.
184 E. J. Park, T. N. Gevrek, R. Sanyal and A. Sanyal, *Bioconjugate Chem.*, 2014, **25**, 2004–2011.
185 M. H. Ghanian, H. Mirzadeh and H. Baharvand, *Biomacromolecules*, 2018, **19**, 1646–1662.
186 F. Yu, X. Cao, J. Du, G. Wang and X. Chen, *ACS Appl. Mater. Interfaces*, 2015, **7**, 24023–24031.
187 K. C. Koehler, K. S. Anseth and C. N. Bowman, *Biomacromolecules*, 2013, **14**, 538–547.
188 G. Wang, X. Cao, H. Dong, L. Zeng, C. Yu and X. Chen, *Polymers*, 2018, **10**, 949.
189 X. Bai, S. Lü, Z. Cao, B. Ni, X. Wang, P. Ning, D. Ma, H. Wei and M. Liu, *Carbohydr. Polym.*, 2017, **166**, 123–130.
190 S. Li, L. Wang, X. Yu, C. Wang and Z. Wang, *Mater. Sci. Eng., C*, 2018, **82**, 299–309.
191 B. Bi, M. Ma, S. Lv, R. Zhuo and X. Jiang, *Carbohydr. Polym.*, 2019, **212**, 368–377.
192 C. M. Madl and S. C. Heilshorn, *Chem. Mater.*, 2019, **31**, 8035–8043.
193 A. Gandini, *Prog. Polym. Sci.*, 2013, **38**, 1–29.
194 T. Elschner, F. Obst and T. Heinze, *Macromol. Biosci.*, 2018, **18**, 1–15.
195 K. C. Nicolaou, S. A. Snyder, T. Montagnon and G. Vassilikogiannakis, *Angew. Chem., Int. Ed.*, 2002, **41**, 1668–1698.
196 P. Farkaš and S. Bystrický, *Carbohydr. Polym.*, 2007, **68**, 187–190.
197 H. S. Abandansari, M. H. Ghanian, F. Varzideh, E. Mahmoudi, S. Rajabi, P. Taheri, M. R. Nabid and H. Baharvand, *Biomaterials*, 2018, **170**, 12–25.
198 A. Cuvellier, R. Verhelle, J. Brancart, B. Vanderborght, G. Van Assche and H. Rahier, *Polym. Chem.*, 2019, **10**, 473–485.
199 B. L. Oliveira, Z. Guo and G. J. L. Bernardes, *Chem. Soc. Rev.*, 2017, **46**, 4895–4950.
200 M. Pagel, *J. Pept. Sci.*, 2019, **25**, 1–9.
201 M. L. Blackman, M. Royzen and J. M. Fox, *J. Am. Chem. Soc.*, 2008, **130**, 13518–13519.
202 T. Reiner and B. M. Zeglis, *J. Labelled Compd. Radiopharm.*, 2014, **57**, 285–290.
203 R. A. Carboni and R. V. Lindsey, *J. Am. Chem. Soc.*, 1959, **81**, 4342–4346.
204 J. Balcar, G. Chrisam, F. X. Huber and J. Sauer, *Tetrahedron Lett.*, 1983, **24**, 1481–1484.
205 J. Schoch, M. Staudt, A. Samanta, M. Wiessler and A. Jäschke, *Bioconjugate Chem.*, 2012, **23**, 1382–1386.
206 A. L. Rutz, E. S. Gargus, K. E. Hyland, P. L. Lewis, A. Setty, W. R. Burghardt and R. N. Shah, *Acta Biomater.*, 2019, **99**, 121–132.
207 A. C. Knall, M. Hollauf, R. Saf and C. Slugovc, *Org. Biomol. Chem.*, 2016, **14**, 10576–10580.

 This journal is © The Royal Society of Chemistry and IChemE 2021

Published on 19 July 2021. Downloaded by University of Virginia on 8/10/2021 5:09:05 PM.

208 F. Jivan, N. Fabela, Z. Davis and D. L. Alge, *J. Mater. Chem. B*, 2018, **6**, 4929–4936.
209 V. X. Truong, M. P. Ablett, S. M. Richardson, J. A. Hoyland and A. P. Dove, *J. Am. Chem. Soc.*, 2015, **137**, 1618–1622.
210 D. N. Kamber, Y. Liang, R. J. Blizzard, F. Liu, R. A. Mehl, K. N. Houk and J. A. Prescher, *J. Am. Chem. Soc.*, 2015, **137**, 8388–8391.
211 A. C. Knall, M. Hollauf and C. Slugovc, *Tetrahedron Lett.*, 2014, **55**, 4763–4766.
212 D. L. Alge, M. A. Azagarsamy, D. F. Donohue and K. S. Anseth, *Biomacromolecules*, 2013, **14**, 949–953.
213 K. Kang, J. Park and E. Kim, *Proteome Sci.*, 2017, **15**, 1–13.
214 V. Delplace, P. E. B. Nickerson, A. Ortin-Martinez, A. E. G. Baker, V. A. Wallace and M. S. Shoichet, *Adv. Funct. Mater.*, 2020, **30**, 1–11.
215 V. Delplace, A. J. Pickering, M. H. Hettiaratchi, S. Zhao, T. Kivijärvi and M. S. Shoichet, *Biomacromolecules*, 2020, **21**, 2421–2431.
216 S. T. Koshy, R. M. Desai, P. Joly, J. Li, R. K. Bagrodia, S. A. Lewin, N. S. Joshi and D. J. Mooney, *Adv. Healthcare Mater.*, 2016, **5**, 541–547.
217 Z. Zhang, C. He and X. Chen, *Polymers*, 2020, **12**, 884.
218 D. S. B. Anugrah, K. Ramesh, M. Kim, K. Hyun and K. T. Lim, *Carbohydr. Polym.*, 2019, **223**, 115070.
219 Y. Zhang, H. Chen, T. Zhang, Y. Zan, T. Ni, M. Liu and R. Pei, *Biomater. Sci.*, 2018, **6**, 2578–2581.
220 Y. Takayama, K. Kusamori and M. Nishikawa, *Molecules*, 2019, **24**, 172.
221 H. Wu and N. K. Devaraj, *Top. Curr. Chem.*, 2016, **374**, 1–22.
222 F. Liu, Y. Liang and K. N. Houk, *J. Am. Chem. Soc.*, 2014, **136**, 11483–11493.
223 F. Liu, R. S. Paton, S. Kim, Y. Liang and K. N. Houk, *J. Am. Chem. Soc.*, 2013, **135**, 15642–15649.
224 M. Vrabel, P. Kölle, K. M. Brunner, M. J. Gattner, V. Lõpez-Carrillo, R. De Vivie-Riedle and T. Carell, *Chem. – Eur. J.*, 2013, **19**, 13309–13312.
225 R. Selvaraj and J. M. Fox, *Curr. Opin. Chem. Biol.*, 2013, **17**, 753–760.
226 M. Wiessler, W. Waldeck, C. Kliem, R. Pipkorn and K. Braun, *Int. J. Med. Sci.*, 2010, **7**, 19–28.
227 A. C. Knall and C. Slugovc, *Chem. Soc. Rev.*, 2013, **42**, 5131–5142.
228 G. J. Bodwell and Z. Pi, *Tetrahedron Lett.*, 1997, **38**, 309–312.
229 S. Agopcan Cinar, S. Ercan, S. Erol Gunal, I. Dogan and V. Aviyente, *Org. Biomol. Chem.*, 2014, **12**, 8079–8086.
230 V. Tamilmani, C. A. Daul and P. Venuvanalingam, *Chem. Phys. Lett.*, 2005, **416**, 354–357.
231 J. W. Wijnen, S. Zavarise, J. B. F. N. Engberts and M. Charton, *J. Org. Chem.*, 1996, **61**, 2001–2005.
232 M. T. Taylor, M. L. Blackman, O. Dmitrenko and J. M. Fox, *J. Am. Chem. Soc.*, 2011, **133**, 9646–9649.
233 A. Lueckgen, D. S. Garske, A. Ellinghaus, R. M. Desai, A. G. Stafford, D. J. Mooney, G. N. Duda and A. Cipitria, *Biomaterials*, 2018, **181**, 189–198.
234 R. M. Desai, S. T. Koshy, S. A. Hilderbrand, D. J. Mooney and N. S. Joshi, *Biomaterials*, 2015, **50**, 30–37.
235 A. Lueckgen, D. S. Garske, A. Ellinghaus, D. J. Mooney, G. N. Duda and A. Cipitria, *Acta Biomater.*, 2020, **115**, 185–196.
236 Y. Hao, J. Song, A. Ravikrishnan, K. T. Dicker, E. W. Fowler, A. B. Zerdoum, Y. Li, H. Zhang, A. K. Rajasekaran, J. M. Fox and X. Jia, *ACS Appl. Mater. Interfaces*, 2018, **10**, 26016–26027.
237 K. H. Vining, A. Stafford and D. J. Mooney, *Biomaterials*, 2019, **188**, 187–197.
238 J. Carthew, J. E. Frith, J. S. Forsythe and V. X. Truong, *J. Mater. Chem. B*, 2018, **6**, 1394–1401.
239 H. Zhang, K. T. Dicker, X. Xu, X. Jia and J. M. Fox, *ACS Macro Lett.*, 2014, **3**, 727–731.
240 J. B. Conant and P. D. Bartlett, *J. Am. Chem. Soc.*, 1932, **54**, 2881–2899.
241 P. Crisalli and E. T. Kool, *J. Org. Chem.*, 2013, **78**, 1184–1189.
242 A. Dirksen and P. E. Dawson, *Bioconjugate Chem.*, 2008, **19**, 2543–2548.
243 J. Kalia and R. T. Raines, *Angew. Chem., Int. Ed.*, 2008, **47**, 7523–7526.
244 L. Moroni, J. A. Burdick, C. Highley, S. J. Lee, Y. Morimoto, S. Takeuchi and J. J. Yoo, *Nat. Rev. Mater.*, 2018, **3**, 21–37.
245 D. K. Kölmel and E. T. Kool, *Chem. Rev.*, 2017, **117**, 10358–10376.
246 S. Hafeez, H. Ooi, F. Morgan, C. Mota, M. Dettin, C. van Blitterswijk, L. Moroni and M. Baker, *Gels*, 2018, **4**, 85.
247 P. E. Farahani, S. M. Adelmund, J. A. Shadish and C. A. DeForest, *J. Mater. Chem. B*, 2017, **5**, 4435–4442.
248 J. M. Poolman, C. Maity, J. Boekhoven, L. Van Der Mee, V. A. A. Le Sage, G. J. M. Groenewold, S. I. Van Kasteren, F. Versluis, J. H. Van Esch and R. Eelkema, *J. Mater. Chem. B*, 2016, **4**, 852–858.
249 N. Boehnke, C. Cam, E. Bat, T. Segura and H. D. Maynard, *Biomacromolecules*, 2015, **16**, 2101–2108.
250 J. Collins, Z. Xiao, M. Müllner and L. A. Connal, *Polym. Chem.*, 2016, **7**, 3812–3826.
251 V. Meyer and A. Janny, *Ber. Dtsch. Chem. Ges.*, 1882, **15**, 1164–1167.
252 G. N. Grover, R. L. Braden and K. L. Christman, *Adv. Mater.*, 2013, **25**, 2937–2942.
253 S. Mukherjee, M. R. Hill and B. S. Sumerlin, *Soft Matter*, 2015, **11**, 6152–6161.
254 R. A. Dilla, C. M. M. Motta, Y. Xu, Z. K. Zander, N. Bernard, C. G. Wiener, B. D. Vogt and M. L. Becker, *Mater. Today Chem.*, 2019, **11**, 244–252.
255 A. E. G. Baker, L. C. Bahlmann, R. Y. Tam, J. C. Liu, A. N. Ganesh, N. Mitrousis, R. Marcellus, M. Spears, J. M. S. Bartlett, D. W. Cescon, G. D. Bader and M. S. Shoichet, *Adv. Mater.*, 2019, **31**, 1–11.
256 G. N. Grover, J. Lam, T. H. Nguyen, T. Segura and H. D. Maynard, *Biomacromolecules*, 2012, **13**, 3013–3017.
257 Z. Zhang, C. He and X. Chen, *Mater. Chem. Front.*, 2018, **2**, 1765–1778.
258 C. Yang and D. Tang, *Comput. Model Eng. Sci.*, 2000, **1**, 119–131.

Published on 19 July 2021. Downloaded by University of Virginia on 8/10/2021 5:09:05 PM.

259 A. A. Kale and V. P. Torchilin, *Bioconjugate Chem.*, 2007, **18**, 363–370.
260 I. Yildiz, *J. Phys. Chem. A*, 2016, **120**, 3683–3692.
261 R. Nguyen, *Chem. Commun.*, 2003, 942–943.
262 D. D. McKinnon, D. W. Domaille, J. N. Cha and K. S. Anseth, *Adv. Mater.*, 2014, **26**, 865–872.
263 D. D. McKinnon, D. W. Domaille, J. N. Cha and K. S. Anseth, *Chem. Mater.*, 2014, **26**, 2382–2387.
264 J. Karvinen, J. T. Koivisto, I. Jönkkäri and M. Kellomäki, *J. Mech. Behav. Biomed. Mater.*, 2017, **71**, 383–391.
265 M. Patenaude and T. Hoare, *Biomacromolecules*, 2012, **13**, 369–378.
266 F. Chen, Y. Ni, B. Liu, T. Zhou, C. Yu, Y. Su, X. Zhu, X. Yu and Y. Zhou, *Carbohydr. Polym.*, 2017, **166**, 31–44.
267 P. K. Sharma and Y. Singh, *Biomacromolecules*, 2019, **20**, 2174–2184.
268 H. Wang, D. Zhu, A. Paul, L. Cai, A. Enejder, F. Yang and S. C. Heilshorn, *Adv. Funct. Mater.*, 2017, **27**, 1–11.
269 F. Xu, A. Lam, Z. Pan, G. Randhawa, M. Lamb, H. Sheardown and T. Hoare, *ACS Biomater. Sci. Eng.*, 2021, DOI: 10.1021/acsbiomaterials.0c01552.
270 T. Kageyama, T. Kakegawa, T. Osaki, J. Enomoto, T. Ito, T. Nittami and J. Fukuda, *Biofabrication*, 2014, **6**, 2.
271 L. L. Wang, C. B. Highley, Y. C. Yeh, J. H. Galarraga, S. Uman and J. A. Burdick, *J. Biomed. Mater. Res., Part A*, 2018, **106**, 865–875.
272 Z. Wei, J. H. Yang, Z. Q. Liu, F. Xu, J. X. Zhou, M. Zrínyi, Y. Osada and Y. M. Chen, *Adv. Funct. Mater.*, 2015, **25**, 1352–1359.
273 W. Huang, Y. Wang, Y. Chen, Y. Zhao, Q. Zhang, X. Zheng, L. Chen and L. Zhang, *Adv. Healthcare Mater.*, 2016, **5**, 2813–2822.
274 Y. Yeo, T. Ito, E. Bellas, C. B. Highley, R. Marini and D. S. Kohane, *Ann. Surg.*, 2007, **245**, 819–824.
275 M. Patenaude and T. Hoare, *ACS Macro Lett.*, 2012, **1**, 409–413.
276 R. Chang, X. Wang, X. Li, H. An and J. Qin, *ACS Appl. Mater. Interfaces*, 2016, **8**, 25544–25551.
277 H. Qian and I. Aprahamian, *Chem. Commun.*, 2015, **51**, 11158–11161.
278 G. Xiao, Y. Wang, H. Zhang, L. Chen and S. Fu, *Carbohydr. Polym.*, 2019, **218**, 68–77.
279 F. Xu, B. Corbett, S. Bell, C. Zhang, M. Budi Hartono, Z. J. Farsangi, J. MacGregor and T. Hoare, *Biomacromolecules*, 2020, **21**, 214–229.
280 M. A. Azagarsamy, I. A. Marozas, S. Spaans and K. S. Anseth, *ACS Macro Lett.*, 2016, **5**, 19–23.
281 H. Ma, A. S. Caldwell, M. A. Azagarsamy, A. Gonzalez Rodriguez and K. S. Anseth, *Biomaterials*, 2020, **255**, 120205.
282 G. N. Grover, J. Garcia, M. M. Nguyen, M. Zanotelli, M. M. Madani and K. L. Christman, *Adv. Healthcare Mater.*, 2015, **4**, 1327–1331.
283 H. Sánchez-Morán, A. Ahmadi, B. Vogler and K. H. Roh, *Biomacromolecules*, 2019, **20**, 4419–4429.
284 F. Lin, J. Yu, W. Tang, J. Zheng, A. Defante, K. Guo, C. Wesdemiotis and M. L. Becker, *Biomacromolecules*, 2013, **14**, 3749–3758.
285 F. Trausel, B. Fan, S. A. P. van Rossum, J. H. van Esch and R. Eelkema, *Adv. Synth. Catal.*, 2018, **360**, 2571–2576.
286 M. Criado-Gonzalez, B. Loftin, J. Rodon Fores, D. Vautier, L. Kocgozlu, L. Jierry, P. Schaaf, F. Boulmedais and E. Harth, *J. Mater. Chem. B*, 2020, **8**, 4419–4427.
287 A. E. G. Baker, R. Y. Tam and M. S. Shoichet, *Biomacromolecules*, 2017, **18**, 4373–4384.
288 J. G. Hardy, P. Lin and C. E. Schmidt, *J. Biomater. Sci., Polym. Ed.*, 2015, **26**, 143–161.
289 L. Koivusalo, J. Karvinen, E. Sorsa, I. Jönkkäri, J. Väliaho, P. Kallio, T. Ilmarinen, S. Miettinen, H. Skottman and M. Kellomäki, *Mater. Sci. Eng., C*, 2018, **85**, 68–78.
290 L. Koivusalo, M. Kauppila, S. Samanta, V. S. Parihar, T. Ilmarinen, S. Miettinen, O. P. Oommen and H. Skottman, *Biomaterials*, 2019, **225**, 119516.
291 D. D. McKinnon, D. W. Domaille, T. E. Brown, K. A. Kyburz, E. Kiyotake, J. N. Cha and K. S. Anseth, *Soft Matter*, 2014, **10**, 9230–9236.
292 S. A. Marchitti, R. A. Deitrich and V. Vasiliou, *Pharmacol. Rev.*, 2007, **59**, 125–150.
293 B. M. Richardson, D. G. Wilcox, M. A. Randolph and K. S. Anseth, *Acta Biomater.*, 2019, **83**, 71–82.
294 B. M. Richardson, C. J. Walker, L. J. MacDougall, J. W. Hoye, M. A. Randolph, S. J. Bryant and K. S. Anseth, *Biomater. Sci.*, 2020, **8**, 3804–3811.
295 D. Zhu, H. Wang, P. Trinh, S. C. Heilshorn and F. Yang, *Biomaterials*, 2017, **127**, 132–140.
296 J. Dahlmann, A. Krause, L. Möller, G. Kensah, M. Möwes, A. Diekmann, U. Martin, A. Kirschning, I. Gruh and G. Dräger, *Biomaterials*, 2013, **34**, 940–951.
297 A. Suo, W. Xu, Y. Wang, T. Sun, L. Ji and J. Qian, *Carbohydr. Polym.*, 2019, **211**, 336–348.
298 C. E. Hoyle and C. N. Bowman, *Angew. Chem., Int. Ed.*, 2010, **49**, 1540–1573.
299 S. Huang, C. Wang, J. Xu, L. Ma and C. Gao, *Bioact. Mater.*, 2017, **2**, 253–259.
300 C. D. Cook, A. S. Hill, M. Guo, L. Stockdale, J. P. Papps, K. B. Isaacson, D. A. Lauffenburger and L. G. Griffith, *Integr. Biol.*, 2017, **9**, 271–289.
301 S. Xin, O. M. Wyman and D. L. Alge, *Adv. Healthcare Mater.*, 2018, **7**, 1–7.
302 A. Lueckgen, D. S. Garske, A. Ellinghaus, D. J. Mooney, G. N. Duda and A. Cipitria, *Biomaterials*, 2019, **217**, 119294.
303 A. Tirella, G. Mattei, M. La Marca, A. Ahluwalia and N. Tirelli, *Front. Bioeng. Biotechnol.*, 2020, **8**, 1–14.
304 Y. Zheng, M. K. Liong Han, Q. Jiang, B. Li, J. Feng and A. Del Campo, *Mater. Horiz.*, 2020, **7**, 111–116.
305 E. Hui, L. Moretti, T. H. Barker and S. R. Caliari, *Cell. Mol. Bioeng.*, 2021, DOI: 10.1007/s12195-021-00672-1.
306 B. D. Fairbanks, M. P. Schwartz, A. E. Halevi, C. R. Nuttelman, C. N. Bowman and K. S. Anseth, *Adv. Mater.*, 2009, **21**, 5005–5010.
307 C. E. Hoyle, A. B. Lowe and C. N. Bowman, *Chem. Soc. Rev.*, 2010, **39**, 1355–1387.
308 A. B. Lowe, C. E. Hoyle and C. N. Bowman, *J. Mater. Chem.*, 2010, **20**, 4745–4750.

This journal is © The Royal Society of Chemistry and IChemE 2021

Published on 19 July 2021. Downloaded by University of Virginia on 8/10/2021 5:09:05 PM.

309 B. D. Fairbanks, T. F. Scott, C. J. Kloxin, K. S. Anseth and C. N. Bowman, *Macromolecules*, 2009, **42**, 211–217.
310 B. D. Fairbanks, M. P. Schwartz, C. N. Bowman and K. S. Anseth, *Biomaterials*, 2009, **30**, 6702–6707.
311 B. L. Ekerdt, C. M. Fuentes, Y. Lei, M. M. Adil, A. Ramasubramanian, R. A. Segalman and D. V. Schaffer, *Adv. Healthcare Mater.*, 2018, **7**, e1800225.
312 S. K. Reddy, N. B. Cramer and C. N. Bowman, *Macromolecules*, 2006, **39**, 3673–3680.
313 S. K. Reddy, N. B. Cramer and C. N. Bowman, *Macromolecules*, 2006, **39**, 3681–3687.
314 P. M. Johnson, J. W. Stansbury and C. N. Bowman, *J. Polym. Sci., Part A: Polym. Chem.*, 2008, **46**, 1502–1509.
315 J. A. Carioscia, H. Lu, J. W. Stanbury and C. N. Bowman, *Dent. Mater.*, 2005, **21**, 1137–1143.
316 C. C. Lin, A. Raza and H. Shih, *Biomaterials*, 2011, **32**, 9685–9695.
317 C. F. H. Allen and W. J. Humphlett, *Can. J. Chem.*, 1966, **44**, 2315–2321.
318 D. L. Elbert, A. B. Pratt, M. P. Lutolf, S. Halstenberg and J. A. Hubbell, *J. Controlled Release*, 2001, **76**, 11–25.
319 A. Metters and J. Hubbell, *Biomacromolecules*, 2005, **6**, 290–301.
320 C. Hiemstra, L. J. van der Aa, Z. Zhong, P. J. Dijkstra and J. Feijen, *Biomacromolecules*, 2007, **8**, 1548–1556.
321 M. P. Lutolf, J. L. Lauer-Fields, H. G. Schmoekel, A. T. Metters, F. E. Weber, G. B. Fields and J. A. Hubbell, *Proc. Natl. Acad. Sci. U. S. A.*, 2003, **100**, 5413–5418.
322 M. P. Lutolf and J. A. Hubbell, *Nat. Biotechnol.*, 2005, **23**, 47–55.
323 S. Khetan, J. S. Katz and J. A. Burdick, *Soft Matter*, 2009, **5**, 1601–1606.
324 A. M. Rosales, S. L. Vega, F. W. DelRio, J. A. Burdick and K. S. Anseth, *Angew. Chem., Int. Ed.*, 2017, **56**, 12132–12136.
325 L. J. Macdougall, K. L. Wiley, A. M. Kloxin and A. P. Dove, *Biomaterials*, 2018, **178**, 435–447.
326 L. E. Jansen, L. J. Negrón-Piñeiro, S. Galarza and S. R. Peyton, *Acta Biomater.*, 2018, **70**, 120–128.
327 N. J. Darling, Y. S. Hung, S. Sharma and T. Segura, *Biomaterials*, 2016, **101**, 199–206.
328 E. A. Phelps, N. O. Enemchukwu, V. F. Fiore, J. C. Sy, N. Murthy, T. A. Sulchek, T. H. Barker and A. J. García, *Adv. Mater.*, 2012, **24**, 64–70.
329 H. N. Chia, M. Vigen and A. M. Kasko, *Acta Biomater.*, 2012, **8**, 2602–2611.
330 B. D. Cosgrove, K. L. Mui, T. P. Driscoll, S. R. Caliari, K. D. Mehta, R. K. Assoian, J. A. Burdick and R. L. Mauck, *Nat. Mater.*, 2016, **15**, 1297–1306.
331 S. R. Caliari, S. L. Vega, M. Kwon, E. M. Soulas and J. A. Burdick, *Biomaterials*, 2016, **103**, 314–323.
332 S. Rezakhani, N. Gjorevski and M. P. Lutolf, *Adv. Funct. Mater.*, 2020, **30**, 1–12.
333 J. Valdez, C. D. Cook, C. C. Ahrens, A. J. Wang, A. Brown, M. Kumar, L. Stockdale, D. Rothenberg, K. Renggli, E. Gordon, D. Lauffenburger, F. White and L. Griffith, *Biomaterials*, 2017, **130**, 90–103.
334 D. D. McKinnon, A. M. Kloxin and K. S. Anseth, *Biomater. Sci.*, 2013, **1**, 460–469.
335 A. Raza, C. S. Ki and C. C. Lin, *Biomaterials*, 2013, **34**, 5117–5127.
336 E. Cambria, K. Renggli, C. C. Ahrens, C. D. Cook, C. Kroll, A. T. Krueger, B. Imperiali and L. G. Griffith, *Biomacromolecules*, 2015, **16**, 2316–2326.
337 M. R. Arkenberg, D. M. Moore and C. C. Lin, *Acta Biomater.*, 2019, **83**, 83–95.
338 T. Y. Lin, C. S. Ki and C. C. Lin, *Biomaterials*, 2014, **35**, 6898–6906.
339 Z. Mũnoz, H. Shih and C. C. Lin, *Biomater. Sci.*, 2014, **2**, 1063–1072.
340 T. Greene and C. C. Lin, *ACS Biomater. Sci. Eng.*, 2015, **1**, 1314–1323.
341 T. Y. Lin, J. C. Bragg and C. C. Lin, *Macromol. Biosci.*, 2016, **16**, 496–507.
342 Y. Hao and C. C. Lin, *J. Biomed. Mater. Res., Part A*, 2014, **102**, 3813–3827.
343 Y. Hao, H. Shih, Z. Muňoz, A. Kemp and C. C. Lin, *Acta Biomater.*, 2014, **10**, 104–114.
344 M. Guvendiren and J. A. Burdick, *Nat. Commun.*, 2012, **3**, 792–799.
345 S. R. Caliari, M. Perepelyuk, E. M. Soulas, G. Y. Lee, R. G. Wells and J. A. Burdick, *Integr. Biol.*, 2016, **8**, 720–728.
346 K. A. Mosiewicz, L. Kolb, A. J. Van Der Vlies, M. M. Martino, P. S. Lienemann, J. A. Hubbell, M. Ehrbar and M. P. Lutolf, *Nat. Mater.*, 2013, **12**, 1072–1078.
347 C. M. Mcleod and R. L. Mauck, *Sci. Rep.*, 2016, **6**, 1–12.
348 C. Loebel, R. L. Mauck and J. A. Burdick, *Nat. Mater.*, 2019, **18**, 883–891.
349 J. Zhao, I. Ullah, B. Gao, J. Guo, X. K. Ren, S. Xia, W. Zhang and Y. Feng, *J. Mater. Chem. B*, 2020, **8**, 2418–2430.
350 D. C. Dieterich, J. J. Lee, A. J. Link, J. Graumann, D. A. Tirrell and E. M. Schuman, *Nat. Protoc.*, 2007, **2**, 532–540.
351 K. M. Mabry, R. L. Lawrence and K. S. Anseth, *Biomaterials*, 2015, **49**, 47–56.
352 A. Khang, A. Gonzalez Rodriguez, M. E. Schroeder, J. Sansom, E. Lejeune, K. S. Anseth and M. S. Sacks, *Acta Biomater.*, 2019, **96**, 354–367.
353 H. Shih, T. Greene, M. Korc and C. C. Lin, *Biomacromolecules*, 2016, **17**, 3872–3882.
354 H. Y. Liu, T. Greene, T. Y. Lin, C. S. Dawes, M. Korc and C. C. Lin, *Acta Biomater.*, 2017, **48**, 258–269.
355 H. Y. Liu, M. Korc and C. C. Lin, *Biomaterials*, 2018, **160**, 24–36.
356 R. J. Wade, E. J. Bassin, W. M. Gramlich and J. A. Burdick, *Adv. Mater.*, 2015, **27**, 1356–1362.
357 W. M. Gramlich, I. L. Kim and J. A. Burdick, *Biomaterials*, 2013, **34**, 9803–9811.
358 S. Khetan and J. A. Burdick, *Biomaterials*, 2010, **31**, 8228–8234.
359 M. A. Daniele, A. A. Adams, J. Naciri, S. H. North and F. S. Ligler, *Biomaterials*, 2014, **35**, 1845–1856.

Published on 19 July 2021. Downloaded by University of Virginia on 8/10/2021 5:09:05 PM.

360 T. E. Brown, B. J. Carberry, B. T. Worrell, O. Y. Dudaryeva, M. K. McBride, C. N. Bowman and K. S. Anseth, *Biomaterials*, 2018, **178**, 496–503.
361 Y. C. Yeh, E. A. Corbin, S. R. Caliari, L. Ouyang, S. L. Vega, R. Truitt, L. Han, K. B. Margulies and J. A. Burdick, *Biomaterials*, 2017, **145**, 23–32.
362 D. Lee, J. P. Park, M. Y. Koh, P. Kim, J. Lee, M. Shin and H. Lee, *Biomater. Sci.*, 2018, **6**, 1040–1047.
363 D. S. Reynolds, K. M. Bougher, J. H. Letendre, S. F. Fitzgerald, U. O. Gisladottir, M. W. Grinstaff and M. H. Zaman, *Acta Biomater.*, 2018, **77**, 85–95.
364 S. Xin, C. A. Gregory and D. L. Alge, *Acta Biomater.*, 2020, **101**, 227–236.
365 N. J. Darling, W. Xi, E. Sideris, A. R. Anderson, C. Pong, S. T. Carmichael and T. Segura, *Adv. Healthcare Mater.*, 2020, **9**, 1–10.
366 A. B. Lowe, *Polym. Chem.*, 2010, **1**, 17–36.
367 P. M. Kharkar, M. S. Rehmann, K. M. Skeens, E. Maverakis and A. M. Kloxin, *ACS Biomater. Sci. Eng.*, 2016, **2**, 165–179.
368 A. B. Lowe and M. A. Harvison, *Aust. J. Chem.*, 2010, **63**, 1251–1266.
369 N. Song, M. Ding, Z. Pan, J. Li, L. Zhou, H. Tan and Q. Fu, *Biomacromolecules*, 2013, **14**, 4407–4419.
370 B. Parrish, R. B. Breitenkamp and T. Emrick, *J. Am. Chem. Soc.*, 2005, **127**, 7404–7410.
371 Y. Chen and Z. Guan, *J. Am. Chem. Soc.*, 2010, **132**, 4577–4579.
372 S. I. Presolski, V. P. Hong and M. G. Finn, *Curr. Protoc. Chem. Biol.*, 2011, **3**, 153–162.
373 L. Li and Z. Zhang, *Molecules*, 2016, **21**, 1–22.
374 C. B. Highley, C. B. Rodell and J. A. Burdick, *Adv. Mater.*, 2015, **27**, 5075–5079.
375 Y. Ding, X. Xu, S. Sharma, M. Floren, K. Stenmark, S. J. Bryant, C. P. Neu and W. Tan, *Acta Biomater.*, 2018, **74**, 121–130.
376 M. L. Grubb and S. R. Caliari, *Acta Biomater.*, 2021, DOI: 10.1016/j.actbio.2021.03.006.
377 C. L. Petrou, T. J. D'Ovidio, D. A. Bölükbas, S. Tas, R. D. Brown, A. Allawzi, S. Lindstedt, E. Nozik-Grayck, K. R. Stenmark, D. E. Wagner and C. M. Magin, *J. Mater. Chem. B*, 2020, **8**, 6814–6826.

This journal is © The Royal Society of Chemistry and IChemE 2021